Evaluation of the efficiency of alternative enzyme production technologies

Albæk, Mads Orla

Publication date:
2012

Document Version
Publisher's PDF, also known as Version of record

Evaluation of the efficiency of alternative enzyme production technologies

Mads Orla Albæk

Ph.D. Thesis

March 2012

Evaluation of the efficiency of alternative enzyme production technologies

Ph.D. thesis

Mads Orla Albæk
Department of Chemical and Biochemical Engineering
Technical University of Denmark

March 30th 2012

Supervisors:

Associate Professor Krist V. Gernaey
Morten S. Hansen
Stuart M. Stocks

Address: **Fermentation Pilot Plant**
Novozymes A/S
Krogshøjvej 36
DK- 2880 Bagsværd
Denmark

Phone: +45 61 26 47 48
Web: www.novozymes.com

Print: **J&R Frydenholm A/S**
København
2012

ISBN: xxx-xx-xx-xx-xxxx

Abstract

Enzymes are used in an increasing number of industries. The application of enzymes is extending into the production of lignocellulosic ethanol in processes that economically can compete with fossil fuels. Since lignocellulosic ethanol is based on renewable resources it will have a positive impact on for example the emission of green house gasses. Cellulases and hemi-cellulases are used for enzymatic hydrolysis of pretreated lignocellulosic biomass, and fermentable sugars are released upon the enzymatic process. Even though many years of research has decreased the amount of enzyme needed in the process, the cost of enzymes is still considered a bottleneck in the economic feasibility of lignocellulose utilization. The purpose of this project was to investigate and compare different technologies for production of these enzymes. The filamentous fungus *Trichoderma reesei* is currently used for industrial production of cellulases and hemi-cellulases. The aim of the thesis was to use modeling tools to identify alternative technologies that have higher energy or raw material efficiency than the current technology.

The enzyme production by *T. reesei* was conducted as an aerobic fed-batch fermentation. The process was carried out in pilot scale stirred tank reactors and based on a range of different process conditions, a process model was constructed which satisfactory described the course of fermentation. The process was governed by the rate limiting mass transfer of oxygen from the gas to the liquid phase. During fermentation, filamentous growth of the fungus lead to increased viscosity which hindered mass transfer. These mechanisms were described by a viscosity model based on the biomass concentration of the fermentation broth and a mass transfer correlation that incorporated a viscosity term. An analysis of the uncertainty and sensitivity of the model indicated the biological parameters to be responsible for most of the model uncertainty.

A number of alternative fermentation technologies for enzyme production were identified in the open literature. Their mass transfer capabilities and their energy efficiencies were evaluated by use of the process model. For each technology the scale-up enzyme production was simulated at industrial scale based on equal mass transfer. The technical feasibility of each technology was assessed based on prior knowledge of successful implementation at industrial scale and mechanical complexity of the fermentation vessel. The airlift reactor was identified as a potential high energy efficiency technology for enzyme production with excellent chances for success.

Two different pilot plant configurations of the airlift reactor technology were tested in nine fermentations. The headspace pressure was varied between 0.1 and 1.1 barg and the superficial gas

velocity in the airlift riser section was varied between 0.02 and 0.06 m/s. The biological model developed in the stirred tank reactor was shown to apply to the airlift reactor with only small modifications: The mass transfer of oxygen in the airlift reactor was studied and a mass transfer correlation containing the superficial gas velocity and the apparent viscosity of the fermentation broth was shown to describe the experimental data well. The mass transfer rate was approximately 20% lower than the literature data for airlift reactors. Mixing in the pilot scale airlift reactor was also studied. As the mixing time was of the same order of magnitude as the characteristic time for oxygen transfer, mixing could also be limiting the process at that scale. The process model for the airlift reactor was also shown to describe the experimental data well for a range of process conditions.

A cost function for oxygen transfer including the equipment cost and running cost for nutrients and electricity was developed for both the stirred tank reactor and the airlift reactor. The cost function was used to identify an optimum range of reactor configuration and process conditions for industrial scale enzyme production fermentors. It was shown that compared to the stirred tank reactor 22% of the electricity cost might be reduced for the airlift reactor, and the capital cost might also be somewhat lower. However, since the electricity cost is a relatively minor part of the total cost, there might currently not be an obvious fiscal motive to change technology. The cost of nutrients is considerably larger than the electricity cost and was shown to be independent of the technology and process conditions. If the cost structure changes in the future and the airlift reactor is chosen as the alternative production technology, suggestions on the practical scale-up procedure are given. These include the use of Computational Fluid Dynamics (CFD) and scale-down models of the production environment.

Dansk resume

I det foreliggende erhvervsph.d.-projekt er forskellige produktionsteknologier for industrielle enzymer blevet undersøgt. Cellulaser og hemicellulaser er enzymer, der kan bruges til produktion af lignocellulose-baseret etanol, og enzymerne produceres ved hjælp af aerob gæring af den filamentøse svamp *Trichoderma reesei*. Normalt foregår produktionen af enzymerne i mekanisk omrørte tanke i størrelsesordenen 100 m^3. Formålet med projektet var at undersøge, om der findes andre gæringsteknologier, som bruger mindre energi og råvarer. Dermed kan prisen på enzymer mindskes og cellulose-baseret etanol kan blive konkurrencedygtig med fossile brændstoffer.

Ved hjælp af en model af gæringsprocessen blev forskellige alternative teknologier vurderet i forhold til deres energieffektivitet for iltoverførsel. En speciel reaktortype uden mekanisk omrøring men med opblanding ved hjælp af beluftning, kaldet airlift reaktor, blev identificeret som en potentiel teknologi med høj energieffektivitet.

To forskellige airlift reaktorkonfigurationer blev undersøgt i 550L skala; iltovergangen i systemet blev målt under 9 gæringer og blandingstider blev bestemt vha konduktivitetsmålinger. Modellen for enzymproduktion i airlift reaktoren blev forbedret, og det blev derefter brugt til at optimere designet af en airlift reaktor i industriel skala. Sammenlignet med en optimeret mekanisk omrørt reaktor kan der spares 22% af elektricitetsforbruget under gæringsprocessen. De resterende udgifter i enzymproduktionen er dog væsentligt større end elektricitetsudgifterne, fx udgør råmaterialer en langt større udgiftspost. Hvis det besluttes at ændre produktionsteknologi anbefales det at undersøge konsekvenserne af denne ændring vha mere detaljerede computerbaserede modeller af processen i stor skala samt yderligere forsøg med airlift reaktoren i forskellige skalaer.

Preface

This thesis is the main result of my industrial Ph.D studies, which were carried out in collaboration between Novozymes A/S and the Department of Chemical and Biochemical Engineering at the Technical University of Denmark. The project was carried out from April 2009 to March 2012 and was financed by Novozymes A/S and the Danish Agency for Science, Technology and Innovation.

The purpose of the project was to obtain new knowledge about the production of industrial enzymes. Specifically, Novozymes was interested in exploring ways to produce cellulases for bioethanol production as energy efficiently and thereby environmentally friendly as possible. One way to do that is to implement various modifications of the current production technology that each will improve the overall performance of the production process. Another approach is to entirely rethink the production setup with the hope to make a step change that could bring energy efficiency to a level that cannot be reached with minor improvements. This project was thought as an attempt to do the latter.

The topic of this project was determined by Novozymes. During my M.Sc. thesis we developed a model to describe enzyme production by *Aspergillus oryzae* and saw very promising results. It was hoped that a similar methodology could be used for the modeling of fermentations of *Trichoderma reesei* for cellulase production. I am very happy that Novozymes had the trust to invite me to pursue the opportunity to carry out a Ph.D. project and continue that work at the Fermentation Pilot Plant in Bagsvaerd.

I have had the pleasure of working with no less than 3 supervisors on this project. It has been very rewarding to work with people with quite different backgrounds and approaches to the project. This is meant in a very positive way, because it taught me the importance of always being able to argue for the decisions and choices that are made. It is not always easy to convince a skeptical supervisor to take a different approach than he would usually have done, but if you succeed, that should be proof that you have built a strong argument.

Morten S. Hansen and Stuart M. Stocks have been my Novozymes supervisors. I have received a lot of insight from working with Morten and Stuart who have many years of experience in this field and who face (and overcome) the difficulties of fermentation technology on a daily basis. Thank you for all your help. I would like to express my gratitude to my supervisor Associate Professor Krist Gernaey, whose advice and great interest in the project have been amazing. I have enjoyed the discussions we all have had during the project and we have made better collective decisions based

on the input from all of us.

During the past years, I have been working in the Novozymes Fermentation Pilot Plant. I would like to thank everyone in “Afdeling 235” and the supporting functions: Laboratory for Production strains, Engineering Support, Maintenance and Planning, the process operators, the quality and laboratory team, the Chemap team, and the chemist group. You have all made me feel like a part of the team and I am truly grateful for that. This project was carried out with strong encouragement from the management team of Fermentation Pilot Plant. I thank Henrik Steen Jørgensen, Morten Carlsen, and Karin Nikolajsen for their continued support throughout the project.

I have also received help from many other colleagues at Novozymes and the Center for Process Engineering and Technology at the Department of Chemical and Biochemical Engineering at DTU. I would like to thank everyone who has helped me by answering my questions and teaching me about your specific areas.

I enjoy learning and investigating new things, and I have been very fortunate to be able to do that all of my life. I owe many thanks to my friends and loving family for supporting my desire to pursue my goals and at the same time reminding me about the other important things in life.

Mads Orla Albæk, March 2012

Contents

Nomenclature

Roman Letters

a, b, c	constants of Eq. (2.9)
A_1, A_2	constants of Eq. (2.8)
A_d	area of the down comer zone (m^2)
A_r	area of the riser zone (m^2)
C	constant of Eq. (2.9)
C_∞	final conductivity output (mS/cm)
C_0	initial conductivity output (mS/cm)
C_1, C_2	constants
C_c	allowance for corrosion (0.0038 m)
C_i	conductivity output (mS/cm)
C_i'	normalized conductivity
C_p	cost factor of pressure vessels ($/kg)
C_{O2}	cost of oxygen transfer ($/kg O_2)
C_s	proportionality constant
CER	carbon dioxide evolution rate (moles $CO_2/m^3/h$)
COP	coefficient of performance (energy removed/energy consumed)
D	impeller diameter (m)

D_L	diffusivity (m^2/s)
DO	oxygen concentration in the liquid phase (moles O_2/m^3)
DO*	oxygen saturation concentration (moles O_2/m^3)
EE_{O2}	energy efficiency of oxygen transfer (kg O_2/kWh)
E_j	efficiency of joints (0.85)
g	gravitational constant (m/s^2)
H_{O2}	Henry's constant for oxygen for water at 25°C (793.4 bar.kg/moles O_2)
k	isentropic exponent
k_s	Metzner and Otto or (shear rate) constant
k_La	volumetric oxygen mass transfer coefficient (1/h)
K	consistency index ($Pa.s^n$)
m_o	maintenance coefficient for oxygen (moles O_2/g DW/h)
m_s	maintenance coefficient for substrate (g substrate/g DW/h)
M_{O2}	molar weight of oxygen (kg O_2/mol)
n	flow behavior index
n	number of impellers
N	impeller speed (rps)
OTR	oxygen transfer rate (moles O_2/m^3/h *or* kg O_2/m^3/h)
OUR	oxygen uptake rate (moles O_2/m^3/h)
p_{O_2}	partial pressure of oxygen in the gas phase (bar)
p_1	absolute compressor inlet pressure (bar)
p_2	absolute compressor discharge pressure (bar)
p_o	absolute pressure at vessel outlet (bar)

pCO_2	partial pressure of carbon dioxide (mbar)
P	agitation power input (kW)
P_a	motor power consumption for agitation (kW)
P_{air}	energy dissipation due to aeration (kW)
P_{broth}	energy dissipation to the broth from agitation and aeration (kW)
P_c	compressor power consumption (kW)
P_g/P_o	relative power draw upon aeration
P_i	maximum allowable internal pressure (kPa, gauge)
P_{loss}	power loss in bearings, seal and gearbox (kW)
Po	unaerated impeller power number
P_w	cooling system power consumption (kW)
Q	total heat generation of the fermentor (kW)
Q_1	volume rate of air flow at inlet conditions (m^3/h)
Q_M	molar rate of air flow conditions (mol/s)
Q_N	aeration rate (Nm^3/min)
R	universal gas constant (J/mol °K)
Re	Reynolds number
S	maximum allowable working stress (79300 kPa)
t	minimum wall thickness (m)
t_{gas}	gas residence time (s)
t_{mt}	mass transfer time (s)
$t_{mix,m}$	mixing time for a degree of mixing of m (s)
T	vessel diameter (m)

T_p	absolute process temperature (°K)
V	liquid volume in the vessel (m^3)
v_b	terminal bubble rise velocity (m/s)
v_g	superficial gas velocity at actual temperature and pressure (m/s)
$v_{l,r}$	riser zone superficial liquid velocity (m/s)
$v_{g,r}$	riser zone superficial gas velocity (m/s)
$v_{g,\,standard}$	superficial gas velocity at standard temperature and pressure (m/s)
W_v	weight of the vessel (kg)
X	biomass concentration (g DW/L)
Y_{SC}	observed yield coefficient of CO_2 per substrate (g CO_2/g substrate)
Y_{SO}	observed yield coefficient of O_2 per substrate (g O_2/g substrate)
Y_{SP}	observed yield coefficient of product per substrate (g product/g substrate)
Y_{SX}	observed yield coefficient of biomass per substrate (g DW/g substrate)
Z	ungassed height of liquid in the column (m)

Greek Letters

ΔH_f	heat development proportionality constant (kJ/mol O_2)
α, β	constants of Eq.(2.13)
$\dot{\gamma}$	shear rate (1/s)
$\dot{\gamma}_{eff}$	effective shear rate (1/s)
ε_g	gas holdup (%)
η_c	compressor efficiency
ρ	broth density (kg/m^3)
ρ_{SS316}	stainless steel 316 density (7840 kg/m^3)

ρ_F	carbon substrate feed density (kg/m^3)
γ_{xo}	stoichiometric coefficient (moles O_2/g DW)
γ_{xs}	stoichiometric coefficient (g substrate/g DW)
σ	surface tension (N/m)
μ	growth rate (1/h)
μ	viscosity (Pa.s)
μ_{app}	apparent viscosity (Pa.s)
μ_w	viscosity of water (Pa.s)
τ	shear stress (Pa)
τ_y	yield stress (Pa)

Abbreviations

ALR	airlift reactor
AR	aspect ratio
B2	Hayward Tyler B2 (formerly titled APV-B2)
CBH	cellobiohydrolase
CFD	computational fluid dynamics
CMC	carboxy methyl cellulose
DCM	dry cell matter
DOT	dissolved oxygen tension
EG	endoglucanase
GH	glycosyl hydrolase
NL	normal liter
RDT	Rushton disc turbine

RQ	respiratory quotient, CER/OUR
SRC	standardized regression coefficient
STR	stirred tank reactor

Chapter 1

Introduction

The first section of this chapter contains the main contents of the project description approved by the Danish Agency for Science, Technology and Innovation. The structure of this thesis follows that of the project description and should be apparent from this first section. In the second section an introduction to modern cellulases and their applications is provided.

1.1 Project description

1.1.1 State of the art

Enzymes are proteins that catalyze chemical reactions inside the cells of living organisms. They can also function outside the biological systems, have high specificity, and involve fast reaction rates. Furthermore enzymes can be used under mild conditions and therefore they are used in many industrial processes to reduce the consumption of chemicals and energy, and to reduce the production of waste (Olsen, 2008). The increasing demand for industrial enzymes is largely driven by decreasing supply of resources such as energy and raw materials. The demand for energy and biomass is ever-increasing and the future will undoubtedly call for a better utilization and higher efficiency of the use of both. There is hope that the global society can transform from dependency of fossil fuels and petrochemical materials towards a bio-based and sustainable energy economy (Bevan and Franssen, 2006). A better utilization of the biomass resources of the Earth requires the use of effective and economical enzymes for the conversion of plant material to valuable sugars that can be further converted to fuels, materials and commodity chemicals (Davenport, 2008).

Within industrial enzymes, Denmark has had a unique position internationally. Until the takeover of Danisco by Dupont in 2011, Danish companies were responsible for 70% of the global enzyme production, and world leading research is still ongoing in Denmark (Ministry of Foreign Affairs of Denmark, 2006). The world market for industrial enzymes is increasing and had an estimated size of ~$5 billion in 2007 (Novozymes estimate (Novozymes A/S, 2007). In the production of industrial enzymes, relatively large amounts of energy, water, and raw materials are used. Novozymes annually consumes 856,000 GJ for primary activities, corresponding to the private electricity consumption of 240,000 Danes (Novozymes A/S, 2007). A reduction in the energy consumption of enzyme production would therefore have large effects on the CO_2 emission and environmental impact. An even greater impact would be the breakthrough of the production of

lignocellulosic ethanol. If enzyme prices can be reduced further, it seems likely that lignocellulosic ethanol economically can compete with fossil fuels in a near future. Since lignocellulosic ethanol is based on a renewable resource it has an obvious environmental advantage over oil derived fuels.

1.1.2 Project content

Industrial enzymes are currently primarily produced in stirred tank reactors, which is the traditional technology for many biotechnological processes. This technology platform is well known, since it has been the preferred technology for this type of operations for approximately 50 years. The enzyme producing microorganisms need substrates for growth and enzyme formation e.g. oxygen, sugars, and other nutrients. In the large production vessels, the greatest challenge is often to ensure proper oxygen supply for the microorganisms. The fermentation broths may become very viscous, which hinders the oxygen transfer. Mechanical stirring with high intensity is one way to overcome this challenge, which is among the reasons for the relatively high energy consumption of the process. Supply and compression of sterile air for the microorganisms also is highly energy consuming. Continuously, scientific studies are initiated in order to improve the current technology platform by minor adjustments such as changes to the feeding strategy, stirrer speed etc. However, a number of alternative technologies to the stirred tank reactor exist as well, which potentially could replace it.

The purpose of this project is "*to investigate the efficiency of alternative enzyme production technologies and objectively evaluate these in a comparison with the existing production platform*". The underlying hypothesis of the research project is, that alternative technologies exist which may be employed in industrial enzyme production such that the energy and/or resource usage is lowered. To evaluate alternative technologies objectively with the traditional production platform, similar dimensions are needed. For research concerning reactors, geometric similarity is a very important parameter, since processes cannot be scaled up by utilization of a volumetric factor. The Novozymes pilot plant is a good setting for the project, as the scales of operation available here, typically are not present in academic environments.

Optimization of the current production technology contributes to minor improvements of enzyme production in the stirred tank reactor; however no ground breaking changes have been introduced to the technology since its origin in the 1950's. In the literature a vast number of alternative technologies are described, which in various ways challenge the traditional production technology. Some are very well known and have been applied for many other biotechnological processes for years while some have just been developed and never been used to perform fungal fermentations. A few examples are given here:

- Rotating jet heads as a means of providing mixing and gas dispersion replacing mechanical stirring (Hua et al., 2007; Nordkvist et al., 2003; Nordkvist et al., 2008)
- Static mixers applied for gas liquid oxygen transfer (Heyouni et al., 2002)

- Different technologies for solid substrate fermentations (Mitchell et al., 2006)
- Bubble columns in various designs (Atkinson and Mavituna, 1991)

Previously, studies have shown that compared to the traditional production technology, alternative technologies have both advantages and drawbacks (Grajek, 1987; Sukumaran et al., 2005). A major challenge is however to perform a reliable and objective comparison of the different available technologies.

One important performance parameter for comparison is the amount of product formation per unit of energy consumed (kg product/kWh), which relates to the energy efficiency of the process or technology. If optimization of this parameter however leads to decreased product concentration, an important drawback is that a larger production volume is required to maintain the amount of product produced. Furthermore parameters such as water- and substrate consumption and the difficulty of product recovery – the cost of product recovery usually increases at lower product concentrations – also play an important role in the comparison of different technologies.

As indicated by the above list of examples, a long list of possible technologies for enzyme fermentations is available through the open literature. Many of the technologies have however only been tested at laboratory or prototype level. A realistic analysis and evaluation of these technologies require experimental data from larger scale or the use of modeling tools that can simulate the effect of various process conditions and parameters.

This research project is very much in line with the recommendation from the Danish AgriFish Agency which in its rapport concludes that "*the upscaling of promising research results from laboratory to pilot-scale studies*" is among the cross disciplinary areas that need research and development "*if Denmark is to retain its competitive edge and become internationally leading in the non-food and feed areas*" (Danish AgriFish Agency (former Direktoratet for FødevareErhverv), 2006)

1.1.3 Scientific novelty

Bioreactor characterization and comparison is not a new concept, and each time a new technology is suggested it should be compared with existing alternatives. This project aims at collecting relevant data from the open literature and by the use of modeling and simulation tools to make a technology comparison for a specific biotechnological process: enzyme production by *Trichoderma reesei*. The cellulases and hemi-cellulases secreted by *T. reesei* are important enzymes in the processing of lignocellulosic biomass to industrial products such as sugars and ultimately bioethanol. A significant strength of this project is the access to a strain with properties very similar to the industrial strains currently used for the production of lignocellulosic enzymes. The process studied will thus closely resemble the actual enzyme production in industrial scale and have the same limiting rates and other process conditions. The development of modeling tools has been strongly

aided by the advances of computer calculating power. The application of a process model for a number of alternative technologies can now be done quite quickly even though it involves relatively heavy computational operations.

1.1.4 Elaboration of the project purpose

The specific purpose of this project is to investigate and compare the efficiency of enzyme production technologies. Enzyme recovery and enzyme formulation or enzyme granulation are operations strongly connected to the fermentation process for some processes, but in various business models for lignocellulosic bioethanol the recovery processes (if any) are very different. For this reason and in order to confine the project and emphasize the focus of fermentation technology comparison it was decided early on that this thesis should be concerned only with the fermentation process.

For commercial reasons this thesis does not contain details about the Novozymes production setup including variable costs, energy consumption and cost, raw material prices, absolute figures on productivity, or product volumes. It is not the intention of this project to minimize the full manufacturing cost of the product, but to explore different technologies for the fermentation process. It is the intension that the approach described in this thesis will be an example of how technology comparison can be done and that it can function as inspiration for others in the future.

1.1.5 Thesis structure

Modeling of the reference process (Chapter 2)

The first part of the project involved the development of a process model of the reference process in the stirred tank reactor. The model is constructed in such a way, that the central part of the model – the oxygen mass transfer model – is easily replaced in the later model applications. The reference process is a fed-batch fermentation of a strain of *T. reesei* with high similarity to the production strains.

Determination of key parameters of the reference process (Chapter 3)

A central problem of the project is to determine the key parameters that will be used for the evaluation of the different technologies. The key parameters are influenced by the process conditions such as the aeration rate, agitation intensity, pressure, concentration of substrate, viscosity etc, and should cover the contribution from these. A number of key parameters are calculated and their abilities to be used for the technology comparison are discussed.

Identification of alternative production technologies (Chapter 4)

A large number of alternative reactor technologies exist. Some of these have previously been

explored by Novozymes, but there is a constant development in the field and new possibilities of combinations also appear. This activity involves a thorough literature search and the development of a reasoned list of potentially interesting technologies based on the previously obtained knowledge of the reference process, the process conditions, and their interactions. If it is not possible to evaluate the particular potential of certain technologies based on the available literature, the information should be obtained by others means (e.g. by contacting the experts and manufacturers in the field).

Research within at least one alternative technology (Chapter 5)

Depending of the results of the identification of alternative technologies, a detailed reactor and process design is to be carried out for at least one alternative technology. This activity involves experimental work with the primary objective of evaluating the potential of this technology as the possible platform for future enzyme production. A central part of the evaluation will be considerations on the possibilities of scaling up of the technology.

Conclusion on at least one alternative technology (Chapter 6)

Whether this last phase of the project can be reached or not depends on the quality of the collected information of the previous activities. The intention is to be able to conclude, whether the proposed alternative technology, in objective comparison with the reference technology, is competitive.

Chapter 7 contains the overall conclusions of the project and provides guidelines for further work.

1.2 Introduction to cellulases and their applications

1.2.1 Structure of cellulosic biomass

Lignocellulose is the structural cell wall component which provides plants their rigidity. The three major components of lignocellulose are cellulose (35-50 wt. % w), hemicellulose (20-35 wt. %), and lignin (5-30 wt. %) (Lynd et al., 2002). The remaining components include small amounts of ash, proteins, and pectin. The composition and amounts of residuals vary depending on the source of biomass (Dashtban et al., 2009).

Cellulose is a linear polymer of β-1,4-linked glucose and is the most abundant organic molecule on the Earth with an annual production of about $7.2 \cdot 10^{10}$ tons (Kubicek et al., 2009). Cellulose is synthesized in nature as individual molecules (linear chains of glycosyl residues) which undergo self assembly at the site of biosynthesis (Lynd et al., 2002). Adjacent chains of cellulose are coupled by hydrogen bonds, hydrophobic interactions, and van der Waal's forces resulting in a parallel alignment of crystalline structures known as fibrils (Dashtban et al., 2009). Cellulose fibers in nature however are not purely crystalline. Regions with kinks, twists, and irregularities also exist and are known as amorphous regions.

The cellulose fibrils are surrounded by hemicelluloses, which are heterogeneous polymers of pentoses, hexoses, and sugar acids (Dashtban et al., 2009). The composition of hemicelluloses in nature varies considerably depending on the plant source, but consists mainly of β-1,4-linked xylans and β-mannans (Kubicek et al., 2009). Hemicellulose often has side chain substituents such as arabinose, galactose, and acetic or glucuronic acid (Mach and Zeilinger, 2003). It is estimated that $6 \cdot 10^{10}$ tons of hemicelluloses are produced annually (Kubicek et al., 2009).

Lignin is the third heterogeneous polymer of lignocellulosic residues and generally contains aromatic alcohols including coniferyl alcohol, sinapyl and *p*-coumaryl (Dashtban et al., 2009). It is the most recalcitrant lignocellulosic material to degrade as it forms linkages to both hemicelluloses and cellulose and thereby efficiently acts as a barrier to any solutions or enzymes (Dashtban et al., 2009).

1.2.2 Degradation of cellulosic biomass by Trichoderma reesei

Trichoderma reesei (teleomorph *Hypocrea jecorina*) is a saprobic ascomycete fungus capable of efficient degradation of plant cell wall polysaccharides (Martinez et al., 2008). The discovery of the strain *Trichoderma viride* QM6a by the US Army during World War II led to extensive research towards the industrial application of its exceptionally efficient enzymes (Schuster and Schmoll, 2010). The organism was identified as the cause of a massive infection of cotton-based army material, and later on this species was renamed *T. reesei* in honor of Elwin T. Reese and is now the most important cellulase producer worldwide (Simmons, 1977).

T. reesei secretes its lignocellulolytic enzymes into its surroundings as the enzymes should act on a macromolecular insoluble substrate. This strategy is known as a noncomplexed lignocellolytic system in contrast to complexed cellulase systems (cellulosomes). Cellulosomes are typically found in anaerobic systems where bacteria growing on cellulosic material form a stable enzyme complex firmly bound to the cell wall but flexible enough to also bind microcrystalline cellulose (Lynd et al., 2002).

The genome of the original isolate QM6a was recently sequenced (Martinez et al., 2008). The genome size was 33.9 Mb and 9,129 genes were identified or predicted. The enzymes involved in degradation of cellulose and hemicellulose work synergistically to allow hydrolysis to smaller oligosaccharides and finally to the corresponding monomers (Mach and Zeilinger, 2003). The cellulolytic enzyme system consists of three types of activities: cellobiohydrolase (CBH) activity, endoglucanase (EG) activity, and β-glucosidase activity (Persson et al., 1991). *T. reesei* encodes at least two CBH enzymes, Cel7A and Cel6A, which are exocellulases hydrolyzing cellulose chain ends. Cel7A and Cel6A act on the cellulose chains from the reducing and non-reducing end, respectively, producing cellobiose as the main product (Dashtban et al., 2009). EG enzymes initiate cellulose breakdown by internally cleaving cellulose chains at amorphous cellulose regions, thereby providing new chain ends accessible for the action of CBH enzymes (Lynd et al., 2002). At least

five EG enzymes (Cel7B, Cel5A, Cel12A, Cel61A, and Cel45A) have been identified for *T. reesei* (Zhang and Lynd, 2004). At least two β-glucosidases are produced by *T. reesei* to facilitate the hydrolysis of cellodextrins (oligosaccharides of glucose) and cellobiose to glucose (Lynd et al., 2002).

T. reesei was found to have 200 genes from the glycosyl hydrolase (GH) family, 103 glycosyltranferases, 16 carbohydrate esterases, and 3 polysaccharide lyases, and 16 genes encoding for hemicellulases (Martinez et al., 2008). As the cellulolytic machinery of *T. reesei* is considered the paradigm for enzymatic breakdown of cellulose and hemicelluloses, it was unexpected that compared to other filamentous fungi *T. reesei* has a considerably smaller set of genes encoding cellulases and hemicellulases (Martinez et al., 2008). However, the efficiency of a cellulase system is not determined by the number of enzymes present. Instead, they act in a coordinated manner to efficiently hydrolyze cellulose (Lynd et al., 2002). Competitive product inhibition of the hydrolysis steps is a well known phenomenon (Dashtban et al., 2009), e.g. an efficient β-glucosidase to prevent the accumulation of cellobiose is needed in order for CBH and GH to be effective since cellobiose inhibits the latter enzymes. Actually, the need for five endoglucanases in the *T. reesei* cellulase system is not fully understood (Lynd et al., 2002) and there still seems to be a lack of ability to rationalize the diversity observed in the composition of cellulolytic enzymes, which underscores the need for further improvement of the understanding of plant cell wall degradation (Martinez et al., 2008).

Expression of extracellular hemicellulases and cellulases is a hugely resource demanding activity for the cell, and tight regulation of the process is needed. Most cellulases are formed adaptively which means that their transcripts are not formed during growth on monosaccharides and full expression of the enzymes requires the presence of an inducer (Kubicek et al., 2009). The genome sequence of *T. reesei* has raised the possibility to use sophisticated gene manipulation methods to further over-production of cellulases by exploitation of the insight into the regulation pathways (Kubicek et al., 2009). However detailed discussion of this matter is beyond the scope of this thesis.

1.2.3 *Industrial applications of cellulases*

Cellulases and hemicellulases have important applications in a number of industries. Industrial strains of *T. reesei* are currently used for the production of these enzymes in relatively large amounts. Early strain improvement with *T.reesei* included classical mutagenesis from treatment with UV light and nitrosoguanine in combination with selection procedures, which resulted in high-yielding strains such as the well known strain *T. reesei* Rut C30 that is also resistant to carbon catabolite repression (Montenecourt and Eveleigh, 1977a). The industrial application of *T. reesei* has led to a well developed toolkit for genetic manipulation of the species (Schuster and Schmoll, 2010). Among the tools currently applied are: transformation, sequential deletions, knock out strategies for functional analysis of genes, and expression of antisense constructs for knockdown (Schuster and Schmoll, 2010).

T. reesei has a long history of safe use in industrial use and the current applications of hemicellulases and cellulases include food (xylanases improve shelf life and quality of bakery products, clarification of fruit juices), animal feed (hemicelluses improve the digestibility of the feed), textile industry (bio-polishing of cotton clothes) and paper and pulp industry (bleaching of cellulose pulp, wood processing) (Nevalainen et al., 1994).

T. reesei represents a principal target cellulase host in the quest to, at least partially, replace gasoline with cellulose-derived ethanol (Ward, 2011). Fuel ethanol production is currently an economically viable industry with a production in the USA of more than 10 billions of gallons produced in 2010 (Renewable Fuels Association, 2011). Lignocellulosic biomass (including agricultural by-products, forestry residues, and woody crops) has a much larger potential as a renewable energy source in the future (Harris et al., 2010; National Academy of Sciences, 2009; Perlack et al., 2005). It is (optimistically) estimated that one billion tons per year of lignocellulosic biomass could be sustainably harvested in the form of crop and forestry residues in the US, which could replace as much as 30% of the total US gasoline consumption (Merino and Cherry, 2007; Perlack et al., 2005). However, a number of challenges have to be overcome before the dream of conversion of cellulosic residues into fuels and chemicals at industrial scale becomes reality.

1.2.4 Challenges of lignocellulosic ethanol

In Figure 1.1 a schematic overview over the process of converting lignocellulosic biomass to ethanol is given. Although a large number of possible variations to the process are suggested and tested, the process can be summarized in five unit operations: (1) desizing, (2), thermochemical pretreatment, (3) enzymatic hydrolysis, (4) ethanol fermentation, and (5) ethanol recovery (Merino and Cherry, 2007).

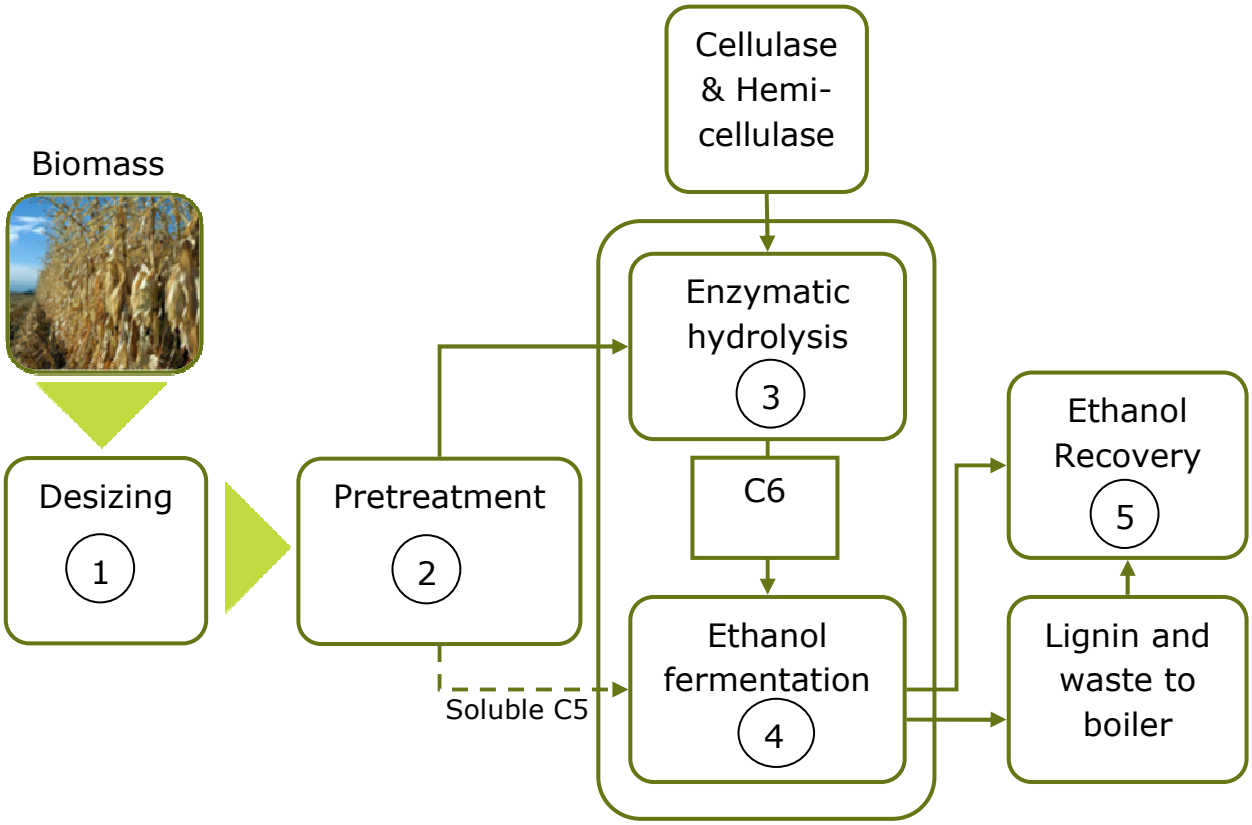

Figure 1.1. Schematic overview of the biomass to ethanol process. *Step 1*: The biomass is milled or chopped to increase the surface area and the uniformity. *Step 2*: Some form of thermochemical pretreatment (exposure to high pressure, temperature, and/or extremes of pH) destroy the plant cell wall and expose the sugars to a liquid phase. *Step 3*: Enzymatic hydrolysis using a complex mix of glycosyl hydrolases to convert sugar polymers to monomeric sugars. *Step 4*: Fermentation of monomeric sugars to ethanol by a fermentation organism. *Step 5*: Ethanol recovery from the fermentation using distillation or another separation technology. C6 refers to glucose derived from cellulose hydrolysis, while C5 refers to pentose sugers (mainly xylose) derived from hemicelluloses. Adapted from Merino and Cherry (2007).

The conversion of lignocellulose to ethanol must become less expensive in both operating cost and capital investment, before the process will have the potential to replace the current liquid fuels (Merino and Cherry, 2007). For one, investment costs are higher for lignocellulosic ethanol plants compared to starch based production facilities due to their larger size to accommodate more dilute sugar streams, more unit operations, and in some cases the need for acid-resistant construction materials (Merino and Cherry, 2007). Furthermore, the operating costs may currently be higher due to higher enzyme dosage required and higher water consumption that might be required to remove compounds that interfere with the hydrolysis and fermentation process (Merino and Cherry, 2007).

Considerable research has been carried out in order to reduce the cost of enzymes used to hydrolyze the pretreated biomass to monomeric glucose. This work includes the quest for better understanding of the synergy between enzymes in the cellulase complex, the use of *T. reesei* transformants

expressing non-native enzymes such as β-glucosidases and members of the GH61 family, use of synergistic hemicellulases, and the search for the optimal hydrolysis conditions (Harris et al., 2010; Merino and Cherry, 2007).

The US National Renewable Energy Laboratory is very active in the promotion of the production of ethanol and other liquid fuels from lignocellulosic biomass. In a recent publication in which a detailed process simulation including material and energy balances and capital and operating costs was published, the minimum ethanol selling price for a plant using dilute-acid pretreatment and enzymatic hydrolysis of corn stover was determined to be $2.15/gal (Humbird et al., 2011). In comparison, market studies showed that the production cost of corn ethanol and sugarcane ethanol were $1.53/gal and $1.13/gal, respectively (Humbird et al., 2011). Of the minimum ethanol selling price $2.15/gal, enzymes in that particular case accounted for $0.34/gal corresponding to 16% of the total costs (Humbird et al., 2011). A reduction of the enzyme cost could therefore significantly improve the financial feasibility of the lignocellulosic biomass to ethanol process.

The aim of this work is to investigate if the production costs of the enzymes can be brought down by using an alternative enzyme fermentation technology. The enzymes are considered a (hemi)-cellulase complex, since the composition of the hemicellulase and cellulase mixture produced in the *T. reesei* strains developed at Novozymes is not stated for proprietary reasons. It is expected that the close future will lead to further improvements in the industrial strains and enzyme complexes, e.g. by expression of ortholog enzymes from thermophilic fungi in exchange for their mesophile counterparts (Berka et al., 2011). Therefore the approach of this thesis has been generic with the intention that the results should apply also to future industrial strains of *T. reesei* even though they most likely will be even more efficient over-expressors of an even more efficient complex of cellulases and hemicellulases.

Chapter 2

Modeling fungal fermentations for enzyme production in stirred tank reactors

---

The content of this chapter is based on following two articles. Figures from the articles are reprinted with permission from John Wiley and Sons, Inc.

Modeling Enzyme Production With *Aspergillus oryzae* in Pilot Scale Vessels With Different Agitation, Aeration, and Agitator Types

Albaek, MO; Gernaey, KV; Hansen, MS; Stocks, SM

Biotechnology and Bioengineering 108: 1828-1840 (2011)

Evaluation of the Energy Efficiency of Enzyme Fermentation by Mechanistic Modeling

Albaek, MO; Gernaey, KV; Hansen, MS; Stocks, SM

Biotechnology and Bioengineering 109: 950-961 (2012)

2.1 Introduction

The investigations of this thesis are focused on fermentations of the mesophilic soft-rot ascomycete fungus *Trichoderma reesei* (teleomorph *Hypocrea jecorina*). *T. reesei* utilizes a remarkably efficacious protein secretion machinery and represents a paradigm for industrial production of cellulases and hemicellulases for hydrolysis of biomass polysaccharides (Martinez et al., 2008).

Most industrial enzymes are produced by submerged fermentation, a process involving cultivation of the production strain in closed fermentation vessels that contain the nutrient medium (Berka and Cherry, 2006). The sparged, mechanically agitated, vertical, cylindrical tank (commonly known as

the stirred tank reactor (STR)) is the traditional design of the fermentation vessel, which dates from the 1940's (Bailey, 1980). Today, this fermentation technology is still preferred (Dodge, 2009).

The majority of large-scale industrial fungal fermentations involve fed-batch mode cultivations with a high concentration of active biomass (Papagianni, 2004). During fermentation, growing hyphal elements tend to entangle and therefore many fungal fermentations suffer from the same problem – high viscosity of the fermentation broth that often leads to mass transfer limitations (Li et al., 2000; Mcneil and Harvey, 1993; Morris et al., 1973; Olsvik and Kristiansen, 1994). For aerobic fermentations the transfer of sufficient oxygen to active cells is critically important. By manipulation of the substrate feed rate it can be guaranteed that the carbon source becomes the rate limiting substrate and the dissolved oxygen tension (DOT) is maintained at the desired level. This mode of operation is reliant on the available oxygen mass transfer in the fermentor. The gas-liquid mass transfer in the fermentor is influenced by the operational conditions, the physicochemical properties of the culture, the geometrical parameters of the system, and the presence of oxygen consuming cells.

A number of models have been proposed in order to describe filamentous growth and growth related production (see for example (Agger et al., 1998; Nielsen, 1993)). Some authors relate cytological events within the hyphae to mycelial growth kinetics (i.e. hyphal extension and branch initiation), but each model seems to be very strain specific and highly dependent on the experimental setup (Pazouki and Panda, 2000). Yang and Allen (1999) have described a model to predict mycelial morphology and mycelial growth in the development of an alternative scale-up strategy to constant energy dissipation, mass transfer coefficient, or impeller tip speed. Their work showed that simulation of mycelial processes can be a valuable tool for developing process understanding and for scale-up of such processes (Yang and Allen, 1999).

The present work represents a relatively simple but more complete mathematical process model describing microbial growth and enzyme production in submerged viscous aerobic fed-batch fermentations. The model has been shown to describe fermentations of both *Aspergillus oryzae* and *T. reesei* well. For each production organism, a number of biological parameters are measured and used in the model as described in this chapter. The model simulates the process performance at different rates of agitation and aeration as well as different headspace pressures; three of the key parameters influencing the oxygen mass transfer. With focus on oxygen mass transfer, it is shown that it is possible to model enzyme production even under very different process conditions.

Here, three mass transfer correlations are tested and compared in their ability to describe the mass transfer characteristics of 550 L fed-batch fermentations with viscous fermentation broth. The data set consists of k_La measurements from 9 fermentations carried out under different process conditions.

An analysis of the model uncertainty is included as well. Assuming a certain distribution of the

model parameter values, Monte Carlo simulations – a widely recognized technique – are performed to explore how the parameter uncertainty influences the simulation results (Heinzle et al., 2006). Also, a sensitivity analysis is conducted which results in a significance ranking of the model parameters. This will help to direct the future experimental work towards reducing the uncertainty of the most influential parts of the model.

Finally, the total energy consumption of the fermentation vessel including agitation, aeration and cooling is considered.

2.2 The model

In this model the progress of the fermentation is simulated by considering the following: (1) a representation of the main reaction equation of the fermentation, (2) a mass transfer prediction, (3) a viscosity prediction, and (4) a mathematical representation of the above components that can be used for simulating the process. In the following each of these four components will be described in more detail.

The reaction equation

It is assumed that the enzyme production process can be described with the following simple reaction equation

$$\text{Substrate} + Y_{SO} \cdot O_2 \rightarrow Y_{SX} \cdot \text{biomass} + Y_{SP} \cdot \text{product} + Y_{SC} \cdot CO_2 + H_2O \tag{2.1}$$

where Y_{SO}, Y_{SX}, Y_{SP}, and Y_{SC} are the observed yield coefficients of substrate and products per unit of carbon source substrate consumed. Since the reaction is carried out in aqueous solution, the relatively small amount of water produced is neglected. A certain amount of nitrogen is needed for biomass and product formation, but the ammonium added in order to adjust and maintain the desired pH is assumed to deliver enough nitrogen. For simplicity this relatively small amount of nitrogen is not included in the reaction equation.

A mass transfer prediction

In a DOT controlled fed-batch fermentation the oxygen mass transfer rate is rate limiting. The oxygen transfer rate per unit of reactor volume (OTR) is often described by

$$\text{OTR} = k_L a \left(\text{DO}^* - \text{DO} \right) \tag{2.2}$$

In the literature, a number of approaches towards estimation of $k_L a$ have been suggested for the STR with non-Newtonian fluids. The flow behavior of these liquids is often described in terms of the Ostwald-de Waele relationship (Nienow, 1990)

$$\mu = K\dot{\gamma}^{n-1} \tag{2.3}$$

The shear rate in the STR is locally non-uniform. Close to the impeller blades the shear rates are high. The shear rate decreases with increasing distance from the stirrer and stagnant zones with zero shear rates might even exist (Herbst et al., 1992). In Table 2.1 three correlations are listed to obtain the effective mean shear rate, which is then used to calculate the apparent viscosity from Eq. (2.3). Graphical representations of the three correlations and the apparent viscosities calculated on data for a fed-batch enzyme production of *T. reesei* are shown in Figure 2.1A and Figure 2.1B, respectively.

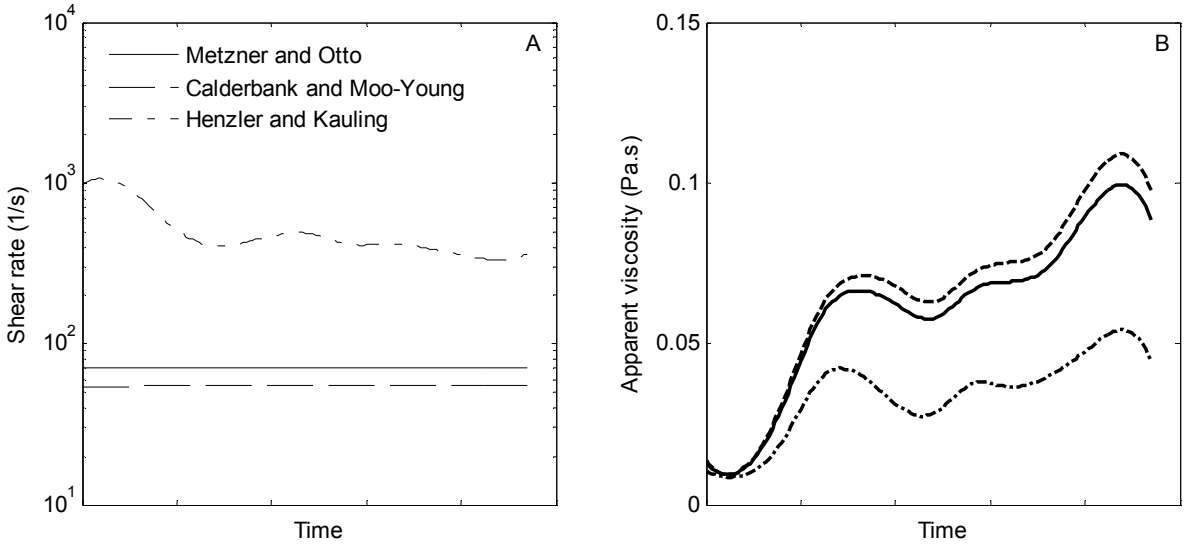

Figure 2.1. A: Comparison of effective mean shear rates estimated with Eq. (2.4) – (2.6) for data from a fed-batch fermentation of *T. reesei* (550L fermentor, B2 impellers, N = 6.33 1/s, 0.58<n<0.92). **B:** Apparent viscosities calculated from shear rates from Figure 2.1A. See Herbst et al. (1992) for similar graphs for xanthan production. Note that time axis labels are not shown on purpose for proprietary reasons. Adapted from (Albaek et al., 2012).

The relationship of Metzner and Otto (1957) (Eq. (2.4)) was modified with a function of n by Calderbank and Moo-Young (1959) (Eq. (2.5)). In the above example, 0.58<n<0.92 which means that the shear rate predicted by Eq. (2.5) is ~20% lower than the one obtained with Eq. (2.4). The resulting difference in apparent viscosity, Figure 2.1B, is limited. Eq. (2.6) predicts a different trend since increasing viscosity is assumed to decrease the effective shear rate in this correlation (Herbst et al., 1992). Intuitively, this might be right. The corresponding development in apparent viscosity is different than predicted by the other relationships as the shear rate is roughly one order of magnitude higher.

In the literature a number of correlations for the volumetric mass transfer coefficient, $k_L a$, have been proposed. Three such mass transfer correlations for non-Newtonian media are presented in Table 2.1. In each correlation a different method for shear rate estimation is employed.

Table 2.1. Top: Estimations of the effective shear rate in stirred tank reactors. Bottom: Selected mass transfer correlations for viscous liquids. Adapted from Herbst et al. (1992).

Reference		Equation	Derivation
Metzner and Otto (1957)[a]	$\dot{\gamma}_{\text{eff}} = k_s N$	(2.4)	Empirical
Calderbank and Moo-Young (1959)[a]	$\dot{\gamma}_{\text{eff}} = k_s N \left(\frac{4n}{3n+1}\right)^{n/(1-n)}$	(2.5)	Semi-empirical
Henzler and Kauling (1985)	$\dot{\gamma}_{\text{eff}} = \left(\frac{P_{\text{broth}}}{V}\frac{1}{\mu_{\text{app}}}\right)^{0.5}$	(2.6)	Dimensional anal.

Reference			Derivation	Shear rate
Kawase and Moo-Young (1988)[b]	$k_L a = 2430 D_L^{0.5} \frac{\rho^{\frac{3}{5}} \left(\frac{P_{\text{broth}}}{\rho V}\right)^{\frac{9+4n}{[10(1+n)]}}}{\left(\frac{K}{\rho}\right)^{\frac{1}{2(1+n)}} \sigma^{\frac{3}{5}}} \times \left(\frac{v_g}{v_b}\right)^{0.5} \left(\frac{\mu_{\text{app}}}{\mu_w}\right)^{-0.25}$	(2.7)	Semi-theoretical	CM (Eq. (2.5))
Henzler (1982)[b]	$\frac{k_L a}{v_g}\left(\frac{{\mu_{\text{app}}}^2}{g}\right)^{1/3} = A_1 \left(\frac{P_{\text{broth}}}{V}\frac{1}{v_g \rho g}\right)^{A_2}$	(2.8)	Various lit. data	HK (Eq. (2.6))
Empirical	$k_L a = C \left(\frac{P_{\text{broth}}}{V}\right)^a v_g^b {\mu_{\text{app}}}^c$	(2.9)	Various lit. data	MO (Eq. (2.4))

[a]In this work a value of $k_s = 11$ is used

[b]The following properties are assumed: ρ = 1050 kg/m^3, σ = 0.047 N/m, $D_L = 2.5 \cdot 10^{-9}$ m^2/s, $v_b = 0.265$ m/s

The theoretical expression suggested in Eq. (2.7) contains only one factor that should be fitted to data for specific surface area and has been determined using data for water (Kawase and Moo-Young, 1988). The correlation proposed by Henzler (1982) (Eq. (2.8)) has been shown to successfully describe many literature data, although with the limitation that the system specific constant A_1 and exponent A_2 are required (Herbst et al., 1992). A commonly used empirical correlation is based on power input per unit volume, superficial gas velocity, and apparent viscosity (Eq. (2.9)). The constant C is said to depend on the geometrical parameters of the vessel and the experimental method used, while it is sure that the exponent values a, b, and c show a wide variation range in different correlations proposed by different authors (Garcia-Ochoa and Gomez, 2009). It is claimed, that there is poor correspondence among most correlations proposed in the literature (Kawase and Moo-Young, 1988). The correlation is however seen to describe the experimental data within ±30% (e.g., Cooke et al., 1988; Zhu et al., 2001). Within this precision, which is realistic for pilot scale and industrial scale vessels, there are multiple examples that k_La is independent of agitator geometry (Albaek et al., 2011; Cooke et al., 1988). The correlation of Kawase and Moo-Young (1988) (Eq. (2.7)) is semi-theoretical and thus no fitting to the data set is performed, while the two empirical correlations are fitted to the data set by least squares regression.

A viscosity prediction

The fermentation broth is known to have power law-like behavior. The power law consistency, K, and flow behavior indices, n, are here correlated in the following way

$$K = C_1 X^{\alpha} \tag{2.10}$$

$$n = C_2 X^{\beta} \tag{2.11}$$

where C_1, C_2, α, and β, are constants estimated by regression. The effective shear rate of the fermentation vessel, $\dot{\gamma}_{\text{eff}}$, is determined by the approach of Metzner and Otto

$$\dot{\gamma}_{\text{eff}} = k_s N \tag{2.12}$$

where k_s is the Metzner and Otto (or shear rate) constant (Nienow, 1996) and N is the rate of agitation. The apparent viscosity, μ_{app}, of the broth is calculated using $k_s = 11$ for both agitator types

$$\mu_{\text{app}} = C_1 X^{\alpha} \left(k_s N \right)^{C_2 X^{\beta} - 1} \tag{2.13}$$

A mathematical representation of the model

It was decided to model the fed-batch fermentation by applying a pseudo steady state assumption; a complex differential equation can then be converted to a simpler algebraic equation. The model consists of balance equations for the total liquid phase volume and the concentrations of biomass,

substrate, product, and dissolved oxygen, respectively, given below.

Volume, V (L/h)

$$\frac{dV}{dt} = \frac{\rho_F F - F_{evap} + M_{O_2} - M_{CO_2}}{\rho} \tag{2.14}$$

Biomass, X (g DW/L/h)

$$\frac{dX}{dt} = \mu X - \frac{X\left(\rho_F F - F_{evap} + M_{O_2} - M_{CO_2}\right)}{V\rho} \tag{2.15}$$

Substrate, S (g substrate/L/h)

$$\frac{dS}{dt} = \frac{c_F F}{V} - \left(\mu\gamma_{xs}^{true} + m_s\right)X - \frac{S\left(\rho_F F - F_{evap} + M_{O_2} - M_{CO_2}\right)}{V\rho} \tag{2.16}$$

Product, P (g product/L/h)

$$\frac{dP}{dt} = \mu Y_{SP} Y_{XS} X - \frac{P\left(\rho_F F - F_{evap} + M_{O_2} - M_{CO_2}\right)}{V\rho} \tag{2.17}$$

Dissolved oxygen, DO (moles O_2/L/h)

$$\frac{d\mathrm{DO}}{dt} = k_L a \frac{\left(\mathrm{DO}_{in}^{*} - \mathrm{DO}\right) - \left(\mathrm{DO}_{out}^{*} - \mathrm{DO}\right)}{\ln\left(\frac{\mathrm{DO}_{in}^{*} - \mathrm{DO}}{\mathrm{DO}_{out}^{*} - \mathrm{DO}}\right)} - \left(\mu\gamma_{xo}^{true} + m_o\right)X - \frac{\mathrm{DO}\left(\rho_F F - F_{evap} + M_{O_2} - M_{CO_2}\right)}{V\rho} \tag{2.18}$$

The derivation of Eq. (2.14) to (2.18) is given in the supplementary material of Albaek et al. (2011). The oxygen transfer in this work is however approximated by use of a logarithmic mean value for the driving force, which corresponds to plug flow of the gas phase.

Dissolved oxygen control

A proportional integral control law is used to regulate the substrate feed rate in such a way that the desired level of dissolved oxygen is obtained.

Estimating the specific growth rate

For cell growth on a single nutrient limiting substrate at low concentrations it is generally seen that the specific growth rate is proportional to the substrate concentration, S. In contrast, with increasing

values of *S* the specific growth rate approaches an upper limit (Nielsen et al., 2003). This can be described with different mathematical models of which the Monod model is frequently used. However use of e.g. the Monod model requires an estimation of the substrate concentration and the upper limit of the growth rate (μ_{max}). Intuitively, the dosing strategy of a DOT controlled fed-batch fermentation yields a very low substrate concentration. If the substrate is consumed immediately and with the same rate as added via the substrate feed, one can assume a steady state of the substrate concentration, dS/dt≈0 {Jahic, 2003 157 /id} The following is then seen from the substrate balance Eq.(2.16)

$$\mu = \frac{\frac{c_F F}{V} - \frac{S\left(\rho_F F - F_{evap} + M_{O_2} - M_{CO_2}\right)}{V_L \rho} - m_s}{\frac{X}{\gamma_{xs}^{true}}} \tag{2.19}$$

μ is a function of the feed flow rate, and is to a lesser degree dependent on the substrate concentration. Note that the balance includes losses to evaporation and CO_2.

Computational methods

The model as described above was implemented in MATLAB, version 2009b (Natick, Massachusetts). Numerical solution of the differential equations was obtained by using the ode23 solver. However, before anything was computed, the yield coefficients and the parameters for the biomass-viscosity and k_La correlations were estimated.

2.3 Materials and methods

Strain and growth conditions

A proprietary, recombinant strain of *T. reesei* was used that originated from the wild strain QM6a (Montenecourt and Eveleigh, 1977a; 1977b) For inoculation, frozen spores were germinated on fresh agarose plates, allowed to sporulate, and used to inoculate a seed fermentation whose vegetative growth was subsequently used to inoculate the main fermentors. Inoculation volume was approximately 10% (volume) of the initial batch volume. The process and batch medium are similar to those of various previously published studies (Lehman, 2011). Addition of the carbon source (approximately 65 w/w% carbohydrate) was controlled in such a way that the dissolved oxygen tension was following a specified set point profile throughout the fermentation. A pulsed-paused feeding mode as previously described (see for example Albaek et al. (2011)) was also employed here.

Enzyme expression and activity assay

A cellulase complex is expressed behind various promoters (e.g., (Mach and Zeilinger, 2003)). The

hydrolytic activity and specific promoter used are not reported for proprietary reasons. Enzyme activity was determined using a proprietary enzyme activity assay, and results are here reported as arbitrary units per litre of fermentation broth.

Experimental design and fermentation conditions

We made a full-factorial design consisting of two levels for three process variables: Specific agitation power input (1.5 kW/m^3 and 15 kW/m^3, respectively), aeration rate (96 NL/min and 320 NL/min, respectively), and headspace pressure (0.1 barg and 1.3 barg, respectively). We included a center point (with values 9 kW/m^3, 208 NL/min, and 0.7 barg, respectively) as recommended in the literature (e.g., (Miller, 2007) and various software packages). Thus in total 9 fermentations were conducted. The fermentation vessels were 550 L pilot plant fermentors with dimensions as previously described (Albaek et al., 2008). Six fermentations were carried out with the dual B2-30/45 (D/T = 0.44) configuration while three fermentations had a single B2-45 (D/T = 0.488) impeller. pH was controlled through feeding of ammonia, and pressure and temperature were kept at constant levels by the process control system (DeltaV, Emerson Process Management). The operation mode of the fermentation process was as follows:

-All fermentations were started with identical batch phases, during which the substrate concentration decreased from a high initial value to its operational range. The agitation power input was 0.15 kW, the aeration rate was 96 NL/min, and the headspace pressure was 0.1 barg.

-The batch phase was followed by a DOT controlled fed-batch phase with process variables as described above and with the carbon substrate feed flow rate as the controlled variable.

Biological parameters

Biomass, specific growth rate, and yield and maintenance coefficients were determined as described in Albaek et al (2011). A simple maintenance model describes the maintenance uptake of substrate and oxygen independent of the growth process (Nielsen et al., 2003)

$$Y_{IX} = \frac{\mu}{\frac{\mu}{\gamma_{ix}^{true}} + m_i} \tag{2.20}$$

where Y_{IX} is the "observed" yield coefficient of biomass per mass of component i, γ_{ix}^{true} is the "true" stoichiometric coefficient, and m_i is the non-growth associated maintenance coefficient of i. The true yield coefficients for biomass formation on substrate and oxygen and the maintenance coefficients were then determined since the specific rates of substrate uptake, r_s, and oxygen consumption, r_o, are correlated the following way (Nielsen et al., 2003)

$$r_i = \frac{1}{\gamma_{ix}^{true}}\mu + m_i \tag{2.21}$$

Determination of k_La

The direct method was used by means of a mass spectrometer (VG Prima dB, Thermo, MA). A logarithmic mean driving force was used to model average driving force, since the gas phase concentration of oxygen is lower in the outlet (Nielsen et al., 2003). Perfect mixing of the liquid phase is assumed. The oxygen concentration at 100% saturation was estimated using Henry's constant for water at 25°C (H_{O2} = 793.4 bar.kg/mol O2 (Rettich et al., 2000)) and the solute concentration was assumed constant ($DO^* = p_{O2}/H_{O2}$). The reported k_La values were calculated as average values for time periods of 1 h.

Rheological measurements

The rheological characterization of the fermentation broth was performed by steady state flow measurements using a "vane-and-cup" geometry ideal for suspension rheology in a controlled strain and stress rheometer (AR-G2, TA Instruments, DE). The vane consists of four blades (14 mm W x 42 mm H) mounted at right angles, and the cup had a 15 mm radius and contained 28.72 mL fermentation broth. The gap between vane and cup was 4000 μm. 15 steady state measurements (<5% variation in three consecutive measurements of 5 s duration) were made for each sample in the shear rate interval from 10 to 200 1/s. The power law model was used to describe the rheological behavior of each sample.

Uncertainty analysis

The Monte Carlo Procedure as described in Sin et al. (2009) was used. 10 model parameters were included in the analysis. The subjective input uncertainty of the model parameters was subject to an expert review process and defined as listed in Table 2.2. A uniform distribution was assumed in all cases. The four observed yield coefficients (Y_{SX}, Y_{SP}, Y_{SO}, Y_{SC}) did not vary much and their variation range was set to 10%. The uncertainty of the viscosity prediction is represented by the uncertainty of the constant C_1 (Eq. (2.13)) and set to 30%. The uncertainty of the mass transfer correlation is represented by the constant C and set to 30%. The largest uncertainty presumably exists around the parameters γ_{xs}, γ_{xo}, m_s, and m_o; since the fermentations are carried out at low growth rates, these four parameters are not easily determined. Therefore the variation range was set to 50%. For proprietary reasons, the actual values of the yield- and maintenance coefficients are not reported.

Table 2.2. Expert review of uncertainty of input parameters

Uncertainty class	Variation range (%)	Parameters
Low	10	Y_{SX}, Y_{SP}, Y_{SO}, Y_{SC}
Medium	30	C, C_1
High	50	γ_{xs}, γ_{xo}, m_s, m_o

100 samples – each containing one value for each parameter – were selected from the input parameter space using the Latin-Hypercube Sampling method (Sin et al., 2009). In lack of detailed knowledge, no correlation was assumed between the parameters. The sampled input matrix was used to perform 100 simulations of a randomly selected fermentation. Fermentation conditions were 1.5 kW/m^3, 320 NL/min, and 1.3 barg, respectively.

Sensitivity analysis

Linear regression (using linear least squares) was used to obtain Standardized Regression Coefficients (SRCs) between the 100 input parameter samples and the output results of the Monte Carlo simulations. The procedure is described in detail in Sin et al. (2009). The scalar outputs required for the calculation of the SRCs were chosen to be the values at the end of the fermentation as the uncertainty in general increased with time.

Power consumption

The power consumption for agitation is calculated by

$$P = \frac{n\mathrm{Po}\rho N^3 D^5 P_g / P_L}{1000} \tag{2.22}$$

where n is the number of impellers, Po is the unaerated impeller power number, and P_g/P_o is the relative power draw upon aeration. The power consumption of the motor includes the power loss in bearings, seal and gearbox, P_{loss}

$$P_a = P + P_{loss} \tag{2.23}$$

Previously, Po for the dual B2-30/45 configuration was determined to be 3.35 (Albaek et al., 2008). As part of the measurements with this study, Po for the single larger B2 (D/T = 0.48) was found to be 2.69 and P_{loss} = 0.15 kW (data not shown). P_g/P_o was set to 0.8 in this work (Albaek et al., 2008).

The power dissipated by aeration is calculated as suggested by Roels and Heijnen (1980)

$$P_{\text{air}} = \frac{V_{\text{g,standard}} R T_{\text{p}} V}{22.4 Z} \ln\left(1 + \frac{\rho g Z}{p_{\text{o}}}\right) \tag{2.24}$$

The total energy dissipated in the fermentation broth due to agitation and aeration is

$$P_{\text{broth}} = P + P_{\text{air}} \tag{2.25}$$

The power consumption for the air compressor is calculated assuming single stage, isentropic compression of Q_1 from p_1 to p_2 (Green and Perry, 2008)

$$P_{\text{c}} = 2.78 \cdot 10^{-2} \frac{k}{k-1} \frac{Q_1 \cdot p_1}{\eta_c} \left[\left(\frac{p_2}{p_1} \right)^{\frac{k-1}{k}} - 1 \right] \tag{2.26}$$

The mechanical and electrical losses of the compressor were represented by the degree of efficiency of the compressor, η_{c}, which was assumed to be 0.7 (Knoll et al., 2005). The isentropic exponent, k, is about 1.4 for air (Kouremenos and Antonopoulos, 1987).

Microbial metabolism and the mechanical power input by agitation dissipate heat to the fermentation broth. The energy removed from the system by water evaporation is not considered here. The metabolic heat development has been shown to be directly proportional to the rate of oxygen consumption and the proportionality constant, ΔH_{f}, is assumed to be 460 kJ/mol (Cooney et al., 1969; Nielsen et al., 2003). The total heat generation of the fermentor, Q, is thus

$$Q = P + \Delta H_{\text{f}} \frac{\text{OTR} \cdot V}{3600} \tag{2.27}$$

The power consumption for cooling of the vessel is estimated by assuming an effective cooling system with a coefficient of performance (COP) of 6 (Curran et al., 1989)

$$P_{\text{w}} = \frac{Q}{\text{COP}} \tag{2.28}$$

The energy efficiency of oxygen transfer includes all energy consumed by the system

$$EE_{\text{O}_2} = \frac{M_{\text{O}_2} \text{OTR}}{\frac{P_{\text{a}} + P_{\text{c}} + P_{\text{w}}}{V}} \tag{2.29}$$

2.4 Results and discussion

2.4.1 Mass transfer

The accumulated oxygen transfer for all fermentations is shown as function of the total specific power input to the fermentation broth and the aeration rate in Figure 2.2. The achieved specific power inputs are slightly lower than the experimental design due to the fed-batch mode of fermentation; the volume generally increased during the course of the fermentation. The average fermentation broth volume is used for these calculations.

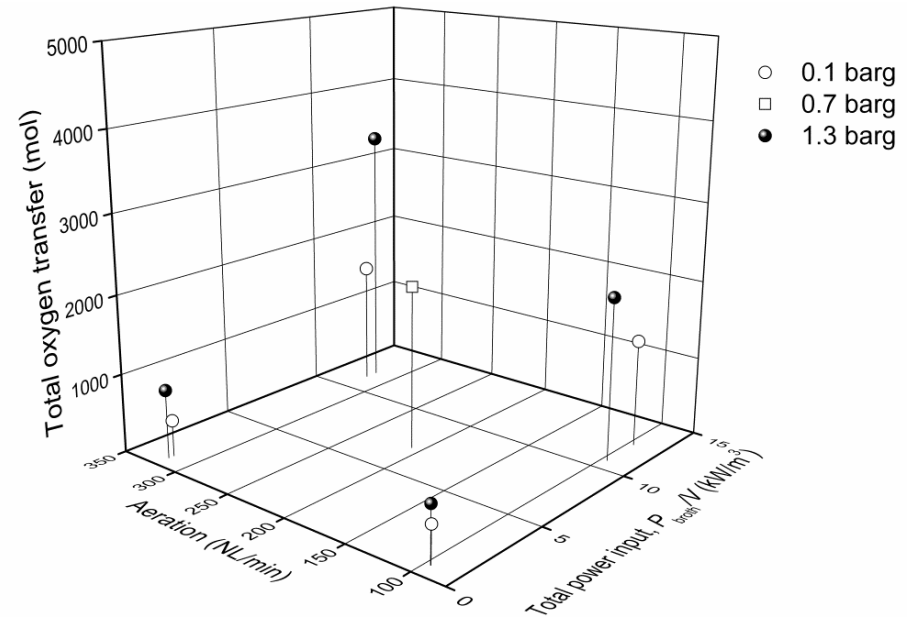

Figure 2.2. Total oxygen transfer for all fermentations as function of aeration rate and total specific power input, P_{broth}/V. Three different headspace pressures were used. Adapted from Albaek et al. (2012).

The oxygen transfer increased with increased aeration, agitation power input and headspace pressure as predicted from Eq. (2.2) and Eq. (2.7) – (2.9). In the data reported in Figure 2.2 there are no exceptions to this observation (in each case an increase in any single process parameter leads to increased oxygen transfer); this provides an indication of the high quality of the equipment and measurements in the pilot plant.

In Figure 2.3A, B, and C the experimental k_La data are shown versus the correlations presented in Table 2.1. The correlation by Kawase and Moo-Young (1988) (Figure 2.3A) is not modified to fit the experimental data. The relationship suggested by Henzler (1982) (Figure 2.3B) has been fitted to the current data set with $A_1 = 1.19$; $A_2 = 0.48$. The best fit obtained with the empirical correlation is shown in Figure 2.3C

$$k_La = 32\left(\frac{P_{broth}}{V}\right)^{0.52} v_g^{0.15}\mu_{app}^{-0.50} \tag{2.30}$$

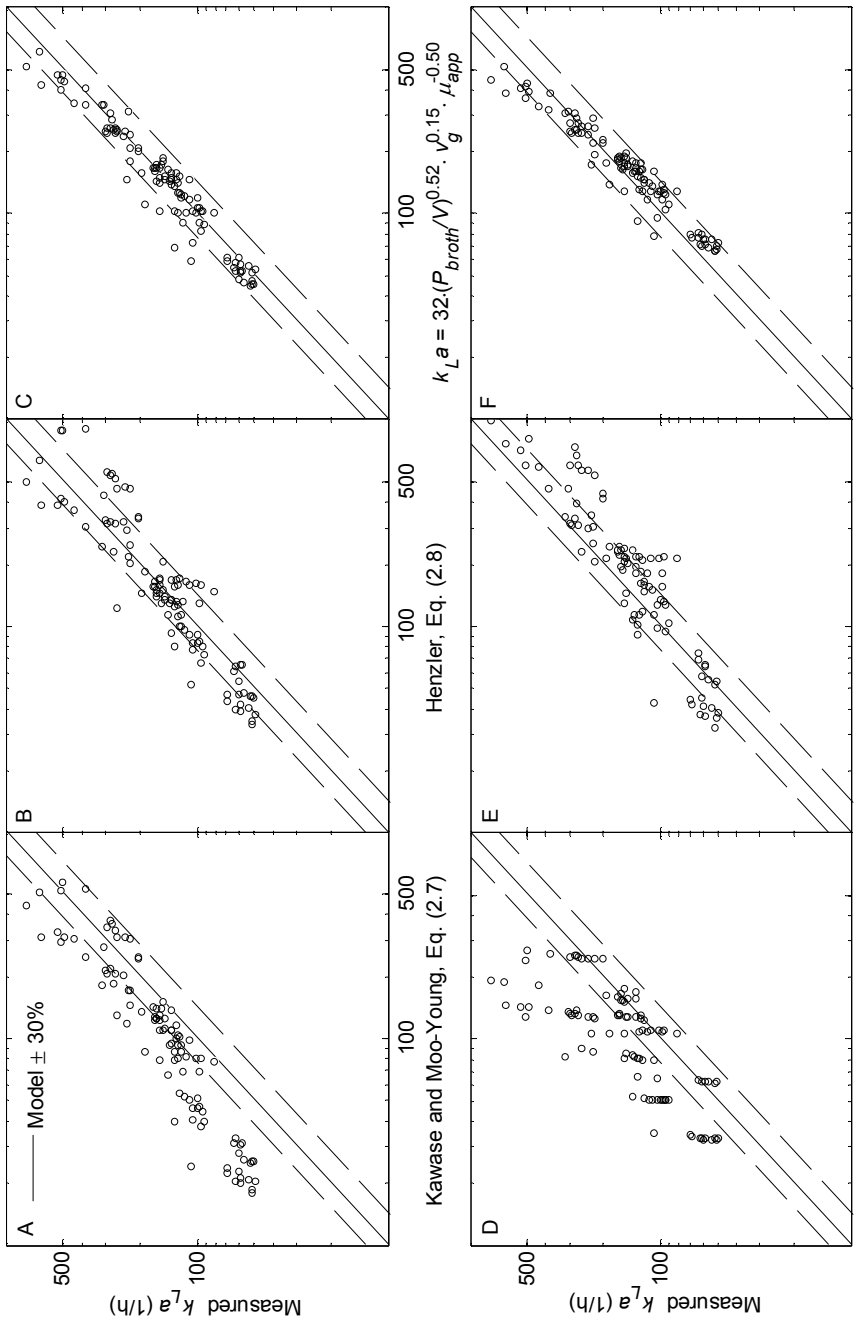

Figure 2.3. Comparison of three correlations for k_La using fermentation data. In each case the experimental data is shown as function of the model. A: Kawase and Moo-Young (1988), Eq. (2.7). Regression curve slope: 0.67 (R^2 = 0.87). B: Henzler (1982), Eq. (2.8). Regression curve slope: 0.75 (R^2 = 0.84). C: Empirical correlation, Eq. (2.9). Regression curve slope: 0.97 (R^2 = 0.93). D: Wang et al., 1979. Regression curve slope: 0.84 (R^2 = 0.58). E: Garcia-Ochoa and Gomez, 1998. Regression curve slope: 0.68 (R^2 = 0.86). F: Albaek et al., 2011. Regression curve slope: 1.21 (R^2 = 0.93). Adapted from Albaek et a.- (2012). [a] P_{broth} is inserted in hp/1000L and v_g in cm/min.

Of the three correlations included in this work, Eq. (2.30) describes the experimental data best with a regression curve slope of 0.97. For 105 available data points, only 8 are not within ±30% of the model prediction. Contrary to previous findings, it is also seen that one correlation describes both geometrical configurations used. The regression curve slopes for the correlations by Kawase and Moo-Young (1988) and Henzler (1982) are 0.67 and 0.75, respectively. Even though it might have been beneficial for a comparison of mass transfer correlations, it has not been possible to include mass transfer data from other scales.

The correlation matrix of the parameter estimates in Eq. (2.9) based on the Fisher Information Matrix (see for example Petersen et al. (2008)) is shown in Table 2.3. The parameters are highly correlated, i.e. most correlation coefficients are higher than 0.5.

Table 2.3. Correlation matrix of the parameter estimation in Eq. (2.9) calculated based on the Fisher Information Matrix.

	C	*a*	*b*	*c*
C	1.0000	-0.5617	0.7264	0.7170
a	-0.5617	1.000	-0.0917	-0.4951
b	0.7264	-0.0917	1.000	0.0960
c	0.7170	-0.4951	0.0960	1.000

The correlation coefficients can vary between -1 and +1. Values close to -1 or +1 indicate a high correlation.

Comparison between Eq. (2.30) and other correlations in the literature is possible. In Figure 2.3D, E and, F the experimental data are shown versus correlations of the same form obtained for non-Newtonian media in STR. The correlation of Wang et al. (1979) does not contain the viscosity term and the fit to the data is not impressive (Figure 2.3D). The correlation of Garcia-Ochoa and Gomez (1998) describes the current data somewhat better (Figure 2.3E). The slope of the regression curve is 0.68, which reflects the differences in the exponents *a*, *b*, and *c* (0.6, 0.67, and -0.67, respectively) compared to those of Eq. (2.30). The correlation found in the previous work with *A. oryzae* in identical fermentors (Albaek et al., 2011) has an excellent fit with the data (Figure 2.3E). It is clearly seen that the two different sets of parameters give very similar predictions of k_La. This underlines the importance of not considering the individual exponents as absolute values. Indeed, they are highly correlated and many combinations of these constants will yield equally good fit to the data.

2.4.2 Yield coefficients

The yield coefficients and maintenance coefficients were determined as described in “Materials and methods”, but their values are not stated for proprietary reasons. However, it was surprising to observe that in some cases higher headspace pressure led to lower cellulase concentrations. Oxygen

transfer to the fermentation broth was shown to follow Eq. (2.2) and Eq. (2.30) in the previous section. In all fermentations, the respiration quotient (RQ) was on average equal to 1.05 and fluctuated only slightly around this value (data not shown), which meant that the CER varied accurately with the process conditions similar to OUR (assuming OUR = OTR). CO_2 has long been known to inhibit microbial growth (Onken and Liefke, 1989). The actual effect of CO_2 is caused by its concentration in the medium; however, assuming efficient exchange between the gas and liquid phases, partial pressure of CO_2 in the gas phase will be the independent variable (pH was constant during the fermentations). The yield coefficients for biomass and protein formation relative to the average yield coefficients for all fermentations are shown in Figure 2.4.

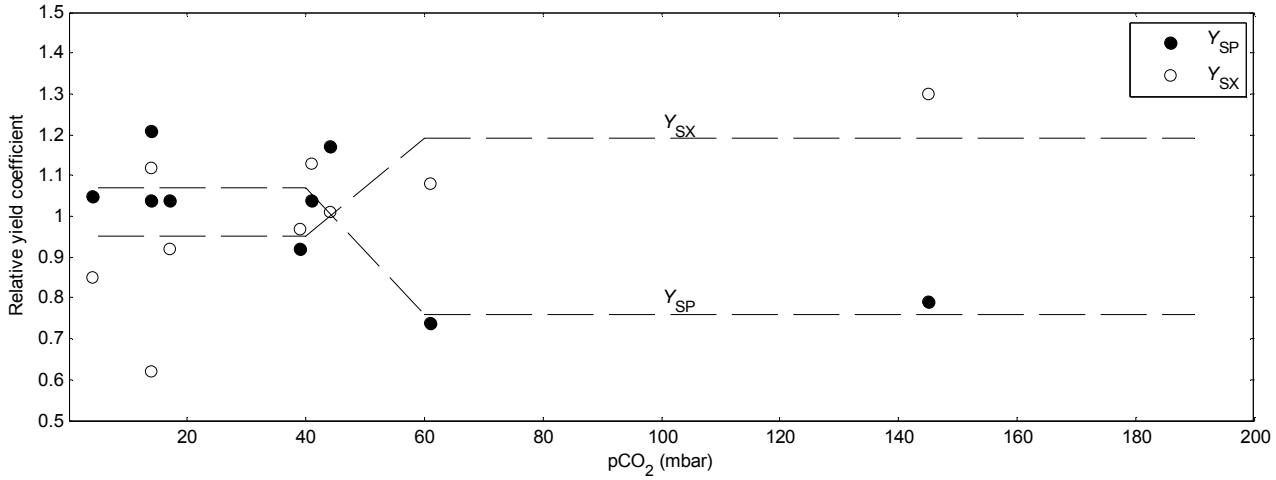

Figure 2.4. Relative Y_{SP} and Y_{SX} versus partial pressure of CO_2. All values are calculated averages of the entire fermentation. Above a threshold value of pCO_2 between 40 and 60 mbar product formation is decreased ~20%. Y_{SX} increases correspondingly. Adapted from Albaek et al. (2012).

At the lowest values (pCO_2 < 50 mbar) no clear trend is seen. In two cases, Y_{SP} and Y_{SX} differ significantly from this situation. Y_{SP} is decreased ~20% when pCO_2 is above what seems to be a threshold level, which lies between 40 and 60 mbar. Biomass formation, Y_{SX}, seems to increase correspondingly to the decrease in product formation. It is important to remember here, that no threshold CO_2 content in the outlet gas (e.g., 3% or 5%) is observed; the essential parameter is the partial pressure. The complex interactions between process conditions, morphology and growth, and productivity of filamentous fungi in general are still to be assessed (McIntyre et al., 2001).

The observed response of *T. reesei* to pCO_2 is perhaps not surprising. Onken and Liefke (1989) compared data from 10 different studies where pCO_2 was varied. There is a general trend of growth retardation for increasing levels of CO_2, but examples where lower CO_2 partial pressures stimulated growth, and growth was only inhibited at higher pCO_2 are also mentioned (Onken and Liefke, 1989). Pirt and Mancini (1975) found reductions in penicillin production of 35% at 50 mbar CO_2 and 50% at 80 mbar CO_2 in chemostat cultures of *Penicillum chrysogenum*. It therefore seems possible that even CO_2 partial pressures in the range of 50 mbar can induce a shift in the metabolism from product to biomass formation.

2.4.3 Viscosity

In Figure 2.5A the measured apparent viscosity is shown as a function of fermentation time for all fermentations. The effective shear rates used for the calculation of the apparent viscosity ranged from 28-91 1/s. The apparent viscosity increases during the fermentation from initial values around 0.001 Pa.s, the viscosity of water, to maximum values of 0.120 Pa.s at the end of the fermentation.

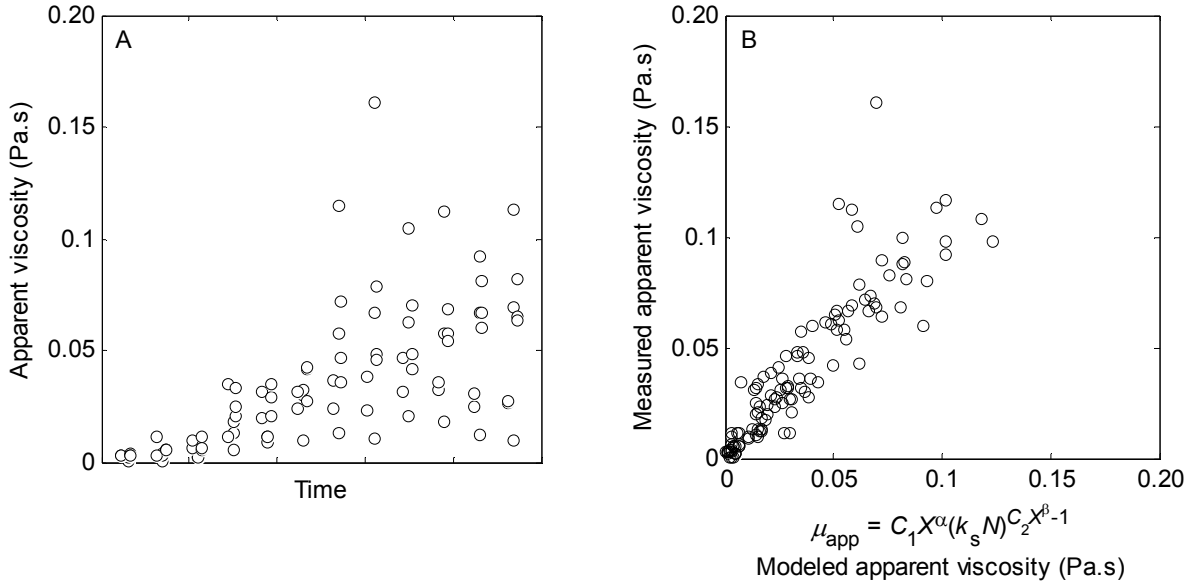

Figure 2.5. A: Development of apparent viscosity as function of fermentation time for all fermentations. The apparent viscosity increases from approximately that of water (0.001 Pa.s) to a maximum of 0.120 Pa.s at the end of the fermentation. B: Parity plot of measured apparent viscosity as function of modeled apparent viscosity. A good modeling prediction is seen (regression curve slope: 1.01, R^2 = 0.80). Note that the time and the constants in the viscosity model are not given for proprietary reasons.

The measured apparent viscosity is shown as function of the modeled apparent viscosity using Eq. (2.13) in a parity plot in Figure 2.5B. For proprietary reasons the values of the constants are not given. The regression slope curve of Figure 2.5B is 1.01 with R^2 = 0.80, which means that the model explains most of the development seen in Figure 2.5A. A few separate measurement point are not predicted by the model, but this can be due to uncertainty in the determination of the biomass concentration or an unrepresentative broth used for the rheological characterization.

2.4.4 Process simulation

Now that the parameters from the individual model components are determined, the complete fed-batch phase can be simulated as proposed. In Figure 2.6 representations of the model prediction and model uncertainty are shown as well as the experimental measurements. It is clear, that uncertainty exists in the model outputs. The degree of uncertainty on different outputs is different; e.g. the uncertainties on biomass and product concentration are relatively larger compared with the uncertainty of the prediction of $k_L a$. The mean values of the simulations in Figure 2.6 overall

describe the fermentation process in quite a satisfactory manner. The mean simulated trajectories of weight, specific growth rate, product concentration, feed flow rate, apparent viscosity and k_La are in fact all very similar to the experimental measurements. The DO is the controlled output and therefore the uncertainty for this output is expected to be small.

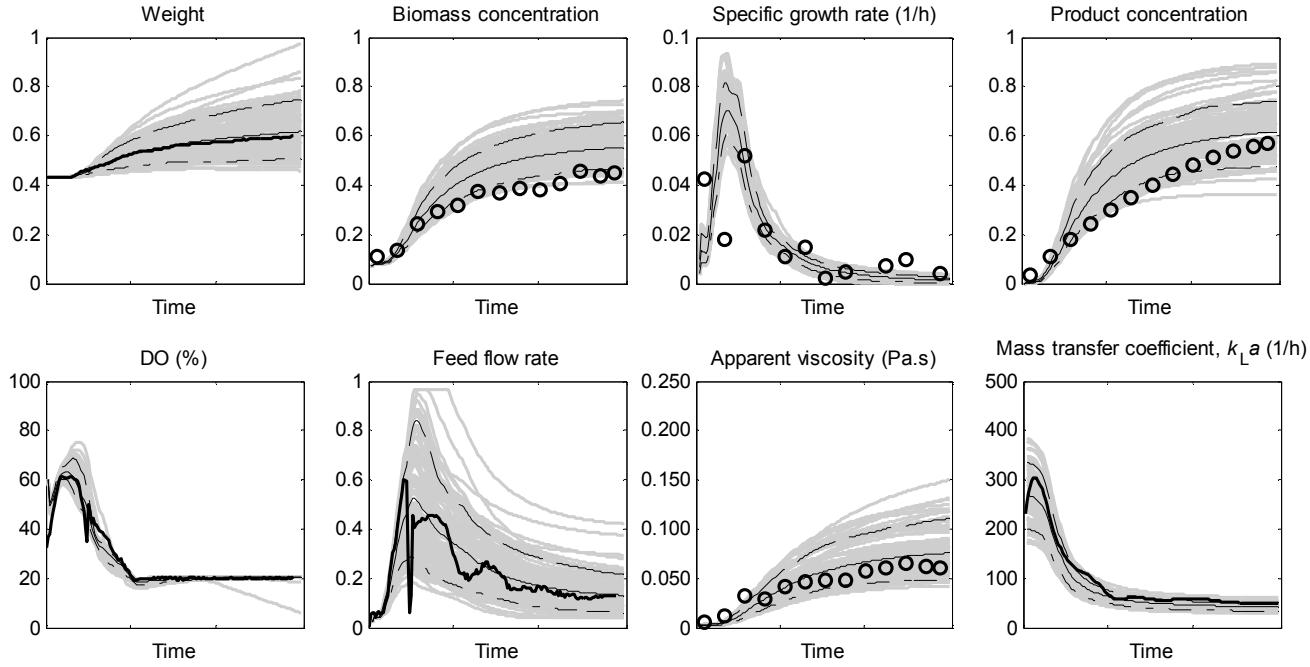

Figure 2.6. Representation of the model prediction and model uncertainty for weight, biomass concentration, specific growth rate, product concentration, dissolved oxygen, feed flow rate, apparent viscosity, and k_La: Monte Carlo simulations (gray), mean (-), 10th (• -) and 90th (- -) percentile of the predictions as well as the experimental measurements (bold) are shown. The fermentation conditions were: 1.5 kW/m^3, 320 NL/min, and 1.3 barg respectively. Adapted from Albaek et al. (2012).

The example shown in Figure 2.6 is typical for the fermentations performed in this study. In two cases however, the model is shown to overestimate the final weight by ~20% even though the oxygen transfer is predicted satisfactory. Interestingly, these two cases are the fermentations with pCO_2 > 50 mbar. One might speculate that the observed change in metabolism from protein formation to increased biomass formation also leads to changes in the oxygen consumption. The model in its current state does not correct for these changes, since such phenomena are not incorporated in the model structure.

It seems that the level of complexity of the model is suitable and that the number of parameters for growth, product formation, and maintenance uptake is sufficient to describe these processes. Future improvements could include the effect of increased pCO_2.

2.4.5 Sensitivity analysis

The SRCs ranked for each model output are given in Table 2.4. First, it is noticed that the degree of

linearization indicated by the coefficient of model determination, R^2, is high for all outputs. The linearized model is thus able to explain most of the variance in the model.

The maintenance oxygen uptake, m_o, is highly influential on all outputs. m_o describes non-growth associated oxygen uptake, and therefore a higher m_o intuitively should lead to less oxygen available for growth. Consequently, the growth rate should decrease. With the decreased growth rate, also the biomass and product concentration, feed flow rate, and viscosity are expected to be lower. Finally, a higher m_o should lead to higher k_La because the viscosity is lower. Encouragingly, the signs of the SRCs of m_o predict exactly these trends. This expected behavior of the system is also seen with C (of the k_La correlation). Increasing C leads to increases in all outputs (positive SRCs). For C_1 (of the viscosity prediction) the analogue (and opposite) behavior is seen.

The maintenance coefficients (γ_{xs}, γ_{xo}, m_s, m_o) in general have high rankings, and at least one of them has a higher ranking than C for all outputs. This might be somewhat surprising, since the fermentation is limited by mass transfer of oxygen. However, the model of the mass transfer is accurate with ±30% and therefore, the uncertainty of the model is primarily seen in the biological parameters. The variations in the yield coefficients (Y_{SX}, Y_{SP}, Y_{SO}, Y_{SC}) only have significant impact on the product concentration. This is expected from Table 2.2 and the model structure, as Y_{SO} and Y_{SC} contribute only to the calculation of the dilution term in the selected model outputs.

Overall, the sensitivity analysis shows that detailed knowledge of the production organism is required in order to use the mechanistic model for quantitative purposes. In future investigations, emphasis could be on improving the knowledge of the biological system and thus decreasing the uncertainty of this part of the model. It seems that the viscosity prediction and the mass transfer correlation at present do have the necessary accuracy.

Table 2.4. Standardized Regression Coefficients (SRCs): The ranking of the 10 model parameters for the model outputs.

	Weight		Biomass		Growth rate		Product		Feed flow rate		μ_{app}		k_La	
R2	0.94		0.97		0.91		0.97		0.85		0.95		0.99	
Rank		SRC		SRC		SRC		SRC		SRC		SRC		SRC
1	γ_{xs}	0.75	m_o	-0.71	m_o	-0.74	m_o	-0.63	m_o	-0.59	m_o	-0.67	m_o	0.76
2	m_o	-0.40	C	0.53	γ_{xo}	0.47	C	0.48	m_s	0.50	C	0.51	C	0.50
3	C	0.34	γ_{xs}	-0.28	γ_{xs}	0.26	Y_{SP}	0.34	γ_{xs}	0.41	C_1	0.34	C_1	-0.25
4	m_s	0.26	C_1	-0.28	m_s	0.23	Y_{SX}	-0.30	C	0.33	γ_{xs}	-0.27	γ_{xo}	0.24
5	γ_{xo}	-0.20	γ_{xo}	-0.22	C	0.17	C_1	-0.26	C_1	-0.14	γ_{xo}	-0.20	γ_{xs}	-0.10
6	C_1	-0.17	m_s	-0.10	C_1	-0.07	γ_{xo}	-0.20	Y_{SX}	0.03	m_s	-0.10	Y_{SP}	-0.01
7	Y_{SX}	0.02	Y_{SX}	0.03	Y_{SO}	-0.05	γ_{xs}	-0.17	γ_{xo}	0.02	Y_{SX}	0.05	m_s	-0.01
8	Y_{SP}	0.02	Y_{SP}	0.01	Y_{SP}	-0.02	m_s	-0.05	Y_{SC}	0.02	Y_{SO}	-0.01	Y_{SO}	-0.01
9	Y_{SC}	0.01	Y_{SC}	0.00	Y_{SX}	0.01	Y_{SO}	0.00	Y_{SO}	-0.01	Y_{SP}	0.00	Y_{SX}	-0.01
10	Y_{SO}	0.01	Y_{SO}	0.00	Y_{SC}	0.01	Y_{SC}	0.00	Y_{SP}	0.00	Y_{SC}	0.00	Y_{SC}	0.00

SRC may take values between 0 and ± 1. The larger the absolute value of a coefficient, the more significant the parameter. The signs indicate a negative or a positive impact of the parameter on the outputs.

2.4.6 Energy efficiency and overall model performance

The efficiency of oxygen transfer is a key process variable, since oxygen transfer completely governs DOT-controlled fed-batch fermentations and protein formation is thus directly coupled to oxygen transfer. In Figure 2.7 the measured efficiencies of oxygen transfer (Eq. (2.29)) at each process condition are shown versus the total specific power consumption including agitation, aeration and cooling. A clear correlation between EE_{O2} and specific power input is seen; as expected efficiency drops with increasing power input. The simulation results are also shown, and in general the agreement with the experimental results is good. On average, the total oxygen transfer of the entire fermentation time is under-predicted by only 13%. A deviation in this order of magnitude is acceptable and within the uncertainty of the model. The simulation "error" is relatively larger in the low power fermentations.

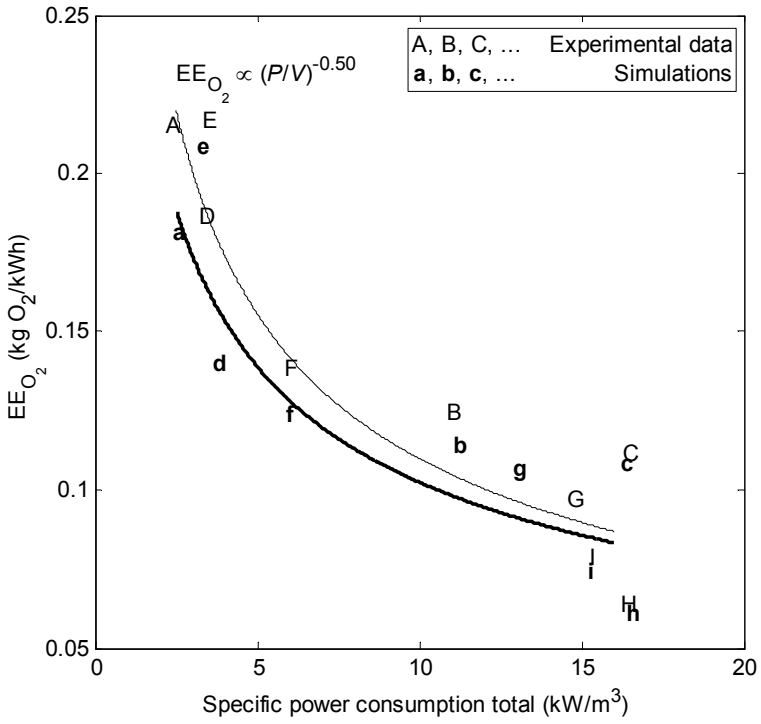

Figure 2.7. Energy efficiency of oxygen transfer versus total specific power consumption for agitation, aeration and cooling. Experimental data are shown in uppercase letters while the corresponding simulation results are shown in bold lowercase letters. The experimentally observed efficiency EE_{O2} drops with increasing specific power input with a negative exponent of -0.50 (R^2 = 0.88). Adapted from Albaek et al. (2012).

If only the power input for agitation is considered, the following relationship is expected (Schügerl, 1990)

$$EE_{02} \propto \left(\frac{P}{V}\right)^{m} \tag{2.31}$$

By theoretically considering the turbulent forces, it has been suggested, that if the power input was only altered by a change in agitation intensity, m would be equal to -0.6 (Schügerl, 1991). In this study, energy consumption for aeration and cooling is however included in order to give a more realistic description of the operation of the STR. We observe a change in oxygen transfer efficiency with specific total power input with an exponent $m \approx -0.5$, and the simulation results predict a similar relationship. Opposed to a purely theoretical relation, the mechanistic model incorporates the complex behavior of the system: Oxygen transfer causes biomass formation; this growth is coupled with increased viscosity, which increasingly hinders oxygen transfer. Even though comparison with other studies is difficult due to differences in media properties such as degree of coalescence-promotion and viscosity, our data is very much in line with other studies in stirred tanks (Schügerl, 1991). We find it encouraging and interesting that $m \approx -0.5$ even after accounting for aeration and cooling. However, at different scales the relative contributions from agitation, aeration and cooling change, making the detailed analysis in Eq. (2.29) necessary. In Figure 2.8 the measured EE_{O2} is shown versus the simulated EE_{O2}. In each end of the wide range of variation of the process parameters, the EE_{O2} is predicted with good accuracy.

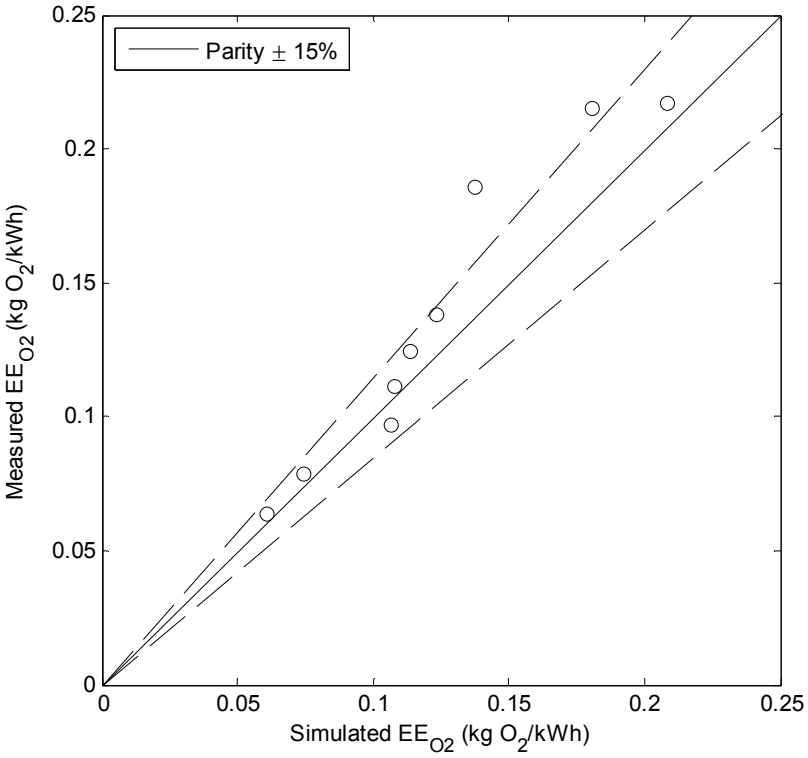

Figure 2.8. Parity plot of the measured EE_{O2} as function of the simulation EE_{O2}. The model covers well the entire range of fermentation conditions. The simulation error on average is 13% and is therefore larger for the high efficiency fermentations, which have the smallest energy consumption.

These kinds of simulations, developed for enzyme production by filamentous fungi, may serve as a basis for development of increased understanding of process economics in the STR. In applying the

model to the actual fermentation plant one must however consider the remaining critical cost functions such as product sale price, plant life time, reactor and compressor purchase costs, energy costs, etc.

2.5 Conclusions

It has been showed that a relatively simple model containing the reaction equation stoichiometry, a mass transfer correlation, and a viscosity prediction can be used to simulate STR pilot scale fed-batch fermentations of *T. reesei* carried out with different agitation, aeration and headspace pressure.

Three oxygen mass transfer correlations have been compared based on experimental data from 9 fermentations. A purely empirical correlation which is commonly used in the STR literature showed to describe the experimental data best. No data from other scales were included in the comparison.

The partial pressure of carbon dioxide seemed to have a threshold level around 40-60 mbar, above which the metabolism is shifted from protein production to more growth in the form of biomass formation.

The process model was shown to describe the important process variables with a satisfactory accuracy during the entire fermentation period. The large variation in oxygen transfer is successfully predicted by the model. The physical part of the model is coupled with a biological part describing growth, product formation and maintenance uptake. The uncertainty and sensitivity analyses suggest that future work could be especially focused on the biological part of the model.

Finally the model is shown to predict the energy efficiency of oxygen transfer for the entire range of process conditions well. This application of the model allows for a quantitative evaluation of the efficiency of the enzyme production in the STR. As the power input is increased, the efficiency is decreased, reflecting the inverse relationship often experienced between productivity and efficiency. The manufacturer can utilize such models to achieve the highest possible profitability if the remaining costs of production are known.

Chapter 3

Identification of key performance indicators for cellulase production

The cellulase production process in the STR is described and modeled in Chapter 2. In the current chapter the focus is on identifying suitable performance indicators that can be used for comparison of bioreactors. In the literature a number of such indicators have been suggested. The data collected during the model construction in Chapter 2 are used to determine these performance indicators for the process studied in this thesis, namely *T. reesei* fermentation.

In this analysis, investment costs and fixed-costs are assumed to be relatively low owing to the long lifespan of the plant (Schügerl, 1991) The operational costs considered here are substrate consumption and energy consumption. Factors such as manual labor, downtime, and raw material preparation are considered to be equal for the technologies considered.

3.1 Introduction of performance indicators

Depending on the process, many different parameters may be used to characterize and compare bioreactors. It is important to keep in mind the type of process and product when defining performance indicators. In this case the product is the extra-cellular (hemi)cellulase complex. The aim of the process is thus efficient formation of this product. The production of the enzyme complex is carried out by the active biomass in the fermentation vessel. The formation of product as well as the growth and existence of active biomass is reliant on oxygen transfer from the gas to the liquid phase (and finally from the liquid phase to the fungal cells). During most of the process oxygen transfer is the limiting rate.

For an extracellular product and an oxygen transfer limited process, four performance indicators was suggested by Schügerl (1991) as seen in Table 3.1. The productivity (product formation per fermentation broth volume per time) and oxygen transfer rate are obvious indicators. The specific productivities (product formation per energy consumption (EE_P) and efficiency of oxygen transfer (EE_{O2})) are indicators of the process efficiency. In this work all energy consumption – including that of mixing, aeration, and cooling – of the fermentation vessel is considered.

Table 3.1. Units of productivity and oxygen transfer rate and the related efficiencies. Adapted from (Schügerl, 1991).

Indicator	Unit	Equation
Productivity[a]	kg product/m^3/h	(3.1)
EE_P[b]	kg product/kWh	(3.2)
Oxygen transfer rate[a]	kg O_2/m^3/h	(2.2)
EE_{O2}[b]	kg O_2/kWh	(2.29)

[a]Using the average broth volume for the process (not vessel absolute capacity). [b]In this work the energy consumption includes all energy for mixing, aeration, and cooling.

In addition to the energy consumption, the consumption of substrate (including chemicals such as anti-foam oil) is another major operational cost. The carbon source used in this process constitutes the largest cost, while the consumption of ammonia used to control pH is also investigated here. The overall consumption of these substrates relative to overall product formation is calculated as shown in Table 3.2.

Table 3.2. Units of overall yield coefficients for product on carbon source and ammonia

Indicator	Unit	Equation
Product yield on carbon substrate, Y_{SP}	g product/g substrate	(3.3)
Product yield on ammonia, Y_{NP}	g product/g NH_3	(3.4)

3.2 Results and discussion

Two fermentations in this data set stand out from the rest. In Chapter 2, the reason for this is argued to be sensitivity of the organism to pCO_2. Throughout this chapter the data from these fermentations are therefore not included in the calculations, but the data are shown in the figures with special markers (gray) for comparison.

3.2.1 Productivity and oxygen transfer

The six indicators introduced above have been determined from the data obtained the modeling of the reference process. In Figure 3.1 the relative productivity and EE_P are shown as function of the total specific power input. The productivity is seen to increase with the power consumption with an exponent of 0.38 (Figure 3.1A), while EE_P decreases with the power consumption with an exponent of -0.66 (Figure 3.1B). Note that the data are shown in relative units for commercial reasons.

OTR and EE_{O2} are shown as function of the total specific power consumption in Figure 3.2. OTR increases with the power consumption with an exponent of 0.50 (Figure 3.2A). The data shown in Figure 3.2B are identical to the experimental data shown in Figure 2.7. EE_{O2} decreases with the power consumption with an exponent of -0.57.

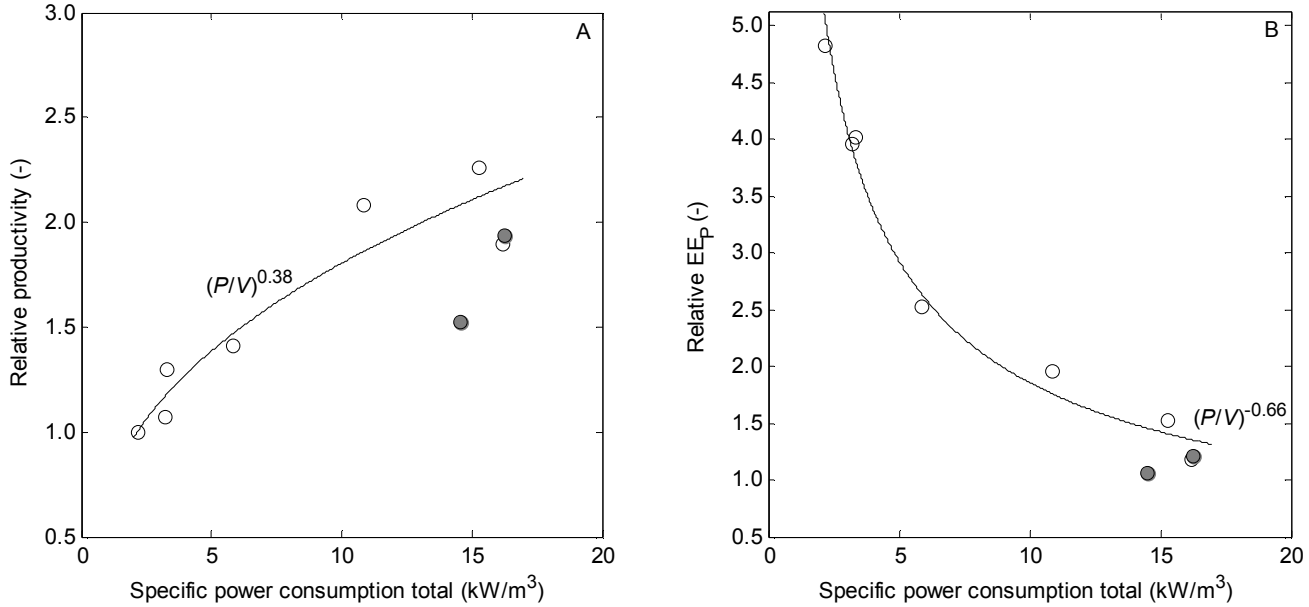

Figure 3.1.A: Relative productivity (Eq. (3.1)) shown as function of total power consumption for the nine fermentations described in Chapter 2. The productivity increases with total power consumption with an exponent of 0.38 (R^2 = 0.92). The data points in gray are shown for comparison but not included in the regression **B:** Relative energy efficiency of product formation (Eq. (3.2)) shown as function of total power consumption. EE_P decreases with the specific power consumption with an exponent of -0.66 (R^2 = 0.98).

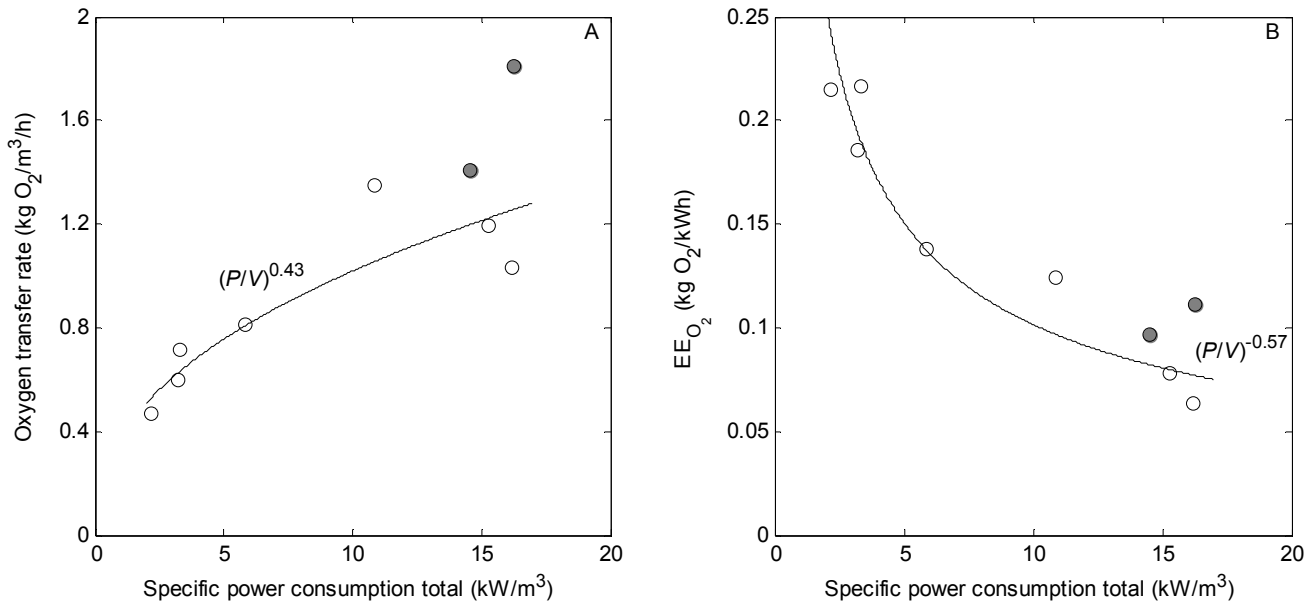

Figure 3.2. A: Oxygen transfer rate (Eq. (2.2)) shown as function of total power consumption for the nine fermentations described in Chapter 2. The oxygen transfer rate increases with total power consumption with an exponent of 0.43 (R^2 = 0.85). **B:** EE_{O2} (Eq. (2.29)) shown as function of total power consumption. The data is identical to the experimental data shown in Figure 2.7. EE_{O2} decreases with the specific power consumption with an exponent of -0.57 (R^2 = 0.91).

The very small difference between the exponents of the regression curves in Figure 3.1 and Figure 3.2 is noteworthy. While the oxygen transfer rate increases with P/V with an exponent of 0.43, the productivity increases with an exponent of 0.38. EE_{O2} decreases with the power consumption with an exponent of -0.57 while EE_P decreases with an exponent of -0.66. Since the values of the productivity and EE_P obtained in the experiments are not given here and thus cannot easily be used in the later comparison, it is interesting to investigate the relation between product formation and oxygen transfer in more detail.

According to the model presented earlier, maintenance consumption of substrates (carbon and oxygen are considered in the model) is non-growth related metabolism needed to maintain the organisms in a healthy state (Pirt, 1965). The amount of dry cell matter (DCM) is shown as function of the total oxygen transfer in Figure 3.3A. In general, one should be careful with the use of DCM since this method (as described in Chapter 2) includes all non-soluble substances as well as live and dead biomass. If however, DCM is assumed to reflect mostly the biomass present in the bioreactor, the biomass formation is linearly proportional to the oxygen transfer. The slope of the regression line gives the yield coefficient of biomass per oxygen, Y_{OX}.

In Figure 3.3B the corresponding graph for product formation is shown. Product formation is almost linearly proportional to oxygen transfer. The second order polynomial regression curve fitted the data slightly better than a linear regression ($R^2 = 0.98$ and $R^2 = 0.97$, respectively).

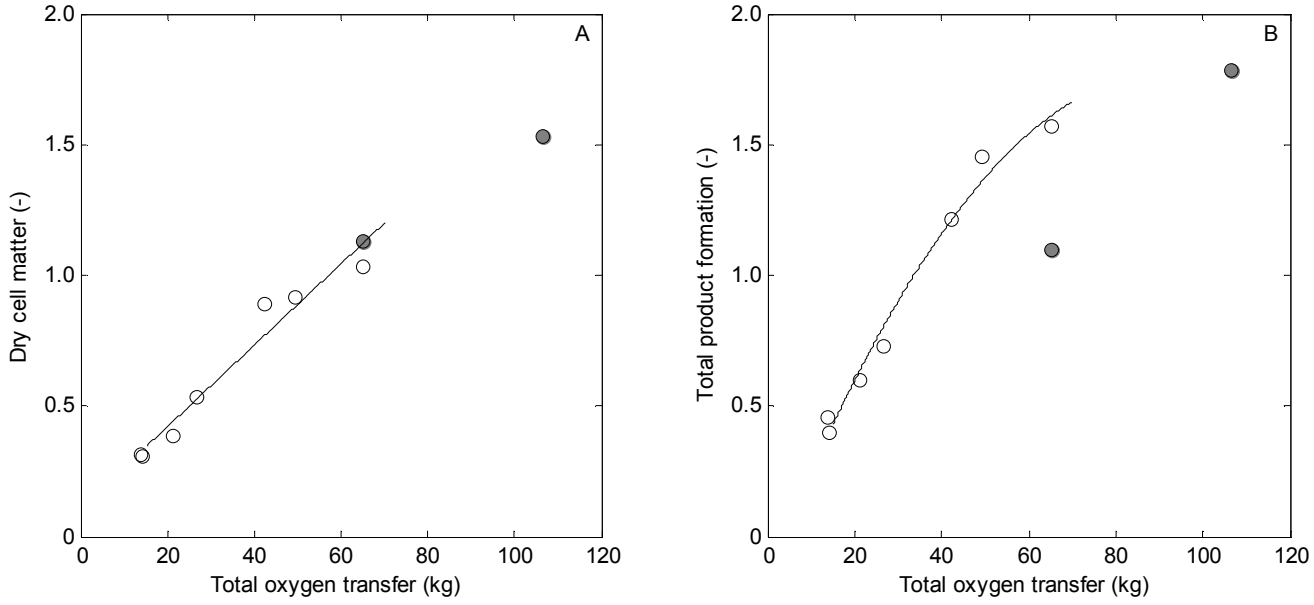

Figure 3.3.A: Dry cell matter in the bioreactor shown as function of total oxygen transfer. A linear relation is seen between dry cell matter and oxygen transfer ($R^2 = 0.95$). The slope of the regression line is the yield of DCM per oxygen, Y_{OX}. **B:** Total product formation shown as function of end total oxygen transfer. An almost linear relation is seen between product formation and oxygen transfer. The slope of the regression curve is the yield of product per oxygen, Y_{OP}. Note that dry cell matter and product formation are shown in arbitrary units for proprietary reasons.

The yield of product per oxygen, Y_{OP}, is shown as function of the average DCM during fermentation in Figure 3.4. No clear correlation is observed between Y_{OP} and average DCM. The data presented in Figure 3.3 and Figure 3.4 indicates that the maintenance consumption of oxygen is relatively small. The presented data shows, that the oxygen transfer almost linearly determines both the formation of biomass and product.

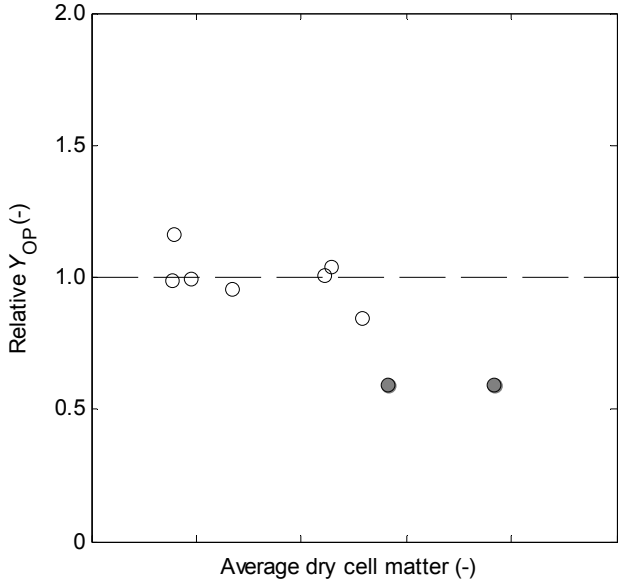

Figure 3.4. Yield of product per oxygen, Y_{OP}, shown as function of average dry cell matter during fermentation. The calculated mean value of Y_{OP} is also shown. The standard deviation from the mean value is 9.4%.

The final comparison of this section is shown in Figure 3.5. OTR and EE_{O2} are shown as function of productivity and EE_P in Figure 3.5A and B, respectively. OTR can be described by a second order polynomial of the productivity ($R^2 = 0.94$). A linear regression line fits the data almost as well ($R^2 = 0.93$). Also EE_{O2} can be described by a second order polynomial of EE_P ($R^2 = 0.97$).

The results of this section show that oxygen transfer completely governs the progress of this process. This is perhaps not unexpected, since the process is oxygen transfer limited. The maintenance uptake and consumption of oxygen is indicated to play a very small role, since the yield of product on oxygen does not seem to vary with the amount of biomass in the reactor. This means that Y_{OP} can be considered almost constant and it also explains why OTR and EE_{O2} are almost linearly proportional with productivity and EE_P. Instead of using productivity and EE_P (which again are not revealed due to commercial reasons) as process indicators it is therefore natural to use OTR and EE_{O2}.

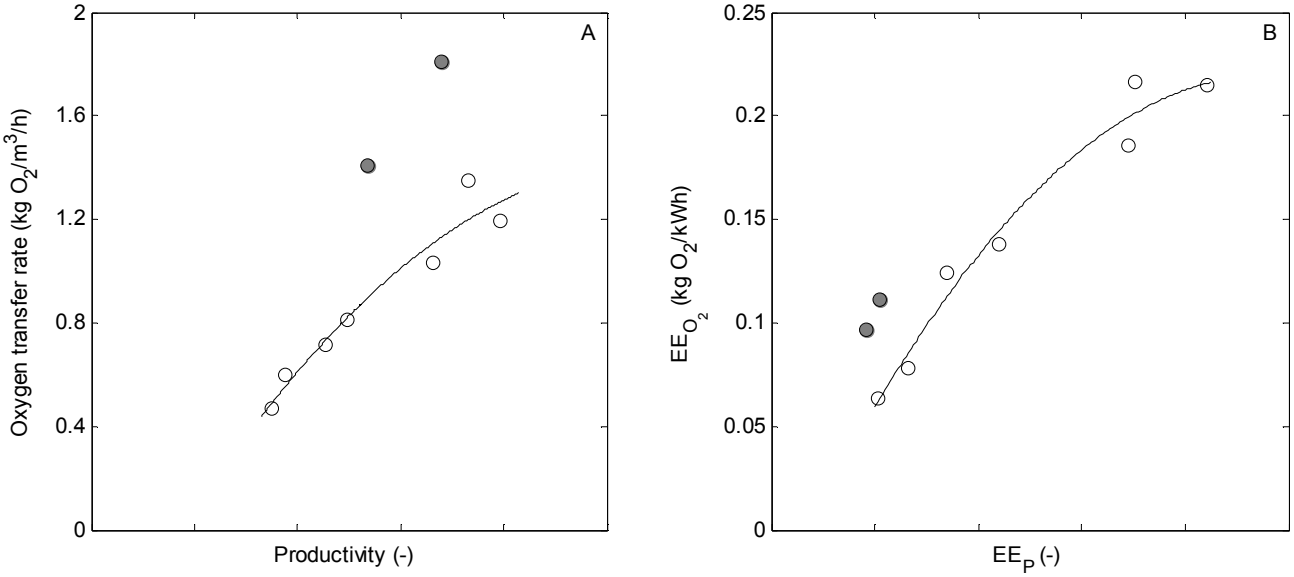

Figure 3.5. **A:** Oxygen transfer rate shown as function of productivity. The regression curve is a second order polynomial (R^2 = 0.94). **B:** EE_{O2} shown as function of EE_P. The regression curve is a second order polynomial (R^2 = 0.97).

3.2.2 Yield coefficients Y_{SP} *and* Y_{NP}

The overall yield coefficients, Y_{SP} and Y_{NP}, specify the influence of the total consumption of the variable substrates, the carbon substrate and ammonia, of the process. All fermentations had identical batch phases and additional substrates in the batch medium are not considered here. Y_{SP} and Y_{NP} are shown as function of the total specific power consumption in Figure 3.6.

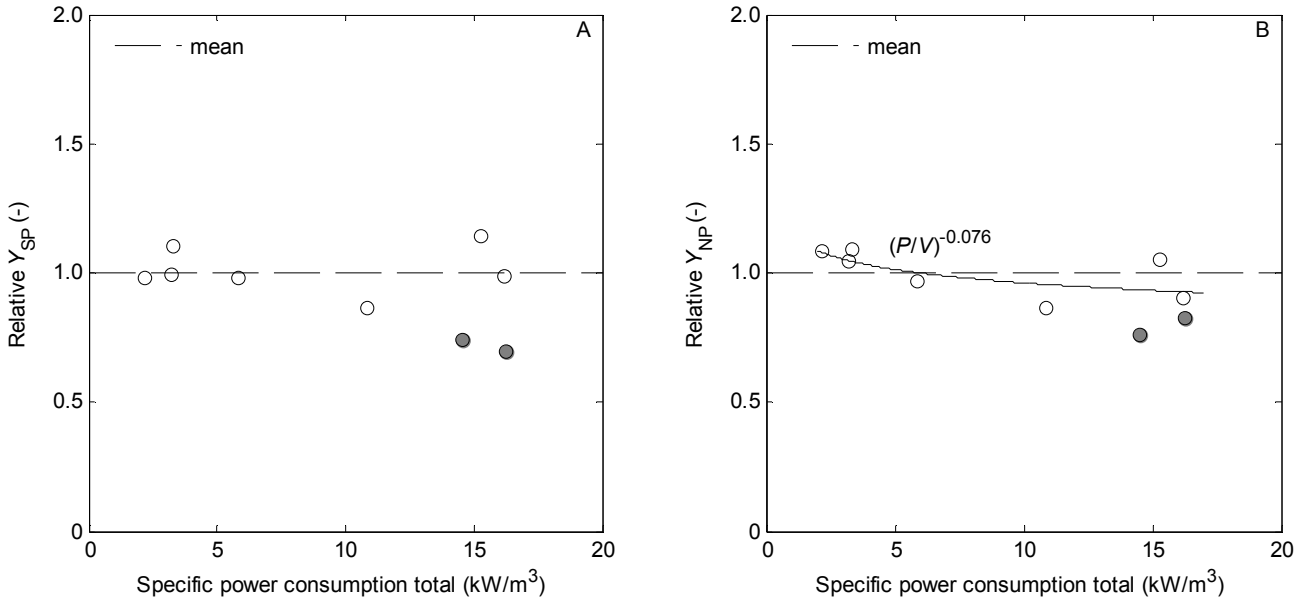

Figure 3.6. **A:** Relative Y_{SP} shown as function of total specific power consumption. The mean value of all nine fermentations is used in the model of Chapter 2. There is no relation between Y_{SP} and P/V. **B:** Relative Y_{NP} shown as function of total specific power consumption. A slightly inverse relation between Y_{NP} and P/V is seen (R^2 = 0.45)

For Y_{SP} no relation with the total specific power consumption is seen. For Y_{NP} an inverse relation with the total specific power consumption is observed. Like Y_{OP}, Y_{SP} and Y_{NP} are shown as function of average DCM in Figure 3.7. No relation is observed between Y_{SP} and the average DCM either, which suggests that in this case not much carbon is used in the maintenance metabolism even at low growth rates. This implies that it is reasonable to assume a constant yield coefficient for product on the carbon substrate. The standard deviation from the mean value is 9.0%.

For Y_{NP} there seems to be a relation with the average DCM (negative exponent of -0.13 and R^2 = 0.55). The standard deviation from the mean value for Y_{NP} is however only 8.9% and it therefore is reasonable also to consider this yield coefficient constant.

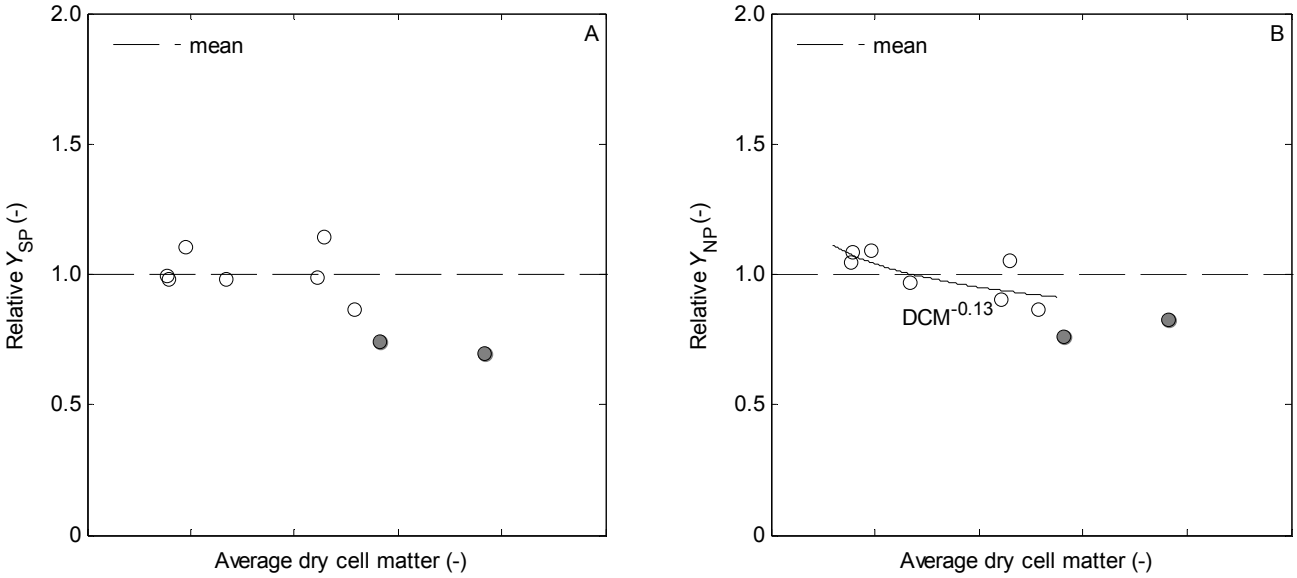

Figure 3.7. **A:** Relative Y_{SP} shown as function of average dry cell matter. There seems to be no relation between Y_{SP} and dry cell matter. Standard deviation from the mean value is 9.0% **B:** Relative Y_{NP} shown as function of average dry cell matter. An inverse relation between Y_{NP} and dry cell matter (R^2 = 0.55) is seen.

3.3 Conclusions

3.3.1 Productivity and oxygen transfer

Since the absolute values of the productivity and energy efficiency of product formation, EE_P, cannot be revealed, the oxygen transfer rate and the efficiency of oxygen transfer, EE_{O2}, are considered the key performance indicators of this process. It has been shown that OTR and EE_{O2} are strongly correlated with productivity and EE_P, and therefore these are equally good indicators of the process.

The data presented in Figure 3.1 and Figure 3.2 show that it is not possible to determine a single value of the four indicators from Table 3.1. Clearly, the performance and characteristics of the STR depends on the process conditions and the operating parameters. An inverse relationship between productivity and efficiency is observed for both product formation and oxygen transfer. For oxygen transfer, this is clearly expected from the exponents a and b of the k_La correlation in Eq. (2.30), since both of these are smaller than 1. This means that a smaller than proportional oxygen transfer increase is achieved when P/V or v_g is raised. Equally importantly, for this type of processes a high oxygen transfer rate leads to higher biomass concentration, higher viscosity, and thus a hindering of oxygen transfer.

One implication of the inverse relation between productivity and efficiency for this process in the STR is that the manufacturer has to choose where on the curve of Figure 3.2 “to be”. This choice is usually made early on in the design phase of the production plant when vessel volume, motor size,

and compressor pressure etc. are determined. However the operating conditions of most STRs can easily be changed, so that in times of excess production capacity the agitation or aeration intensity – and thereby also the overall productivity – is reduced, while the energy efficiency is increased.

The data collected from this process might be quite different to other data available in the literature due to differences in the media. Coalescence and viscosity of the medium highly influence the oxygen transfer. It should also be remembered that the power consumption considered in the literature is often only that delivered to the broth by the agitator.

3.3.2 Yield coefficients Y_{SP}, Y_{NP}, *and* Y_{OP}

The yield coefficients for product formation on carbon substrate, ammonia, and oxygen can be considered constant for the conditions used in this study. No or only very weak correlations were found between each of the coefficients and the specific power input and average DCM. The yield coefficients therefore cannot be used as key performance indicators for this process. The results suggest that the maintenance consumption of carbon substrate, ammonia, and oxygen is of minor importance for this process. This finding might be somewhat surprising if compared to the results of Table 2.4, where the maintenance coefficients were found to have high SRCs. However, that analysis in fact showed that uncertainty of the model developed in Chapter 2 is caused by the uncertainty concerning the value of the maintenance coefficients. The results of Chapter 3 do not contradict that conclusion; the results rather indicate that the maintenance coefficients for oxygen and substrate are quite small.

Chapter 4

Identification of alternative enzyme production technologies

Using current technology, large amounts of enzymes are needed if the ambitions of lignocellulosic ethanol and commodity chemicals are to come true. The United States congress set an annual goal of 16 billion gallons of cellulosic ethanol by 2022 along with 15 billion gallons of ethanol from conventional sources like corn starch (U.S.Congress, 2007). Currently, conversion of lignocellulosic biomass realistically results in approximately 80 gallons of ethanol per dry ton of feedstock, which corresponds to about 75% of the maximum theoretical conversion (Humbird et al., 2011). If an enzyme loading of 20 mg/g cellulose is assumed, approximately $1 \cdot 10^6$ kg of cellulase protein is needed annually in order to comply with the US ambitions (Humbird et al., 2011).

The work described so far in the thesis has been conducted at pilot plant scale, while the commercial production of enzymes will surely take place at very large scale, since the increase of production capacity is governed by the principles of the economy of scale. Collection of cost data for a wide range of plant construction has given rise to the so-called six-tenth factor, which means that as the plant capacity is doubled, the cost will only be $2^{0.6}$ higher (Votruba and Sobotka, 1992). The purpose of this chapter is to compare different enzyme production technologies that have been described in the literature and evaluate their potential as the platform for industrial enzyme production. The approach is to utilize the process model that has been constructed for *T. reesei* enzyme production in Chapter 2 and evaluate the fermentation technologies at large scale based on available knowledge for each technology.

The list of technologies is not exhaustive. Innumerable minor and major variations of fermentation technologies have been suggested, patented, and published. It is not the aim of this work to include all technologies that have ever existed; it is however the hope that the significant types of alternative technologies for enzyme production at the moment are covered. For more detailed descriptions of each technology in this chapter the reader is referred to books dealing entirely with the subject (Schügerl, 1991; Schügerl and Sittig, 1982).

4.1 Scale-up strategy

An enormous number of book chapters, reviews, and original papers have dealt with the subject of scale-up (Reuss, 1993). Scale-up of biotechnological processes is usually the final step in a research and development program leading to the large scale industrial manufacture of a biotechnological product by fermentation (Hewitt and Nienow, 2007). The term scale-up has become almost identical with the attempt to duplicate a seemingly optimal solution from small-scale fermentors in large scale aerated STRs (Charles, 1985). That task has proven to be very difficult, as the process of scaling up a fermentation system is often governed by a number of important engineering considerations and not simply a question of increasing culture and vessel volume (Hewitt and Nienow, 2007).

Scale-up can however also be the problem associated with the design of a fermentor or a production plant, assuming that the designer has the flexibility to select and develop a system to meet the process requirements (Reuss, 1993). This perception of scale-up fits well to the procedure presented here. The enzyme production fermentation described in Chapter 2 will be used as the reference process in a screening of technologies based on their energy efficiency. The following procedure for this screening was employed:

1. Oxygen transfer was assumed to be the rate limiting step of the process. Oxygen transfer was modeled using Eq. (2.2) and the logarithmic mean value for the driving force as shown in Eq. (2.18) was used.
2. Mass transfer data were obtained from the open literature for each technology and inserted in the process model. Preferably, mass transfer data collected in non-Newtonian media were used in order to access the influence of increasing viscosity on mass transfer. The viscosity model obtained in Chapter 2 was used to estimate the viscosity of the fermentation broth.
3. The process model of Chapter 2 including the DOT-controlled substrate feed flow was used to simulate the progress of the fermentation.
4. Geometric similarity was assumed and the operating conditions at large scale were equal or similar to the ones used to obtain the mass transfer data.
5. The fermentation length was the same for all technologies (between 100-200h). For proprietary reasons the exact fermentation length is not stated.
6. The fermentation vessel volume was iterated such that the total oxygen transfer at the fermentation end was equal for all technologies. The total oxygen transfer was in the range 10,000-30,000 kg but the exact amount is not revealed for proprietary reasons. The vessel volumes needed were in the range of 100 m^3.
7. The total energy consumption during fermentation was estimated as shown in Chapter 2.

Since product formation is proportional to oxygen transfer, this procedure ensured that an equal amount of product was formed for each technology. Mixing was not quantitatively considered in this procedure, since this process could not be predicted at other scales for all technologies. The

scale-up procedure described here thus includes a constant DOT as this is the way the fermentation process is controlled, while other parameters such as superficial gas velocity, k_La, and OTR might vary significantly from the laboratory experiments. This is only natural since completely different conditions are often provided at large scale (Garcia-Ochoa and Gomez, 2009).

The technologies included in this chapter were subject to an assessment of their technical feasibility at large scale. Each technology was scored from 0-10; with 10 ranging as very high likelihood of successful implementation at large scale. Assessments of this kind are inherently subjective and the score given here should not be considered a "hard number".

4.2 Technology screening

Fermentation technologies are often grouped according to the primary method of energy input: energy input through expansion of compressed gas, energy input by means of liquid kinetic energy generated by a liquid pump, or energy input by mechanically moving agitators (Schügerl, 1991). This classification is also used here. Solid state fermentation is treated in a separate section, as this fermentation technology differs significantly from the other groups.

4.2.1 Power input by compressed gas

Mixing and mass transfer of these reactor types relies on compressed gas dispersed into the liquid through a sparger. The energy consumption of these reactors was determined as the sum of the energy consumption of the compressor calculated by Eq. (2.26) and the energy consumption for cooling by Eq. (2.28).

4.2.1.1 *Bubble column*

These reactors are only controlled by the aeration, which is usually supplied by a porous plate of a perforated ring at the bottom of the reactor (Schügerl, 1985). The dispersion of gas leads to density differences within the fluid body, which induces convective flows in the reactor sufficient enough for mixing and mass transfer for a variety of biotechnological processes (Lübbert, 2010). Bubble columns are often utilized when the medium has a viscosity only slightly higher than that of water and a commonly mentioned disadvantage is a limited top-to-bottom mixing in slender columns (Lübbert, 2010).

Bubble columns have however also been employed for fermentations of filamentous fungi such as *Penicillium chrysogenum* (Deckwer et al., 1982). The effect of apparent viscosity on mass transfer in a bubble column was also studied by Godbole et al. (1984) by testing various concentrations of carboxy methyl cellulose (CMC) solutions in a rather large bubble column. An overview of the conditions tested in the study is given in Table 4.1.

Table 4.1. Summary of experimental conditions for a bubble column (Godbole et al., 1984)

Property	Value
Vessel volume (m^3)	0.250
Operating volume (m^3)	0.183
Diameter (m)	0.305
Height (m)	3.4
Fluid	CMC solutions
Superficial gas velocity (m/s)	0.0025-0.25
k_La values (1/h)	72-144

The k_La values obtained in the study were sufficient for oxygen transfer of fermentations of filamentous fungi; however increasing viscosity was shown to have a large impact on k_La. The mass transfer correlation recommended was the following (Godbole et al., 1984)

$$k_La = 3.006 v_g^{0.44} \mu_{app}^{-1.01} \tag{4.1}$$

The mass transfer of Eq. (4.1) was inserted in the process model and a superficial gas velocity of 0.15 m/s was assumed. The simulation of the bubble column gave the following results

Performance indicator	Value
Oxygen transfer rate (kg $O_2/m^3/h$)	0.83
EE_{O2} (kg O_2/kWh)	0.18

The technical feasibility of the bubble column is indisputable. This type of reactor is widely used in large production scale for commodity products such as baker's yeast and citric acid (Lübbert, 2010). The technical feasibility at industrial scale was assessed at 10 on the scale from 0-10.

4.2.1.2 *Airlift reactor with internal loop*

This reactor type has a defined liquid flow directed by the geometry of the reactor or the reactor internals. The liquid flow is caused by a density difference between an aerated part of the liquid and a non-aerated part. In turn this driving force is caused by a difference in gas hold-up (Chisti and Moo-Young, 1987).

Airlift reactors exist in a variety of configurations. The reactor may have internal or external loops and may be fitted with internals such as static mixers (Chisti, 1989). Airlift reactors with various combinations of internal fittings such as draft tubes and perforated plates also exist (Fukuda et al.,

1978), and even mechanically agitated airlift reactors have been proposed (Chisti and Jauregui-Haza, 2002). In Table 4.2 a summary of the experimental conditions are given for a study of a simple internal loop airlift reactor with a central draft tube.

Table 4.2. Summary of experimental conditions for a internal loop airlift reactor (Barker and Worgan, 1981)

Property	Value
Vessel volume (m^3)	0.140
Operating volume (m^3)	0.100
Diameter (m)	0.30
Height (m)	2.00
Fluid	0-1 % (w/v) starch solution
Riser superficial gas velocity (m/s)	0.018-0.069
k_La values (1/h)	40-100

Increasing viscosity was shown to lead to a decrease of k_La and different broth viscosities were tested, but no general relationship between k_La and viscosity was found (Barker and Worgan, 1981). The mass transfer correlation recommended by Barker and Worgan (1981) for the gas-air system was the following

$$k_La = 853 v_{g,r}^{0.78} \tag{4.2}$$

In order to incorporate the anticipated influence of increased viscosity, in the simulation of the airlift reactor with this geometry, a 25% smaller constant was assumed, and thus the constant of Eq. (4.2) was set to 640. The airlift simulation was carried out using $v_{g,r} = 0.069$ and gave the following results

Performance indicator	Value
Oxygen transfer rate (kg $O_2/m^3/h$)	0.54
EE_{O2} (kg O_2/kWh)	0.40

This type of reactor is popular; its use is widespread and it is used for microorganism, plant and animal cell cultivation (Blenke, 1979; Hatch, 1975; Schügerl, 1991; Sittig, 1982). The technical feasibility at industrial scale was assessed at 9.

4.2.1.3 *The pressure cycle reactor*

A noteworthy variation of the airlift reactor with internal loop is the so-called pressure cycle

reactor. In Billingham, England, Imperial Chemical Industries constructed a very well known and very large reactor of this type with an operating volume of about 1500 m^3, see Figure 4.1 (Westlake, 1986). The reactor was constructed for single cell protein fermentation of the species *Methylophilus methylotrophus*. The organism was grown in a medium containing methanol as the sole carbon substrate (Westlake, 1986). The process was run with a high cell mass concentration and in order to match the biological kinetics, an extremely high oxygen transfer rate of approximately 10 kg $O_2/m^3/h$ was required (Hines et al., 1975). Under pressure, this can be achieved by intense mechanical agitation in small vessels, but is prohibitive in power consumption for large scale equipment (Hines et al., 1975). For this reason an airlift fermentor was developed in which the air for biological oxidation also provided the liquid circulation (Hines et al., 1975).

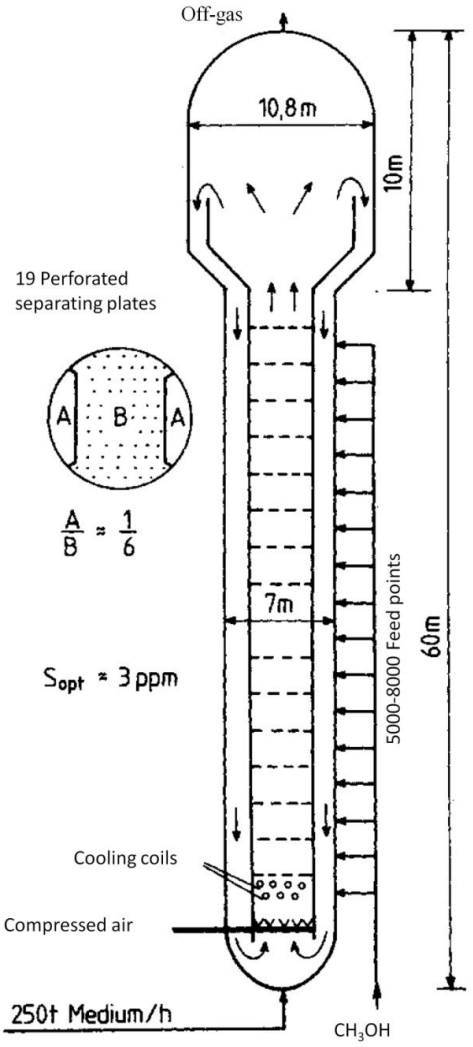

Figure 4.1. Pressure cycle fermenter. Reprinted from Schügerl (1983) with permission from John Wiley and Sons, Inc.

The reactor had an inner diameter of 7 m and was 60 m tall; thus the operating ungassed liquid height would have been around 40 m. The top of the fermentor was widened to enable the gas

bubbles to separate from the ascending liquid stream before the liquid returns in the downcomer zones (Smith, 1980). The reactor contained an internal draft tube for the aerated section, and in order to reduce the liquid velocity perforated plates were mounted in this section. The difficulty of the operation of such a large reactor with fast-growing bacteria is that of maintaining the supply of power, oxygen, and substrate while still ensuring their uniform distribution in the reactor (Schügerl, 1991). The air was claimed to be added with a pressure of 6 bar at the base of the fermentor, whilst CO_2 is drawn off at the top with a pressure of about 3 bar (Westlake, 1986). However, this does not fit together with a liquid height of at least 40 m. The distribution system of the toxic methanol substrate was attached to the 19 perforated plates, and uniform distribution was accomplished by having 5000-8000 injection points throughout the height of the fermentor (Schügerl, 1991). This means that the oxygen demand created by the methanol injection was primarily in the riser of the fermenter.

Before dealing with the energy consumption of this reactor type, the biological aspects of the technology are worth considering. The fermenting mass is circulated between areas of high and low pressure driving the liquid circulation (Smith, 1980). The ability of the micro organism to withstand these changes in physiological conditions was tested in laboratory scale, but it is specifically stated that the distinct design of the reactor was unlikely to be suitable, without further research and design, for other fermentations (Smith, 1980).

There seems to be disagreement over the energy consumption of the reactor. The energy dissipation rate of the reactor was claimed to be 1.6 kW/m^3 by Westlake (1986), while the oxygen transfer efficiency stated by Hines et al. (1975) was 1.5 kg O_2/kWh with an OTR of 10 kg O_2/m^3/h. This corresponds to a specific energy consumption of 6.6 kW/m^3. The aeration rate of the reactor has been stated to be 93000 Nm^3/h (Schügerl, 1983). If the pressure at the bottom of the reactor is assumed to be 6 bar, the power consumption of the compressor estimated using Eq. (2.26) is 9,300 kW. With a liquid volume of 1500 m^3 this corresponds to 6.2 kW/m^3, which is close to the number of Hines et al. (1975). However, the aeration rate of 93000 Nm^3/h corresponds to a mean superficial gas velocity of 0.225 m/s (based on the total reactor cross-sectional area), which means that the power input per unit liquid is about 2.2 kW/m^3 (Chisti and Moo-Young, 1987). This number is in turn very close to that of Westlake (1986). This kind of seemingly divergent data is a general problem that will be examined closer in a later chapter of this thesis.

The mass transfer coefficient achieved in the reactor can be estimated using Eq. (2.2). If the mass transfer is assumed to take place throughout the height of the fermentor, the average pressure in the fermenter is assumed to be 4 bar, and DO of the medium is set to zero one obtains (Schügerl, 1991):

$$k_L a = \frac{\mathrm{OTR}}{\mathrm{DO}^*} = \frac{10\ \left(\mathrm{kg\ O_2/m^3/h}\right)}{4 \cdot 0.008\left(\mathrm{kg\ O_2/m^3}\right)} = 313\ \left(1/\mathrm{h}\right) \tag{4.3}$$

By use of the process conditions from the above discussion of the pressure cycle reactor, a simulation based on this technology was completed. The impact of increasing viscosity could not be determined. The pressure cycle reactor has a high oxygen transfer rate, but in this simulation it did not match the 10 kg $O_2/m^3/h$ mentioned in the literature, since the simulated reactor was shorter and thus the driving force for oxygen transfer was smaller. The simulation was performed assuming only a headspace pressure of 0.5 barg; otherwise the partial pressure of CO_2 was unacceptably high. The following results were obtained

Performance indicator	Value
Oxygen transfer rate (kg $O_2/m^3/h$)	2.17
EE_{O2} (kg O_2/kWh)	0.31

The technical feasibility of the reactor has been proven on a very large scale, but its complex design with many feeding points is not desirable from a sanitary point of view. Furthermore the fermenter height and slenderness potentially involve unacceptably high levels of pCO_2. The technical feasibility at industrial scale was assessed at 5.

A variant of the pressure cycle reactor was also designed and operated for use in the sewage and effluent treatment business and sold under license with the trade name “Deep Shaft” (Smith, 1980; Walker and Wilkinson, 1979). It has not been possible to obtain data for this type of reactor for this comparison. However, its large volume and thin design (the depth was in the range 50-150 m (Schügerl, 1985)) makes it a questionable candidate for other purposes than waste-water treatment.

4.2.1.4 *Airlift reactor with external loop*

A 1000-tons per year single cell protein reactor of this type was constructed as a pilot scale fermentor by Imperial Chemical Industries (Gow et al., 1975). However, no construction and operational data were published on the unit.

The mass transfer capability of an airlift reactor with external loop was improved by insertion of static mixers in the riser section of the reactor (Chisti et al., 1990). The plastic static mixer elements were fitted inside the tube of the riser with the intension of increasing the surface for gas-liquid transfer by physically breaking down larger gas bubbles into smaller ones (Chisti et al., 1990). The energy needed for the break-up of bubbles in static mixers was delivered by a pressure drop through the loop. The mass transfer in different CMC solutions was studied, and it was found that for highly viscous fluids the viscosity did not permit sufficiently rapid fluid circulation and the reactor became stagnant (Chisti et al., 1990). For highly viscous fluids the use of static mixers therefore also requires the use of a liquid pump to force circulation in the loop (Chisti et al., 1990).

Table 4.3. Summary of experimental conditions for a external loop airlift reactor with static mixers (Chisti et al., 1990)

Property	Value
Vessel volume (m^3)	0.0149
Operating volume (m^3)	0.0120
Diameter, riser (m)	0.050
Diameter, downcomer (m)	0.075
Height (m)	1.8
Fluid	0-0.6 % (w/v) CMC solution
Riser superficial gas velocity (m/s)	0.02-0.08
k_La values (1/h)	4-108

Increasing viscosity was shown to result in a decrease of k_La as expected for this technology. The data for the 0.2% (w/v) CMC are reported here, since this CMC concentration was most similar to the medium of *T. reesei* fermentations. The mass transfer correlation recommended by Chisti et al. (1990) for the 0.2% (w/v) CMC solution was the following

$$k_La = 241 v_{g,r}^{0.83} \tag{4.4}$$

For the simulation of this technology an aspect ratio of 15 was used and a riser superficial gas velocity of 0.06 m/s. The increasing viscosity of the fermentation broth was simulated, but this did not affect mass transfer since this is not included in Eq. (4.4). The simulation gave the following results

Performance indicator	Value
Oxygen transfer rate (kg $O_2/m^3/h$)	0.16
EE_{O2} (kg O_2/kWh)	0.12

Highly viscous fermentation broths may not be possible to circulate through the static mixers without the aid of a liquid pump. Furthermore the static mixers might impose serious sanitary problems. The technical feasibility at industrial scale was assessed at 5.

4.2.1.5 *Gas fluidized bed reactor*

Baker's yeast has been grown aerobically in the form of solid particles in reactors known as gaseous fluidized beds (Schügerl, 1985). In such beds, air would be used to fluidize the solid yeast particles and to supply the oxygen necessary for aerobic growth, while the concentrated nutrient solution is

sprayed above the bed surface (Mishra et al., 1982). This system possibly eliminates the requirement for cooling, and drying of the yeast could take place in the production vessel (Mishra et al., 1982). However, only low growth rates could be realized and the technology was found noncompetitive for industrial biomass production (Mishra et al., 1982).

Since this technology differs significantly from the submerged fermentation type used for the industrial enzyme production, no further investigation of these reactor types was made. Whether *T. reesei* could grow in the form of solid particles and maintain its high secretion of proteins is not known.

4.2.2 Power input by liquid circulation

This type of reactor requires a loop in which the liquid is accelerated. The kinetic energy produced is then used to disperse the gas in the reactor, providing the mixing and mass transfer needed for successful fermentation (Schügerl, 1991). Pump efficiencies are in the range 0.75-0.95; in this section the pump efficiency is assumed to be 0.80 (Schügerl, 1985). Cooling may be achieved by a heat exchanger in connection with the loop and thus internal cooling coils of the reactor may be avoided.

4.2.2.1 *Plunging jet reactor*

A nozzle is directed downwards and a liquid jet hits the liquid surface of the fermentor vessel, which plunges into the liquid taking some of the surrounding air with it (Schügerl, 1991). An example of the set-up is given in Figure 4.2, where a two-phase jet is produced in the nozzle (6) dispersing the gas in the liquid phase. The mass transfer in the system is largest between the bubbles dispersed in the pool liquid (Schügerl, 1991)

The main variables are the distance between the nozzle and the liquid pool surface, the pool geometry, and the angle of jet inclination from the vertical position (Schügerl, 1985). A 20 m^3 plunging jet reactor has been used to produce single cell protein from whey (Moebus and Teuber, 1979), however the main application of the reactor is in waste-water treatment (Schügerl, 1985).

The production of xanthan was studied in the plunging jet reactor depicted in Figure 4.2 by Zaidi et al. (1991). A summary of the experimental conditions of the study is given in Table 4.4. The effect of the power input on mass transfer was studied at the end of a fermentation, where the viscosity of the broth was approximately 0.2 Pa.s (with a shear rate of 80 1/s). The influence of different aeration rates was not studied.

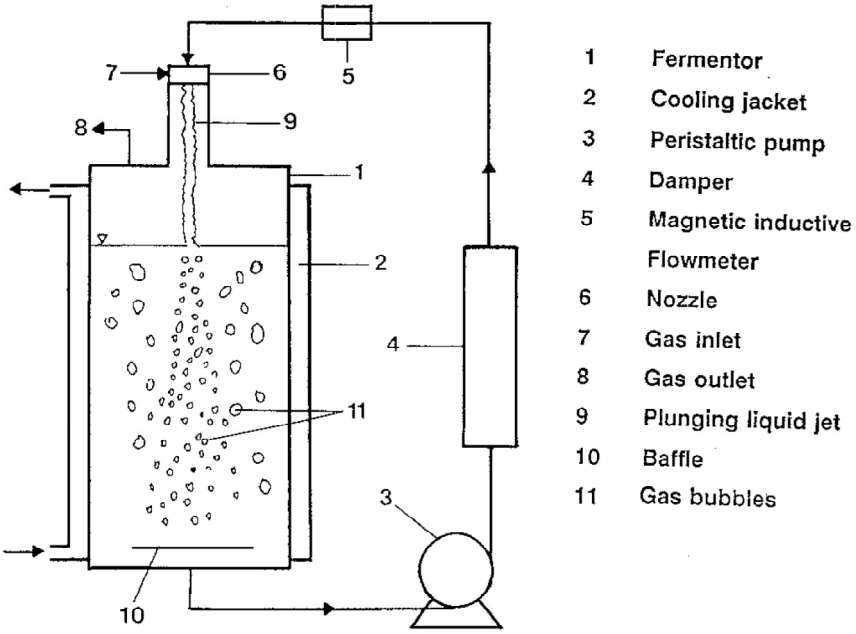

Figure 4.2. Experimental set-up for xanthan production in a plunging jet reactor by Zaidi et al (1991). Figure reprinted with permission from Springer.

Table 4.4. Summary of experimental conditions for a plunging jet reactor (Zaidi et al., 1991)

Property	Value
Vessel volume (m^3)	0.100
Operating volume (m^3)	0.040-0.080
Diameter, vessel (m)	0.40
Height (m)	0.8
Pump power input (kW/m^3)	0.07-0.5
Fluid	xanthan fermentation broth
Vessel superficial gas velocity (m/s)	0.003
k_La values (1/h)	32-83

The mass transfer correlation obtained for the system was the following

$$k_{\mathrm{L}}a = 111\left(\frac{P}{V}\right)^{0.45} \tag{4.5}$$

In order to simulate the plunging jet reactor it was assumed that multiple jets are used simultaneously. No data on the pressure in the external loop were given, so the minimum outlet

pressure for the gas compressor was assumed to be 1 barg. The superficial gas velocity was assumed to be 0.06, which is however larger than the range of the study, but this is a natural consequence of scale-up. Fermentation broths of *T. reesei* probably have lower viscosity than the xanthan fermentation broth, so the energy efficiency for *T. reesei* might be higher than predicted here. The simulation gave the following results

Performance indicator	Value
Oxygen transfer rate (kg $O_2/m^3/h$)	0.60
EE_{O2} (kg O_2/kWh)	0.13

The technical feasibility for this system has been proven for pilot scale fermentations of *Xanthomonas campestris*. The fitting of multiple jets in a large reactor might be associated with technical difficulties and mixing limitations. How other filamentous fungi are impacted by the pump and pressure drop in the nozzle is not known. The technical feasibility of the technology is set to 6.

4.2.2.2 *Rotating jet heads*

Jets are a well known low power input alternative for mixing in large tanks and are also used in waste-water treatment and in storage tanks to avoid stratification (Revill, 1985; Schügerl, 1980). This reactor system is a special kind of jet nozzle reactor developed based on a “cleaning in place” machine produced by Toftejorg, Denmark. A liquid stream is taken out of the reactor and recirculated into the reactor along with gas. In stationary jet systems the flow patterns are constant which may lead to stagnant zones in the tank resulting in compartmentalization and poor mixing in the tank (Kold, 2010). In this system the recirculated fermentation broth is distributed by four nozzles into the tank, while the pressure of the incoming liquid drives a turbine that via a gearing system, makes the “head” rotate around both the horizontal and the vertical axes (Nordkvist et al., 2008). The jets of mixed recirculated fermentation broth and gas continuously change direction and are thus designed to cover the entire reactor volume.

In a recent study, Kold (2010) investigated mass transfer of a rotating jet head during fermentation of *X. campestris*. The experimental conditions of the study are shown in Table 4.5.

Table 4.5. Summary of experimental conditions for a rotating jet head (Kold, 2010)

Property	Value
Vessel volume (m^3)	0.310
Operating volume (m^3)	0.300
Diameter, vessel (m)	0.750
Height (m)	0.750
Pump power input (kW/m^3)	0.4-4.2
Fluid	xanthan fermentation broth
Vessel superficial gas velocity (m/s)	0.001-0.005
k_La values (1/h)	132-180

No complete mass transfer correlation could be derived for the system. However the individual influences of increased power input by the pump P/V, the reactor superficial gas velocity, and the increasing viscosity was estimated. The apparent viscosity studied was in the range 0.004-0.011 Pa.s, while there was very little variation in the superficial gas velocity. The correlations between the variables were found to be

$$k_La \propto \left(\frac{P}{V}\right)^{0.122} v_g^{\ 0.4} \mu_{app}^{\ -0.8} \tag{4.6}$$

In order to simulate the rotating jet heads it is assumed that multiple devices can be fitted inside an industrial scale reactor and provide the same mass transfer efficiency. The power input of the pump was set to 1.0 kW/m^3, which corresponds to a pressure increase of 1.5 barg in the external loop, which is the minimum outlet pressure for the gas compressor (Kold, 2010). The superficial gas velocity was assumed to be 0.06, which is however larger than the range of the study by Kold (2010), but this is a natural consequence of scale-up. The simulation gave the following results

Performance indicator	Value
Oxygen transfer rate (kg $O_2/m^3/h$)	0.91
EE_{O2} (kg O_2/kWh)	0.18

The technical feasibility for this system has been proven for pilot scale fermentations of *A. oryzae* and *X. campestris*. To my knowledge it has not been proven for commercial fermentation of filamentous fungi. The fitting of multiple rotating jet heads in a larger reactor might be associated with technical difficulties. Furthermore, how other filamentous fungi are impacted by the pump and

pressure drop in the rotating jet head is yet to be determined. The technical feasibility of the technology is set to 6.

4.2.2.3 *Pumped loop reactor with static mixers*

This type of fermentor is a pumped loop type reactor with static mixers, which bears resemblance to the airlift reactor with external loop. An example of this reactor type is shown in Figure 4.3. A circulation pump is installed in the loop to ensure the flow through the static mixers. This reactor type has been used for xanthan production with a high viscosity fermentation broth (Olivier and Oosterhuis, 1988).

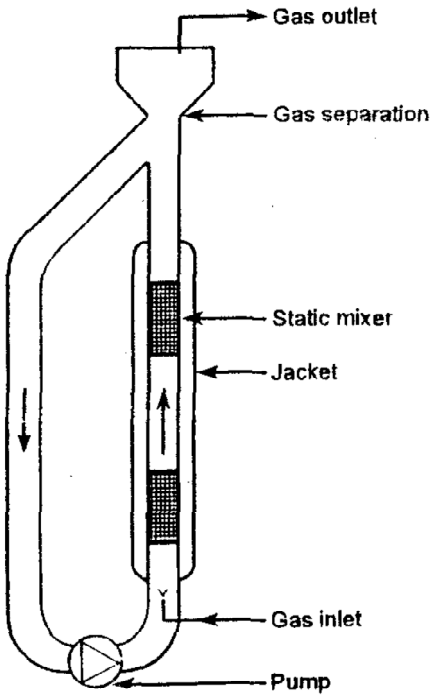

Figure 4.3. Pumped loop reactor with static mixers in the riser section. A mechanical pump is inserted in the loop for the circulation of the fermentation broth. Gas is fed into the loop before the static mixers where the bubbles are dispersed for a larger total interfacial area. Figure reprinted from Meesters et al (1996) with permission from Springer.

The performance of a pumped loop reactor with static mixers has been studied in a 4 m^3 fermentor with the experimental conditions shown in Table 4.6. The reactor had an inner tube diameter of 0.5 m and was equipped with Sulzer SMV mixers. In the mixers a swarm of bubbles and a large, continuously renewed interfacial surface are formed (Streiff et al., 1997).

Table 4.6. Summary of experimental conditions for a pumped loop reactor with static mixers (Olivier and Oosterhuis, 1988)

Property	Value
Vessel volume (m^3)	4.0
Tube diameter (m)	0.5
Height (estimated) (m)	5
Fluid	xanthan fermentation broth
P/V (kW/m^3)	4.3-4.5
v_g (m/s)	0.06-0.14
v_l (m/s)	0.4-1.2
k_La values (1/h)	15-130

Sulzer, a manufacturer of static mixers, has studied the properties of their mixers in dept. For liquid-liquid and gas-liquid dispersion the drop sizes and drop size distributions have been studied in a spectrometer drop size analyzer, and correlations for drop size and mass transfer have been published (Streiff et al., 1997). The mass transfer coefficient is mainly a function of the specific energy dissipation caused by the pressure drop in the static mixer (Streiff et al., 1997)

$$k_La \propto \left(\frac{P}{V}\right)^{0.766} \tag{4.7}$$

The mass transfer correlation obtained by Olivier and Oosterhuis (1988) was however based on superficial gas velocity in addition to the liquid velocity

$$k_La = 245 v_l^{1.5} v_g^{0.5} \tag{4.8}$$

This mass transfer correlation can be used for the scale-up estimation of a pumped loop reactor, since the power input for the circulation pump was also given (Table 4.6). The power consumption for aeration is also included in this simulation. The superficial liquid velocity was assumed to be 1.2 m/s with an average vessel power input from the pump of 4.3 kW/m^3, and the superficial gas velocity was assumed to be 0.25 m/s, which could be realistic for large scale equipment. The fermenter was assumed to have an aspect ratio of 10. The viscosity of the xanthan fermentation broth was higher than that of a typical *T. reesei* fermentation, so a slightly better oxygen transfer should be expected. The scale-up simulation of the pumped loop reactor had the following results

Performance indicator	Value
Oxygen transfer rate (kg $O_2/m^3/h$)	0.96
EE_{O2} (kg O_2/kWh)	0.09

The OTR of this simulation is very similar to the maximum OTR of 0.94-1.27 kg/m^3/h obtained by Olivier and Oosterhuis (1988), but the EE_{O2} is about half of the range 0.21-0.30 kg O_2/kWh recorded in that study. This is most likely because the pump efficiency and power consumption of the compressor is included in this work. Compared to a STR, the pumped loop reactor produced considerably higher concentrations of xanthan at similar power inputs (Olivier and Oosterhuis, 1988). It could be hypothesized that mixing, not mass transfer, was limiting in those STR experiments, which would not be unexpected for highly non-Newtonian fluids. That would also explain why the pumped loop reactor performed better in that study.

The pumped loop fermentor has been used for fermentations of yeast and production of xanthan at scales of at least 4 m^3, so the technology seems feasible (Meesters et al., 1996; Olivier and Oosterhuis, 1988). It is not known how different micro organisms are impacted by the technology, and the static mixers could impose sanitary problems. The technical feasibility at industrial scale was assessed at 7.

4.2.3 Power input by mechanically moved internal devices

The stirred tank reactor – certainly the most well-known example of this reactor category – became the standard bioreactor in the last half of the twentieth century (Schügerl, 1985). However, a great number of alternative reactors in this category have been developed. The energy consumption for these reactors includes the mechanical power by the moving device, the energy consumption for the compressor, and the energy for cooling.

4.2.3.1 *Reactor with mechanical agitators*

The STR falls into this category. The STR is naturally included in the comparison since the experiments in Chapter 2 were carried out using this reactor type. It therefore might be regarded as the reference technology. Recent developments of the STR include new impeller types with improved gas handling capabilities (Albaek et al., 2008; Nienow, 1996). In our study of the fed-batch *A. oryzae* fermentation, the k_La measurements of the RDT and the B2 impellers could not be distinguished at equal power input (Albaek et al., 2011).

The mass transfer correlation of Eq. (2.30) is used. This correlation was determined over a wide range of conditions and in fermentation medium but solely at pilot plant scale. Contradictory reports on the effect of scale on the exponents *a* and *b* of the mass transfer correlation exist. It has been claimed that both *a* and *b* decrease as function of fermentor size (Bartholomew, 1960), but it has

also been shown that a single value of b described k_La data from 0.55 m^3 to 80 m^3 with for a wide range of P/V (Pedersen, 1997).

A simulation using the process model and mass transfer correlation proposed in this work assuming P/V = 3 and a superficial gas velocity of 0.08 m/s was carried out. The simulation gave the following results at industrial scale

Performance indicator	Value
Oxygen transfer rate (kg $O_2/m^3/h$)	1.33
EE_{O2} (kg O_2/kWh)	0.13

The technical feasibility of the STR in large scale has been proven by many industrial manufactures. The technical feasibility is 10.

4.2.3.2 *Mechanically stirred loop reactor*

This type of reactor is similar to the STR but has an internal coaxial cylinder (draft tube) in order to create a defined circulation pattern of the fermentation broth. The introduction of the draft tube was aimed at improving the performance of the STR by providing a more homogeneous reactant distribution (Kura et al., 1993). No quantitative data on the influence of viscosity were given, but experimental data obtained in water as well as small amounts of polyethylene oxide were described by the same mass transfer correlation, because the high viscosity fluids required a higher specific power input (n was kept constant). A summary of the relevant parameters for this reactor type is shown in Table 4.7.

Table 4.7. Summary of experimental conditions and results for a mechanically stirred loop reactor (Kura et al., 1993)

Property	Value
Vessel volume (m^3)	0.050
Diameter (m)	0.35
Height (m)	0.60
Fluid	0-1000 ppm polyethylene oxide
P/V (kW/m^3)	1.8-5.8
v_g (m/s)	0.002-0.009
k_La values (1/h)	0.1-108

The mass transfer correlation found to best describe the experimental data was (Kura et al., 1993):

$$k_L a = 1.222\left(\frac{P/V + P_{air}}{P_{air}}\right)^{0.5} v_g^{1.0} \quad (4.9)$$

Since this study was carried out in a relatively small fermentor, the superficial gas velocities investigated were low. In simulations using the process model this leads to very high levels of CO_2 in the offgas. According to Eq. (4.9), $k_L a$ is proportional to the superficial gas velocity, and upon scale-up of this technology, high values of $k_L a$ will be predicted (if pCO_2 is to be held at an acceptable level). The scale-up simulation of the stirred loop reactor had the following results

Performance indicator	Value
Oxygen transfer rate (kg O_2/m^3/h)	0.62
EE_{O2} (kg O_2/kWh)	0.20

There has been a PhD thesis on the subject of relatively thin columns (H/T from 5-15) within this reactor category (Schügerl, 1991), but the data could not be retrieved for this technology. As this technology is quite similar to the STR, its technical feasibility is quite likely although the introduction of a draft tube makes the design for fed-batch operation more complicated. The technical feasibility at industrial scale was assessed at 8.

4.2.3.3 *Reactor agitated and aerated with gas-inducing impellers*

The impeller shaft of this reactor type is hollow and air is induced through holes in the impeller rather than introduced from a sparger located under the impeller. In some systems the stirrer automatically draws in air from the space above the liquid (Zlokarnik, 1978), or the gas might be provided through the shaft while liquid is sucked in through the impeller and the gas-liquid phase is released in a radial direction together (Poncin et al., 2002). Many variations of this reactor type exist, including internal draft tubes directing the fluid flow and aspect ratios up to 5 (Scargiali et al., 2007). This reactor type does not require a gas compressor, and has been claimed to have given higher $k_L a$ than other types of contactors at same unit power consumption in water (Chen et al., 2003).

A mass transfer correlation, which is very similar the ones found for the STR, for the self-aspirating impeller system has been suggested for a coalescence promoting media (pure water) (Zlokarnik, 1978)

$$k_L a = 1.1 \cdot 10^{-4}\left(\frac{P}{V}\right)^{0.8} \quad (4.10)$$

In a study of self-aspirating impellers with neutralized fermentation broth of *Aspergillus niger*, it

was found that an upper limit to the power input existed above which mass transfer was not increased (Heim et al., 1995). This speed, above with no additional air was aspirated, was found to be 7.39 1/s, which corresponded to 0.45 kW/m^3. The apparent viscosity at this speed was 0.003 Pa.s and k_La was 68 1/h, which was inferior to data for a conventional STR (Heim et al., 1995).

Mass transfer in this reactor was assumed to decrease with viscosity similarly to the STR since the principal mixing mechanism is the same. The following results were obtained upon scale-up by the process model

Performance indicator	Value
Oxygen transfer rate (kg O_2/m^3/h)	0.18
EE_{O2} (kg O_2/kWh)	0.29

The technical feasibility of the gas-inducing impeller is regarded as quite likely, since this contacting device has been used for a variety of applications (Zlokarnik, 1978). The technical feasibility at industrial scale was assessed at 8.

4.2.3.4 *Horizontal loop reactor with gas-inducing impellers*

This reactor type is also known as the Torus reactor and is made up of a horizontal, ring-shaped tube as shown in Figure 4.4 (Gschwend et al., 1983). A gas-inducing propeller provides the aeration and mixing of the medium, and the outlet gas is withdrawn through a foam destroyer. To my knowledge, no large scale versions of this reactor type exist despite the claims of superior performance for xanthan production (Krebser et al., 1988). A summary of the operating conditions used to obtain mass transfer data for this reactor is given in Table 4.8.

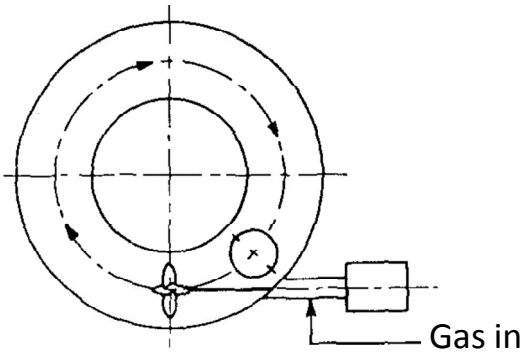

Figure 4.4. Example of a Torus reactor. Figure adopted from Adler and Fiechter (1988) with permission from Springer.

Table 4.8. Summary of experimental conditions and results for the Torus reactor (Krebser et al., 1988)

Property	Value
Vessel volume (m^3)	0.115
Operating volume (m^3)	0.075
Inner diameter (m)	0.50
Outer diameter (m)	1.0
Tube diameter (m)	0.25
Fluid	0-3 % (w/v) xanthan
P/V (kW/m^3)	3.5
Aeration rate (m^3/s)	0.00125
k_La values (1/h)	25-350

Since the power input was constant in the study, it is not possible to estimate the mass transfer as a function of P/V. However, at P/V = 3.5 kW/m^3 the influence of increasing viscosity is correlated with mass transfer in the following way

$$k_La = 34.72\mu_{app}^{-0.34} \tag{4.11}$$

The following results were obtained upon scale-up with the process model (the untraditional design was simulated in a cylindrical tank with aspect ratio of 0.16):

Performance indicator	Value
Oxygen transfer rate (kg $O_2/m^3/h$)	0.47
EE_{O2} (kg O_2/kWh)	0.11

The feasibility of the Torus reactor has not, to my knowledge, been proven on large scale. The design would probably require additional optimization, but mechanically it should be possible to construct and operate the reactor at a larger scale. The technical feasibility at industrial scale was assessed at 5.

4.2.3.5 *Cascade reactor with rotary agitators*

These reactors are slender columns separated into stages by perforated plates. The reactor is typically aerated in the bottom, while each stage is equipped with one or multiple agitators for mixing and gas dispersion (Schügerl, 1991). The following characteristics were found in a study of the a 9 stage reactor with a single flat bladed agitator per stage, unfortunately using a water-gas

system.

Table 4.9. Summary of experimental conditions and results for a the multistage reactor (Meister et al., 1979)

Property	Value
Vessel volume (m^3)	0.035
Operating volume (m^3)	0.032
Diameter (m)	0.15
Height (m)	2.00
Fluid	Water
P/V (kW/m^3)	0.5-1.5
Superficial gas velocity (m/s)	0.05-0.1
k_La values (1/h)	120-280

The mass transfer correlation for the water-gas system is provided below (Meister et al., 1979) The influence of viscosity was unfortunately not investigated.

$$k_La = 581.8\left(\frac{P}{V}\right)^{0.801} v_g^{0.248} \tag{4.12}$$

The influence of P/V for this reactor type is notably high compared to the STR. The stirrer type is similar to those used in STRs, so the concept is considered to be technically feasible. The reactor is however complicated by the internal plates, which might constitute a problem during cleaning and sterilization. The results of the up-scaled reactor (P/V = 0.5) were:

Performance indicator	Value
Oxygen transfer rate (kg $O_2/m^3/h$)	0.99
EE_{O2} (kg O_2/kWh)	0.25

The high aspect ratio of 12 for the reactor investigated leads to very high power consumption for the compressor, which counteracts the efficient mass transfer. The industrial scale reactor will be very tall, which might give significant problems with the construction of the reactor. The impact of viscosity is not known. The technical feasibility at industrial scale was assessed at 6.

4.2.3.6 *Reciprocating plate reactor*

These reactors have mixing elements (called plates) attached to an axially oscillating central shaft.

The element oscillates up and down by a crank-driven motor (Schügerl, 1991). The plates are perforated and liquid is forced through the holes as jets, which creates complex vortex movements ensuring the mixing. Air is fed at the base of the reactor, while the power consumption can be measured from a force transducer on the shaft. The reciprocating plate reactor has been investigated as the production vessel for microbial polysaccharides, where oxygen mass transfer is also crucial (Audet et al., 1996). The operation conditions of that study are shown in Table 4.10. Experiments were carried out in water and in aqueous solutions containing various concentrations of dextran, a complex branched glucan.

Table 4.10. Summary of experimental conditions for a reciprocating plate reactor (Audet et al., 1996)

Property	Value
Vessel volume (m^3)	0.014
Operating volume (m^3)	0.012
Diameter (m)	0.206
Height (m)	0.430
Fluid	0- 100 g/L dextran solution
P/V (kW/m^3)	0.7-5
Superficial gas velocity (m/s)	0.015-0.105

The mass transfer correlation for a 20 g/L non-Newtonian dextran solution is given here. The authors were not able to describe the mass transfer as a function of the apparent viscosity or the measured rheological parameters (Audet et al., 1996)

$$k_{\mathrm{L}}a = 4617\left(\frac{P}{V}\right)^{1.2\pm0.2} v_{\mathrm{g}}{}^{0.8\pm0.3} \tag{4.13}$$

Remarkably, for $P/V > 0.7$ kW/m^3, $k_{\mathrm{L}}a$ increases more than proportionally to the power input, a result not unusual for this type of reactor (Lounes et al., 1995). For the process simulation no effect of viscosity increase during fermentation was considered, but the mass transfer correlation of the non-Newtonian dextran solutions was used independently of fermentation time. The simulation results for $P/V = 1$ are given below

Performance indicator	Value
Oxygen transfer rate (kg O_2/m^3/h)	1.84
EE_{O2} (kg O_2/kWh)	0.41

The technical feasibility for this reactor type is questionable. The reactor is complicated by the upwards and downwards movement of the shaft. This requires sophisticated sealing technology if aseptic production is to be maintained. Cleaning of the internal parts of the reactor might also impose severe problems. The technical feasibility at industrial scale was assessed at 2.

4.2.3.7 *Pulsed baffled reactor*

This reactor is constructed as a slender column with horizontal baffles on the reactor wall with air being sparged in the bottom through a ring sparger. The column base is connected to a piston, which oscillates the system with amplitudes from 1-14 mm and frequencies from 1 to 12 Hz (Ni et al., 1995a; Ni et al., 1995b). The oscillations are intended to increase gas hold-up and thereby increase oxygen mass transfer. Different baffle geometries were tested in yeast culture medium and the best results are reported here.

Table 4.11. Summary of experimental conditions for a pulsed baffled reactor with mixed central and wall baffles (Ni et al., 1995b)

Property	Value
Vessel volume (m^3)	0.001
Operating volume (m^3)	0.0008
Diameter (m)	0.050
Height (m)	0.50
Fluid	resuspension of yeast
P/V (kW/m^3)	0-10
Superficial gas velocity (m/s)	0.0017-0.0068
k_La values (1/h)	50-250

The mass transfer correlation for the geometry with central baffles and wall baffles mixed together is given here. The influence of viscosity on mass transfer was not investigated.

$$k_La = 17500\left(\frac{P}{V}\right)^{0.353} v_g^{0.92} \tag{4.14}$$

The experiments with this reactor type were performed in relatively small scale and thus at very low superficial gas velocities. The impact of superficial gas velocity therefore might be overpredicted when applied in a scale-up of the process. The simulation results for P/V = 1 and superficial gas velocity of 0.016 m/s are given below

Performance indicator	Value
Oxygen transfer rate (kg $O_2/m^3/h$)	0.81
EE_{O2} (kg O_2/kWh)	0.38

The technical feasibility for this reactor type is highly questionable. The movement of the system might be feasible for a laboratory reactor, but if the amplitude of the movement is also subject to scale-up, a very complicated mechanical design is required. The technical feasibility at industrial scale was assessed at 1.

4.2.3.8 *Other reactor types with mechanical energy input*

A number of different surface aerators are used – allegedly exclusively - in biological effluent treatment (Schügerl, 1991). These technologies are used in relatively slow systems and have their advantages at power inputs over the range P/V = 0.01-0.2 kW/m^3 (Schügerl, 1991). Usually such technologies cannot be operated under aseptic conditions and therefore they were not included in this screening. Also horizontal reactors with internal paddle wheels have been developed especially for aeration of inhomogeneous fluids and waste water treatment applications (Zlokarnik, 1975), for example the rotating biological contactors. Horizontal reactors with paddle wheels now seem to have found use in cultivation of microalgae (Grima et al., 2009), but other commercial utilization of this reactor type related to fermentation is not described in the open literature to my knowledge. Therefore this technology was not investigated further in this screening.

4.2.4 Solid state fermentation

Solid-state fermentation (SSF) involves the growth of microorganisms on moist solid particles where the spaces between the particles contain a continuous gas phase and a minimum of visible water (Mitchell et al., 2006). Traditionally SSF has been used in the production of fermented foods and in the composting process. In the food industry in Asia SSF is the state-of-the-art technology, and enzymes and metabolites are produced on a large scale by processes with a very long history (Hölker and Lenz, 2005).

The comparison of SSF and submerged fermentation is difficult due to the large density difference. It has been generally claimed that enzyme titers are higher for SSF than for submerged fermentation when comparing the same strain and fermentation broth (Viniegra-González et al., 2003). However, no established scale or method to compare product yields in SSF and submerged fermentation in

true terms exist (Pandey, 2003), and the definition of "productivity" is often very different from study to study (Hölker et al., 2004).The volumetric productivity of submerged fermentation may be measured in activity per liter, while compared with the volumetric productivity of SSF in activity per g (Tengerdy, 1996). As is often the case, there might be a trend for researchers to have a biased view on SSF.

SSF is said to simulate the natural environment of filamentous fungi and should therefore be a better choice for cultivation because evolution of higher fungi took place on solid growth substrates (Hölker et al., 2004). On the other hand, since research with submerged fermentation accelerated in the 1940s because of the necessity to produce antibiotics on a large scale (Hölker and Lenz, 2005), very efficient microbial strains well adapted to submerged fermentation have been developed (amongst other ways) by genetic engineering (Hölker et al., 2004). When considering the SSF as an alternative to submerged fermentation it should be noted that submerged fermentation is often an "easier" system to work with (Mitchell et al., 2006). The handling of liquid substrates instead of moving solids and the better possibility for applying measurement and control are among the advantages of submerged fermentation systems.

In this work, SSF has not been included in the technology comparison. The reference process utilized a strain of *T. reesei* which has clearly been optimized and selected for high enzyme expression in submerged fermentation systems. To objectively compare SSF and submerged fermentations, the technologies should be equally developed. It is possible that further development within large scale operations of SSF will lead to commercial production of industrial enzymes including cellulases (Mitchell et al., 2006). A separate project might be needed to follow up looking specifically at the potential application of SSF.

4.3 Results and discussion

The results of applying the mass transfer relationships to the process model are summarized for all technologies in Figure 4.5. The key performance indicator EE_{O2} is shown as function of the oxygen transfer rate, since the oxygen transfer rate is a measure of the required fermentor volume. The size of the bubbles in Figure 4.5 refers to the judgment of the technical feasibility of fermentation using the technology in industrial scale.

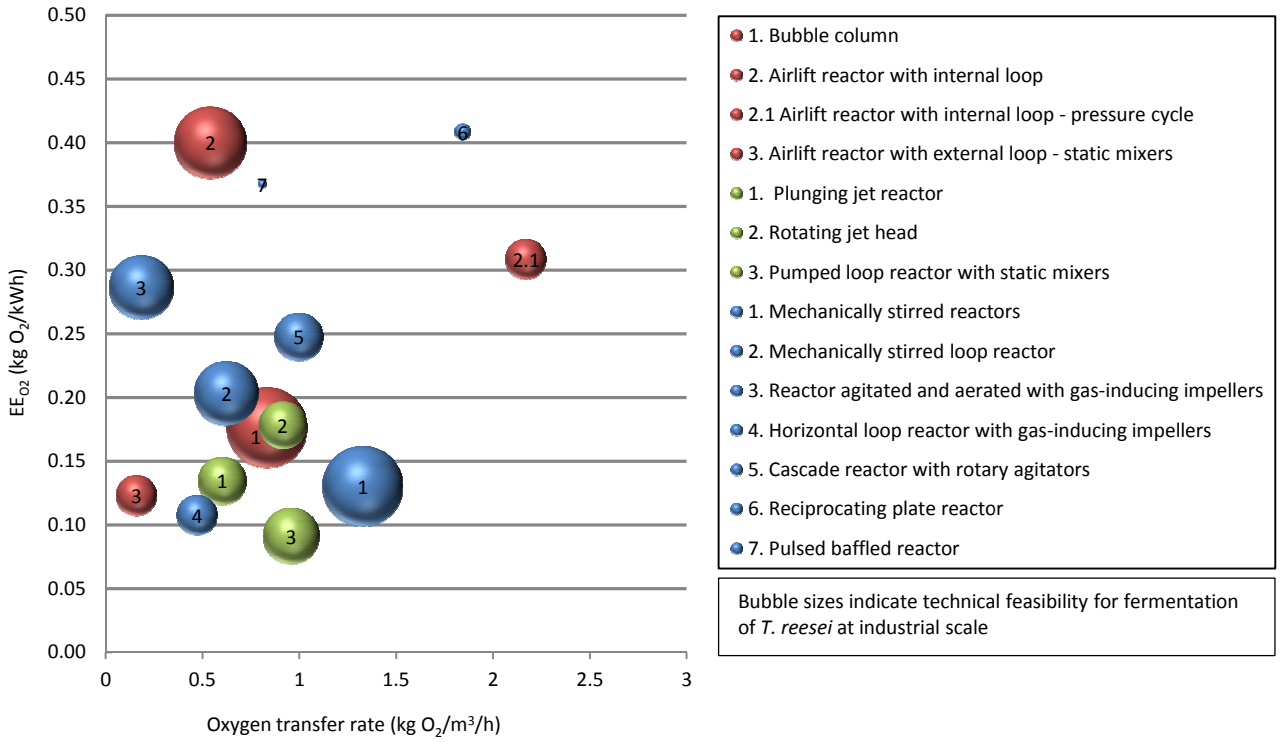

Figure 4.5. Technology screening using the *T. reesei* fed-batch fermentation process model. The EE_{O2} of the technologies is shown as function of oxygen transfer rate, while the bubble size refers to the technical feasibility of the technology at industrial scale. The highest EE_{O2} is predicted for the reciprocating plate reactor, which also provides a high oxygen transfer rate but has an unlikely feasibility at industrial scale. Airlift reactors are predicted to have high EE_{O2} and have been proven to be feasible at very large scale.

The highest energy efficiency was predicted for the reciprocating plate reactor, which also had a high oxygen transfer rate. However, the mechanical challenges of this technology are overwhelming and the technology is not considered an alternative in large scale, especially since the airlift reactor was predicted to have almost the same energy efficiency.

The pressure cycle reactor has the highest oxygen transfer rate, since it is operated with headspace pressure. The pressure cycle even had an EE_{O2} of 0.28, but since the mass transfer data was obtained in low viscosity fermentation broth, the viscosity of filamentous fermentation broth is expected to lower this number significantly.

The traditional stirred tank reactor is capable of delivering a high oxygen transfer rate, but not at the higher EE_{O2}. It was decided to investigate airlift reactors further, since they have the second highest EE_{O2} and have been employed for a range of large scale operations of fermentation processes. The oxygen transfer rate of airlift reactors is inferior to some other technologies but it is acceptably high.

An overview of the assessments of the technical feasibility of the technologies resulting from this screening is given in Table 4.12. The assessments are not definitive, and some technologies that are regarded questionable might already have proven their usefulness for industrial application. This does not however change the estimation of energy efficiency and oxygen transfer rates, which are the essential parameters applied here for comparison.

The screening procedure chosen here was seen as the most objective way to compare the fermentor technologies (Hatch, 1975). Mixing was not considered yet, as the oxygen transfer is assumed to be the limiting rate. A completely different approach for screening the reactor technologies would have been to evaluate the mixing capabilities of each reactor first and subsequently estimate the power consumption required for achieving sufficient mixing. The disadvantages of this approach however include that little information on the large scale mixing capabilities has been published for a number of these technologies. Furthermore, the impact of the (imperfect) mixing in the process and micro organism is not fully understood, and therefore this process is currently run with oxygen transfer as the limiting rate.

Table 4.12. Assessment of the technical feasibility for all technologies of the screening.

Technology	Technical feasibility at industrial scale
Bubble columns	10
Airlift reactors with internal loop	9
Airlift reactors with internal loop – pressure cycle reactor	5
Airlift reactors with external loop – static mixers	5
Plunging jet reactor	6
Rotating jet head	6
Pumped loop reactor with static mixers	7
Mechanically stirred reactors	10
Mechanically stirred loop reactors	8
Reactors agitated and aerated with gas-inducing impellers	8
Horizontal loop reactor with gas-inducing impellers	5
Cascade reactors with rotary agitators	6
Reciprocating plate reactors	2
Pulsed baffled reactor	1

.

Chapter 5

Airlift reactor experiments

Nine fermentations have been carried out using airlift technology. The objective of the airlift reactor experiments was to obtain data from this technology at pilot scale, to evaluate the feasibility of fermentations of *T. reesei* in airlift reactors, and revise the process model for the airlift reactor if needed. Specifically, the mass transfer and mixing characteristics were investigated and compared with available knowledge. The data collected from these experiments are used to increase the reliability of the model based scale-up of airlift reactors in Chapter 6.

5.1 Airlift reactor design

5.1.1 Reactor type and shape

Airlift reactors are pneumatically agitated gas-liquid or gas-liquid-solid contacting devices that are characterized by fluid circulation in a defined cyclic pattern through channels built specifically for this purpose (Merchuk and Gluz, 2002). The liquid pool is divided into two distinct zones, where only one of them is usually sparged by the gas (Chisti and Moo-Young, 1987). The different degrees of gas holdup in the gassed (riser) and ungassed (downcomer) zones result in a density difference which causes the circulation of the fluid by a gas-lift action. Airlift reactors can be divided into two main types of reactors based on their structure (see Figure 5.1): 1) Internal loop (or baffled) vessels in which strategically placed internal devices create the channels needed for circulation, and 2) external-loop reactors which have separate and distinct circuits for circulation. The simplest airlift reactor geometry is arguably the internal-loop split cylinder. External loops increase the risk of infections and the amount of material needed for construction. It was therefore decided to investigate the split cylinder internal loop airlift reactor due to the flexibility of the design: 1) the baffle system is more flexible than a tube because different geometries can easier be obtained, and 2) rectangular vessels are much harder to construct in a design that can be pressurized.

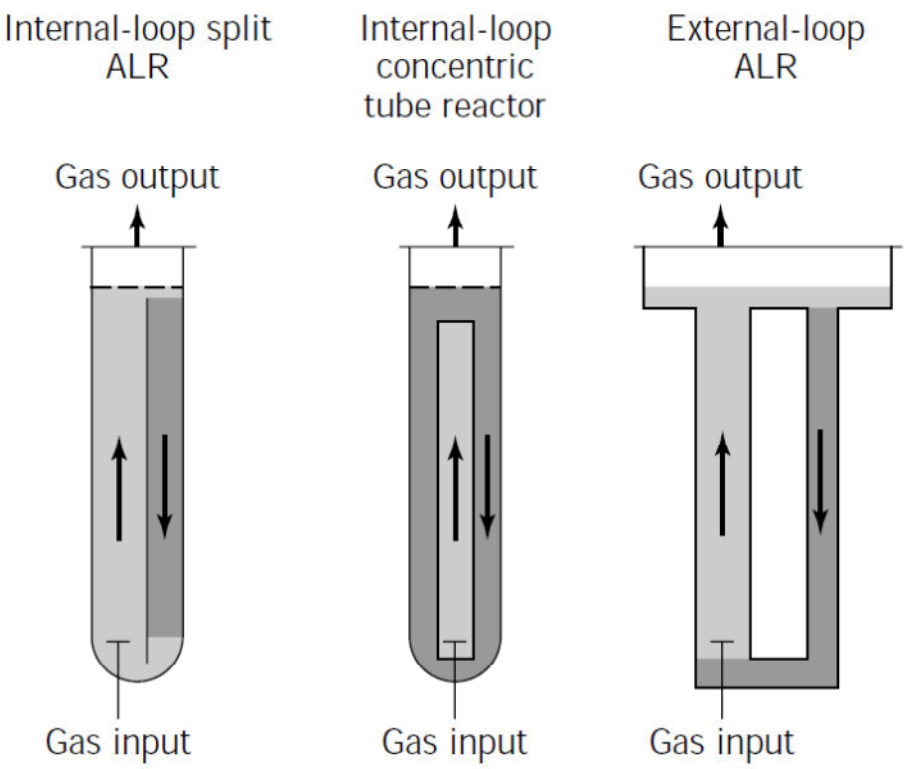

Figure 5.1. Different types of airlift reactors. Left: Internal loop split airlift reactor. Middle: Internal loop concentric tube reactor. Right: External loop airlift reactor. Figure adapted from (Merchuk and Gluz, 2002) with permission from Wiley.

5.1.2 Baffle position

The effect of the downflow/upflow area ratio on the airlift reactor performance has previously been investigated by use of a mathematical model (Hatch, 1975). The studied airlift geometry was an airlift reactor with an inner draft tube. The performance ratio achieved a maximum value at an area ratio of approximately 0.8. However the difference between the performance ratio at area ratios 0.8 and 1.0 was ~3% (Figure 5.2). The simplest baffle construction was achieved by placing the baffle in the middle of the vessel.

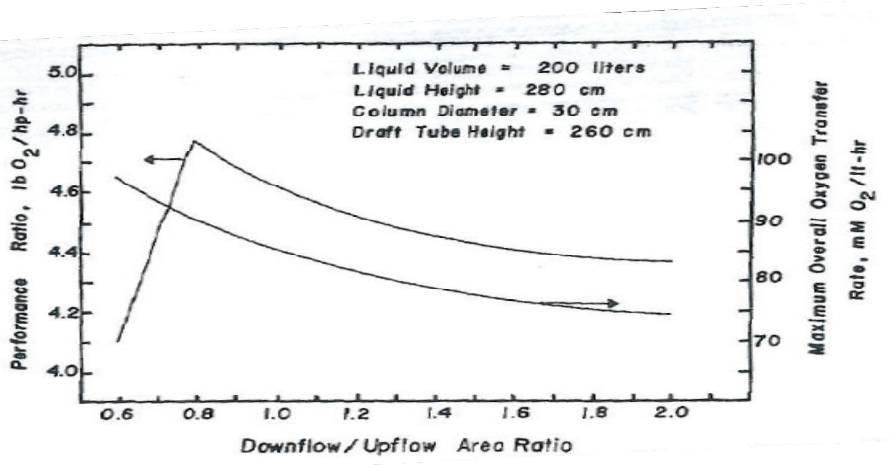

Figure 5.2. Computer simulated dependency of the performance ratio (~oxygen transfer efficiency (lb O_2/hp-hr)) and oxygen transfer rate on the downflow/upflow area ratio. Figure from (Hatch, 1975).

5.1.3 Reactor hydrodynamics and flow configurations

The gas introduced in the bottom of the airlift reactor is the main variable of the system (Chisti and Moo-Young, 1987). The hydrodynamics of the multiphase flow of the airlift reactor have controlling influence on its mixing, mass transfer, and heat transfer characteristics. The gas and liquid velocities of the reactor as well as the gas holdup in the riser and downcomer are determined by the gas flow (Merchuk and Gluz, 2002). The viscosity is also a variable, but in case of non-Newtonian fluids the viscosity is a function of the liquid velocity and it furthermore changes with time of the fermentation due to biomass growth.

Several different gas-liquid flow regimes may be observed based on the gas flow (Brauner and Barnea, 1986). In the riser, the gas velocity is usually higher than that of the liquid. At low gas flows small gas bubbles rise almost straight up the riser section with little interaction amongst them. The free rising velocity of the gas bubbles is here negligible with respect to the liquid velocity (Merchuk and Gluz, 2002). The turbulence is low and this regime is known as the homogenous (or bubbly) flow regime. As the gas flow is increased the bubble density gradually increases which leads to bubble interactions, increased bubble collision frequency, and greater turbulence in a transitional regime known as coalesced bubble flow (Chisti and Moo-Young, 1987). A further increase in the gas flow eventually leads to a fully developed churn turbulent regime in which larger bubbles occur frequently along with many small bubbles. The shape of the bubbles fluctuates quite randomly due to the very high turbulence fields (Chisti and Moo-Young, 1987). The fully developed slug flow obtained at even higher gas flow rates is characterized by spherical caps or bullet nosed bubbles with dimensions that may attain those of the riser. The large bubbles may bridge the entire riser cross section and offer very poor mass transfer, and this regime is important only as a situation to be avoided at all costs (Merchuk and Gluz, 2002). The transition from churn turbulent to slug flow depends, in addition to the gas flow, on the properties of the liquid and on the

geometry of the reactor (Chisti and Moo-Young, 1987). Highly viscous fluids and mycelial media are known to promote spherical cap bubbles, and slug flow occurs earlier in small diameter tubes than in vessels of larger size (Chisti and Moo-Young, 1987). Flow regime maps that are aimed at simplifying the identification of the flow regime of bubble columns do exist, but the transition regions are not clearly or easily defined (Merchuk and Gluz, 2002). In airlift reactors quite high linear liquid velocities may be generated which shift the incipient slugging of airlift reactors to higher gas velocities than is usually seen in bubble columns (Chisti and Moo-Young, 1987).

5.1.4 Pilot scale airlift reactors

Based on the previous fermentations of *T. reesei* in STRs it was assumed that the viscosity of the fermentation broth would reach 0.02-0.04 Pa.s (thus 20-40 times that of water) in airlift reactor fermentations. In order to avoid slug flow, the above considerations of the hydrodynamics of airlift reactors suggest that as large a vessel diameter as possible should be exploited. Two airlift reactor configurations (ALR1 and ALR2) were tested, see Figure 5.3. Both configurations were split cylinder airlift reactors with a total diameter of 0.688 m. The split baffle bottom clearance was 0.20 m. Air was supplied using a perforated pipe sparger (number of holes = 44, hole diameter = 0.0045 m) in the riser section in either downwards (against the direction of the liquid flow) or upwards (in the direction of the liquid flow) direction. The specifications of the reactors are provided in Table 5.1. It was not possible to perform experiments using other scales of operation.

Table 5.1. Airlift reactor configurations tested

	Baffle height (m)	Baffle clearance(m)	Baffle perforated	Sparger direction	Aspect ratio[a]
ALR1	0.80	0.20	Yes	Down	1.0
ALR2	0.80	0.20	No	Up	1.7

[a]Unaerated aspect ratio at the beginning of the fermentations

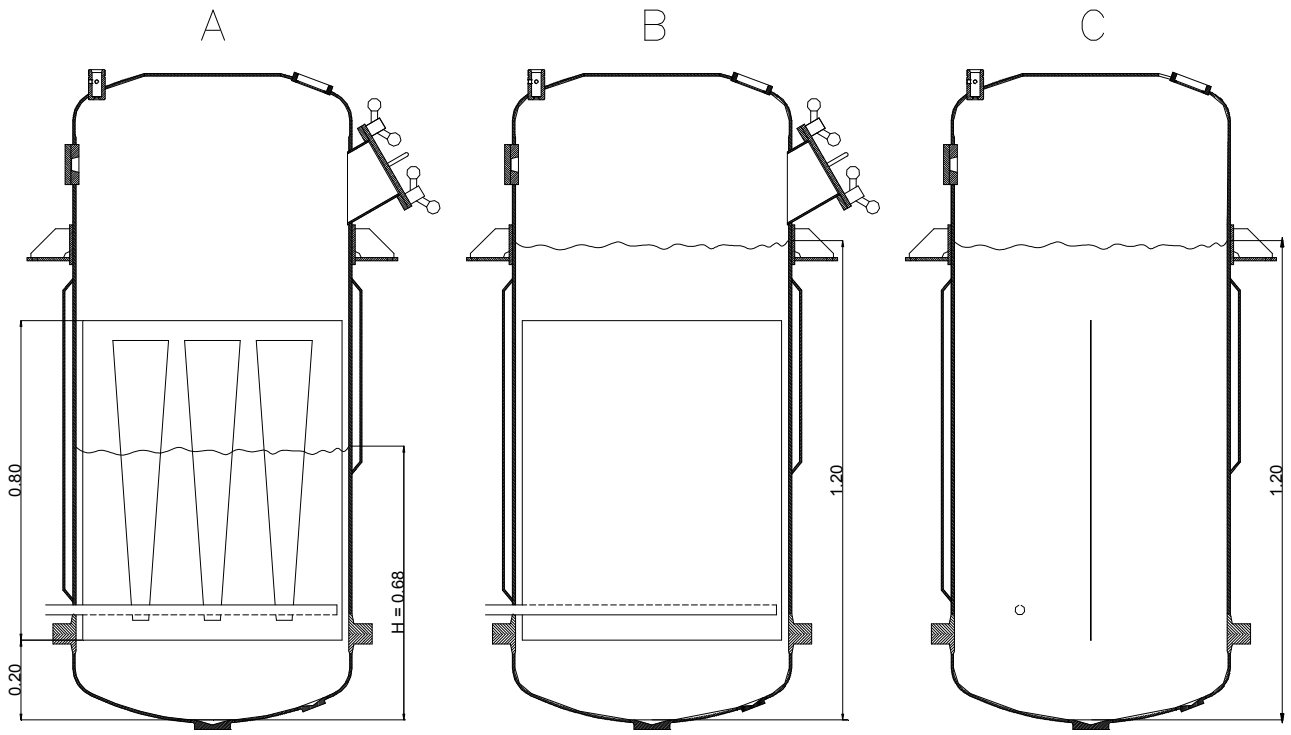

Figure 5.3. Airlift reactor configurations tested. **A:** Front view of ALR1: Perforated split baffle. The initial, unaerated aspect ratio was 1.0. The sparger was in the downwards direction **B:** Front view of ALR2: Split baffle. The initial, unaerated aspect ratio was 1.7. The sparger was in the upwards direction. **C:** Side view of ALR2.

5.2 Materials and methods

In order to compare as objectively as possibly with the STR experiments, all methods employed earlier were unchanged. The strain and growth conditions were the same as described in Chapter 2, as were the enzyme assay and the measurements of rheology, biomass, and $k_L a$.

Experimental design and fermentation conditions

Two process variables were varied: Headspace pressure and superficial gas velocity. For airlift reactors the superficial gas velocity must be based on the riser cross section to have a real meaning. Unless otherwise stated, the superficial gas velocity of airlift reactors is considered based on riser cross section. Importantly, the axial variation in volumetric flow of gas due to changes in hydrostatic pressure must be considered. The headspace pressure must therefore be considered, and the mean superficial gas velocity is given by (Chisti and Moo-Young, 1987):

$$v_{g,r} = \frac{Q_M R T_p}{A_r \rho g Z} \ln\left(1 + \frac{\rho g Z}{p_o}\right) \tag{5.1}$$

From Eq. (5.1) it can be seen that the superficial gas velocity, and thus the turbulence intensity and parameters depending on it (e.g. mixing, mass transfer, and gas hold-up), declines with increasing

reactor headspace pressure, even with constant molar gas flow into a reactor.

The extreme ends of the experimental design were determined by the equipment. It was discovered that a minimum aeration rate of 400 NL/min was needed for establishing a circulating flow during the batch phase of ARL1 fermentations. The maximal obtainable aeration rate was 1180 NL/min. The objective of the experimental design was to explore the experimental space in such a way to determine possible correlations between the varied process variables and the performance of the fermentations. The summary of the experimental design is shown in Table 5.2.

Table 5.2. Experimental design for airlift reactor fermentations

Fermentation nr	Headspace pressure (barg)	Aeration rate (NL/min)	$v_{g,r}$ (m/s)
ALR1.1	0.10	635	0.05
ALR1.2	1.10	1180	0.05
ALR1.3	0.10	400	0.03
ALR1.4	0.10	505	0.04
ALR1.5	1.10	708	0.03
ALR1.6	0.60	545	0.03
Fermentation nr	Headspace pressure (barg)	Aeration rate (NL/min)	$v_{g,r}$ (m/s)
ALR2.1	1.10	475	0.02
ALR2.2	0.75	1180	0.06
ALR2.3	0.10	505	0.04

The fermentation conditions and fed-batch strategy were identical to the STR experiments (of course without agitation as a process variable). The operation mode of the fermentation process was as follows:

-All fermentations were started with identical batch phases, during which the substrate concentration decreased from a high initial value to its operational range. The aeration rate was 400 NL/min and the headspace pressure was 0.1 barg.

-The batch phase was followed by a DOT controlled fed-batch phase with process variables as described above and with the carbon substrate feed flow rate as the controlled variable.

Yield coefficients and carbon balance

The yield coefficients were determined as average values for all three fermentations. The carbon substrate in the batch medium was included in the calculation of Y_{SC}. For low growth rates the

composition of *T. reesei* cell mass can be set to $CH_{1.80}N_{0.116}O_{0.710}$ (Ross et al., 1983). For the elemental composition of the enzyme complex the distribution of the four major cellulases secreted by the strain RutC30 was assumed to represent all the protein since they represent 85% of all components (Tolan and Foody, 1999). The amino acid sequence of each enzyme was found on the publicly available protein knowledge base UniProt (www.uniprot.org) and analyzed using the software GPMAW (Peri et al., 2001). The composition including glycosylation was calculated by use of high-mannose glycans (Hui et al., 2001; Hui et al., 2002).

Table 5.3. Distribution, composition, and glycosylation of the four major components of the *T. reesei* cellulase complex.

Enzyme	Distribution (%)	Composition	Glycosylation (%)	Composition glycosylated
Cel7A	50[a]	$CH_{1.50}N_{0.28}O_{0.34}S_{0.01}$	9.7[b]	$CH_{1.54}N_{0.25}O_{0.40}S_{0.01}$
Cel6A	20[a]	$CH_{1.52}N_{0.27}O_{0.31}S_{0.01}$	20.9[c]	$CH_{1.60}N_{0.23}O_{0.43}S_{0.01}$
Cel7B	10[a]	$CH_{1.52}N_{0.28}O_{0.35}S_{0.02}$	14.8[c]	$CH_{1.58}N_{0.24}O_{0.42}S_{0.01}$
Cel5A	5[a]	$CH_{1.52}N_{0.28}O_{0.32}S_{0.01}$	14.3[c]	$CH_{1.58}N_{0.24}O_{0.40}S_{0.01}$
Weighted average				$CH_{1.56}N_{0.25}O_{0.41}S_{0.01}$

[a](Tolan and Foody, 1999), [b](Hui et al., 2001), [c](Hui et al., 2002)

Mixing time measurements

Mixing time was measured using the conductivity method using a Conducell 4 USF ARC 425 probe (Hamilton, Bonatuz, Switzerland). Data from the conductivity probe were collected once per second. Three different media were used: Water, 0.125% (w/v) xanthan gum, and 0.25% (w/v) xanthan gum (Rhodopol, Rhodia, Albertville, France). All media furthermore contained 0.43% (w/v) sodium benzoate and 0.21% (w/v) KH_2PO_4. The salt pulse used was 400 mL of 0.25% (v/v) NaCl. The salt tracer pulse was injected within 10 s and the addition time was included in the mixing time. The addition of the salt tracer occurred on top of the fermentation broth. Average numbers and standard deviations of three mixing time determinations are used.

Airlift reactor shear rate estimations

In the context of correlating hydrodynamic parameters in non-Newtonian fluids, many investigations of bubble columns have assumed that the average (effective) shear rate is proportional to the superficial gas velocity:

$$\dot{\gamma}_{\text{eff}} = C_s v_g \tag{5.2}$$

As shear originates from the relative velocity between the bubble and the liquid, it is argued that $\dot{\gamma}_{\text{eff}}$ increases with gas holdup ($\dot{\gamma}_{\text{eff}} \sim \varepsilon_g$) and with the mean bubble rise velocity ($\dot{\gamma}_{\text{eff}} \sim v_g/\varepsilon_g$) which in

combination yield Eq. (5.2). The approach has been questioned from a rheological point of view because it predicts the same shear rate for a certain superficial gas velocity no matter which fluid is used (Merchuk and Gluz, 2002). A number of different proportionality constants for Eq. (5.2) have been suggested as shown in the literature, and as the disparity among the constants is large. It is generally agreed that the correct solution is still to be found (Chisti, 1989; Merchuk and Gluz, 2002).

For airlift reactors a common approach also involves assuming that an average shear rate in the airlift reactor exists, even though the area is surrounded with considerable debate (Allen and Robinson, 1991; Chisti and Moo-Young, 1989; Nishikawa, 1991). It has been assumed that the active (predominant) zone for oxygen mass transfer, gas holdup and gas/liquid interfacial area is in the riser section of the reactor (Allen and Robinson, 1989; Popovic and Robinson, 1989). Therefore is seems reasonable that the relevant effective viscosity is that of the riser section of the reactor and the effective shear rate is deduced from the conditions of the riser (Allen and Robinson, 1991)

$$\dot{\gamma}_{\text{eff}} = C_{\text{s}} v_{\text{g,r}} \tag{5.3}$$

In this work, a value of $C_{\text{s}} = 2800$ is assumed (Schumpe and Deckwer, 1987). In Appendix A other constants have been compared.

Mass transfer correlations for airlift reactors

Two different mass transfer correlations were investigated in which the riser zone superficial gas velocity was related to the mass transfer coefficient $k_{\text{L}}a$. The apparent viscosity was included in one of them by analogue to the empirical mass transfer correlation of Chapter 2

$$k_{\text{L}}a = C v_{\text{g,r}}^{a} \tag{5.4}$$

$$k_{\text{L}}a = C v_{\text{g,r}}^{a} \mu_{\text{app}}^{b} \tag{5.5}$$

5.3 Results and discussion

5.3.1 Fermentations

The airlift fermentations were somewhat difficult to execute compared with the STR fermentations. The primary reason for this is that the medium and the fermentation procedure has been optimized for the STR and transferred directly to the ALR. The six fermentations carried out with the ALR1 configuration suffered from biomass growth on the DOT electrodes, which made DOT controlled carbon feeding impossible. As a consequence of that growth, about halfway through the fed-batch phase the signals from the DOT electrodes were at 0% and the carbon feeding was conservatively set manually based on the historical feed rate observed at each set of fermentation conditions. An

example of the ALR1 fermentations is shown in Figure 5.4 The decision to continue feeding the fermentations carbon substrate even though the DOT apparently was 0% was based on the fact that OUR and CER were not behaving unexpectedly and RQ was unaffected (around ~1.05). In the ALR2 configuration, equipment was installed for steaming (or more precisely blowing steam condensate on) the DOT electrodes. When the DOT signal in the ALR2 started to drop due to fouling of the electrode, the steam successfully removed the beginning fouling and the correct signal was restored.

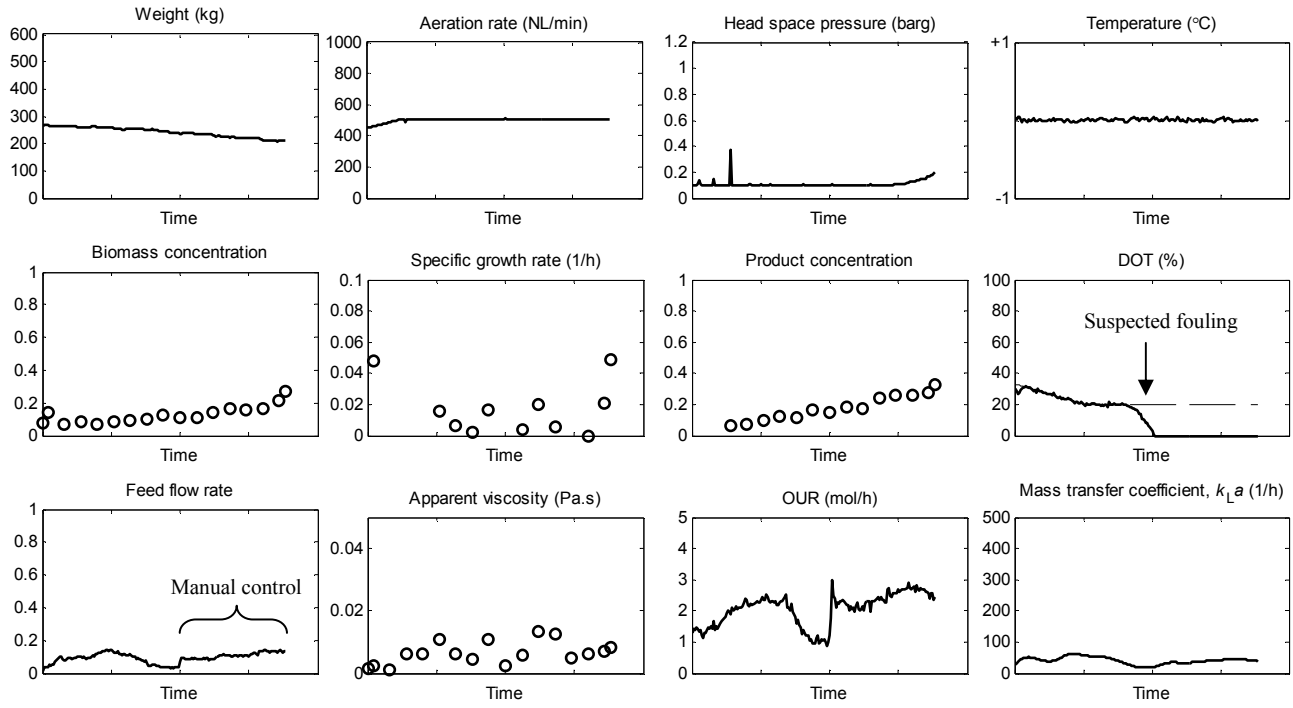

Figure 5.4. Fermentation profile of ALR1.4. From the top left: The weight of the fermentation is seen to decrease due to evaporation. This was similar to the other fermentations with 0.1 barg headspace pressure. The aeration rate was controlled at the set point throughout the fermentation (505 NL/min). The headspace pressure was controlled well at the set point (0.1 barg) except for the final part. The reason for the increase up to 0.2 barg is not known. Temperature was controlled well throughout the fermentation. The biomass concentration increased steadily except for the last two measurement points. The specific growth rate was always below 0.02 1/h, except for the last measurements. The product concentration increased steadily during the fermentation. The DOT is seen to follow the set point nicely until the suspected fouling of the DOT electrode occurs around halfway through the fermentation. The feed flow rate was the control variable of the DOT and when the DOT signal dropped, manual control of the feed flow rate was needed for the remainder of the fermentation. The apparent viscosity was calculated based on (Schumpe and Deckwer, 1987) with $\dot{\gamma}_{eff}$ = 112 1/s and remained in the interval 0.002-0.011 Pa.s. OUR followed the feed flow rate as expected. The drop in OUR at the moment that the suspected fouling of the DOT electrode occurred indicated that the feed could be increased. The measured k_La was in the interval 33-64 1/h and did not decrease significantly towards the end of the fermentation.

Another example of a challenge encountered was the suspension of the denser particles of the fermentation medium. Some insoluble particles were apparently not well suspended in the reactor which led to some sampling difficulties since the particles would gather at the sampling port which

was located in the bottom of the reactor. This is also a minor problem that could be overcome in time by medium optimization and by gaining more experience with ALR operation.

The ALR2 fermentations were performed in accordance with the described fermentation conditions and control methods even though ALR2.1 and ALR2.2 were terminated earlier than planned this time due to fouling of the pH electrodes. Anti-foam oil was preventively added periodically to all fermentations, and in none of the fermentations foaming was observed. The non-foaming property of this strain of *T. reesei* allowed operation with liquid heights quite close to the total vessel height.

5.3.2 Yield coefficients and carbon balance

The absolute values of the yield coefficients are confidential and are therefore not provided. Instead, a comparison with the nine previous fermentations in the STR of Chapter 2 is given in Table 5.4.

Table 5.4. Relative average yield coefficients, C-balance, and RQ for all fermentations. The carbon balances of the ALR fermentations are not shown for proprietary reasons.

	Y_{SX}	Y_{SP}	Y_{SO}	Y_{SC}	C-balance	RQ
STR (9 batches)	1.00±0.18	1.00±0.15	1.00±0.11	1.00±0.10	0.92±0.06	1.05±0.02
ALR1 (6 batches)	0.66±0.22	0.99±0.16	0.99±0.14	1.00±0.14	-	1.07±0.06
ALR2 (3 batches)	0.67±0.07	0.98±0.17	0.98±0.02	0.99±0.02	-	1.07±0.04

The data presented in Table 5.4 are encouraging for future modeling purposes since it can be seen that except from the measured biomass yield coefficients, all yield coefficients (and hence the RQ and the carbon balance) for the ALR fermentations are very close to the equivalent STR data and certainly within the uncertainty of the measurement methods. This shows that the enzyme producing strain behaved similarly for two quite different fermentation technologies and indicates that the model developed in the STR can be applied also to make predictions about other technologies and certainly for the ALR. The lower yield of biomass on carbon substrate is most likely due to biomass loss at the reactor wall above the liquid level in those cases where the volume of the STR was seen to decrease during the course of the fermentation (see Figure 5.5 and caption). Optimization of the carbon content in the carbon feed could probably help to eliminate this problem. The carbon balance closed at 0.92±0.06 for the STR fermentations, and the ALR results were quite similar, but cannot be shown for proprietary reasons. Since only Y_{SX} differs from the STR fermentations, its value could have been estimated easily by the observant reader.

The fact that the yield coefficients of ALR1 and ALR2 are so consistent with each other and also (with the exception of Y_{SX}) with the STR fermentations, indicates that the ALR1 fermentations were not overfed. This was a major concern during the manual feed flow rate adjustment, but the RQ was also observed to be only slightly higher than the STR fermentations. If the feed flow rate had been too high, Y_{SP} had probably been lower while Y_{SC} and/or Y_{SX} had increased. On the other hand the

yield coefficients do not reveal whether the feed flow rate could have actually been higher as OUR kept increasing with increasing feed flow rate, see Figure 5.4.

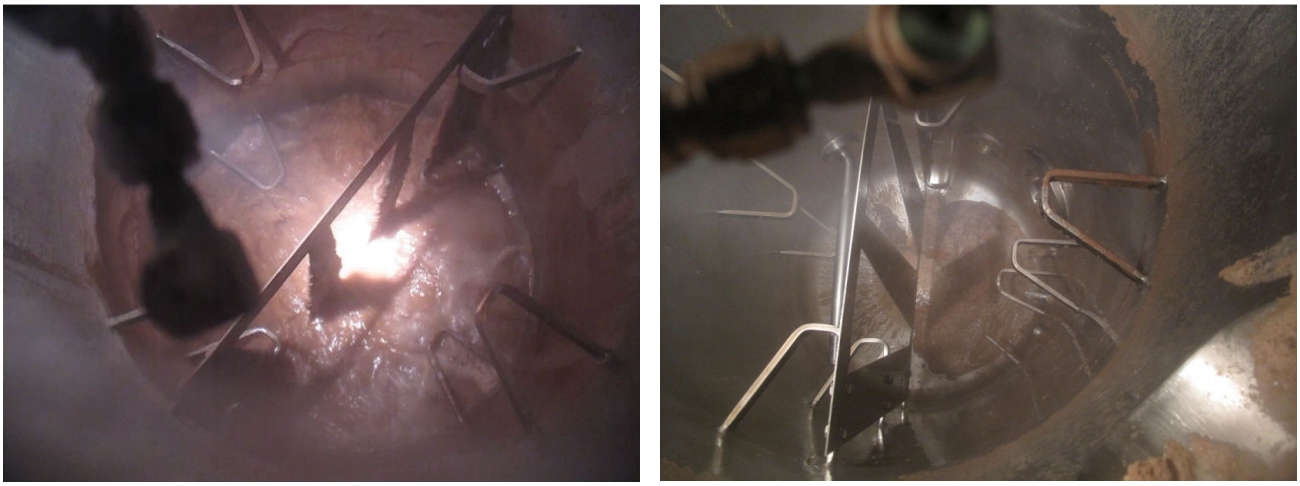

Figure 5.5. **Left:** Photograph inside the reactor with the ARL1 configuration during fermentation. Biomass is seen on the reactor wall. If just 2 mm biomass is left on the reactor wall, a 15 cm drop in liquid level due to evaporation corresponds to 0.6 kg assuming a density of 1000 kg/m^3. **Right:** Photograph inside a reactor after fermentation when the tank has been emptied. No wall growth was ever observed below the liquid surface level.

5.3.3 Rheology of the fermentation broth

The data obtained with the ALR configuration are compared with the data reported in Chapter 2 in Figure 5.6. The biomass concentrations obtained using the ALR are lower than those obtained with the STR as the OTR was in general lower in the former. Eq. (2.10) and (2.11) were also used for modeling the STR in Chapter 2. The exponents α and β were found to be 2.29 and -0.32, respectively, for the STR fermentations. Since the relation between the rheological parameters and the biomass concentration represented by α and β seems to differ between the ALR and the STR fermentations, it could be argued that the morphology seems to be different in the ALR compared to the STR.

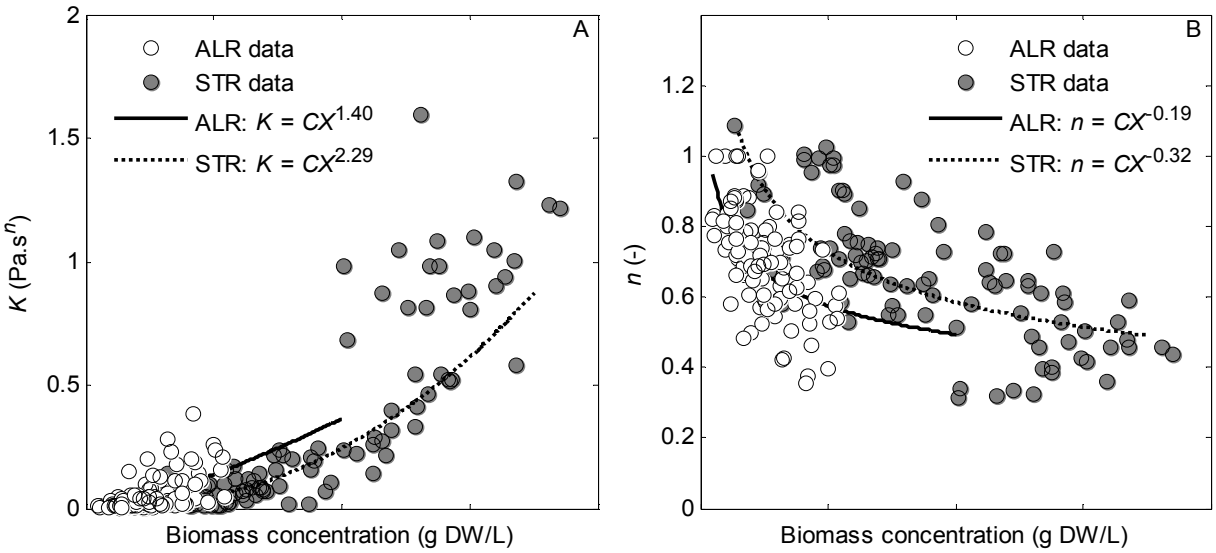

Figure 5.6. A: *K* shown as function of biomass concentration for both ALR and STR fermentations (Chapter 2). Both the highest values of *K* and biomass concentrations were obtained in the STR. **B:** *n* shown as function of biomass concentration for both ALR and STR fermentations (Chapter 2). At the higher biomass concentrations achieved in the STR, the values of *n* were lower than for the ALR.

If the morphology is in fact different for the ALR and the STR, it would perhaps not be surprising. The STR is known to provide zones with very high power input per unit mass (Zhou and Kresta, 1996) and it has previously been shown that the morphology of filamentous fungi is affected by mechanical stress of the STR. The productivity of some organisms seems to be influenced by the morphological state (e.g., *Penicillum chrysogenum*) while the productivity of other organisms appears unaffected (e.g., *A. oryzae*) (Amanullah et al., 1999; Amanullah et al., 2002; Jüsten et al., 1998).

However, as the yield coefficients of the present strain of *T. reesei* are very similar for the ALR and the STR fermentations while the relation between the rheological parameters and biomass concentration apparently differ it would seem that the productivity of the current strain of *T. reesei* is not affected by morphological differences between the reactor technologies. It could therefore be argued that the possible mycelial damage in the STR is actually beneficial since it helps to lower the viscosity of the fermentation broth. A more certain confirmation of the proposed difference in morphology would require more detailed investigations such as advanced image analysis or particle size distribution (Petersen et al., 2008).

5.3.4 Mass transfer correlations

The direct method of measuring k_La was used. The ALR reactor had only a single DOT probe and therefore no distinction between different zones of the reactor could be made. The direct method as used here implies in principle that the reactor is perfectly mixed such that the measured k_La is the same in the entire volume of the whole vessel (Merchuk and Gluz, 2002). If all gas liquid mass

transfer occurs in the riser section as argued in the section on effective shear rate, the broth volume used for mass transfer corresponded to only half of vessel volume. This means that the measured k_La would be twice as large in the riser zone and zero in the downcomer zone. The average vessel k_La would be the same as assuming that the entire vessel volume is utilized for mass transfer. Therefore it is simpler in this case to consider the k_La equal in the entire vessel.

The measured k_La values are shown as function of $v_{g,r}$ in Figure 5.7. The ALR fermentations have been carried out in the range $0.02<v_{g,r}<0.06$ and the k_La values are in the range 15-62 1/h. At each level of $v_{g,r}$, a range of k_La measurements were made as function of fermentation time. Therefore, naturally, there is a certain scatter in the data. For each ALR configuration, there seems to be different exponents for the mass transfer correlation of Eq. (5.4). The ALR1 data with the lowest $v_{g,r}$ deviate from the behavior seen from ALR2 and the correlation from the literature. The ALR1 data suggest an exponent of $a = 1.67$. It is quite unexpected that $a>1$, and it is interesting that as $v_{g,r}$ was increased in the ALR1, the data is very similar to that of ALR2. One reason may, perhaps in combination with other causes, explain this: the mixing achieved with the ALR1 configuration was suboptimal and especially at the lowest power inputs the entire vessel was not well mixed. This would lead to lower average k_La values.

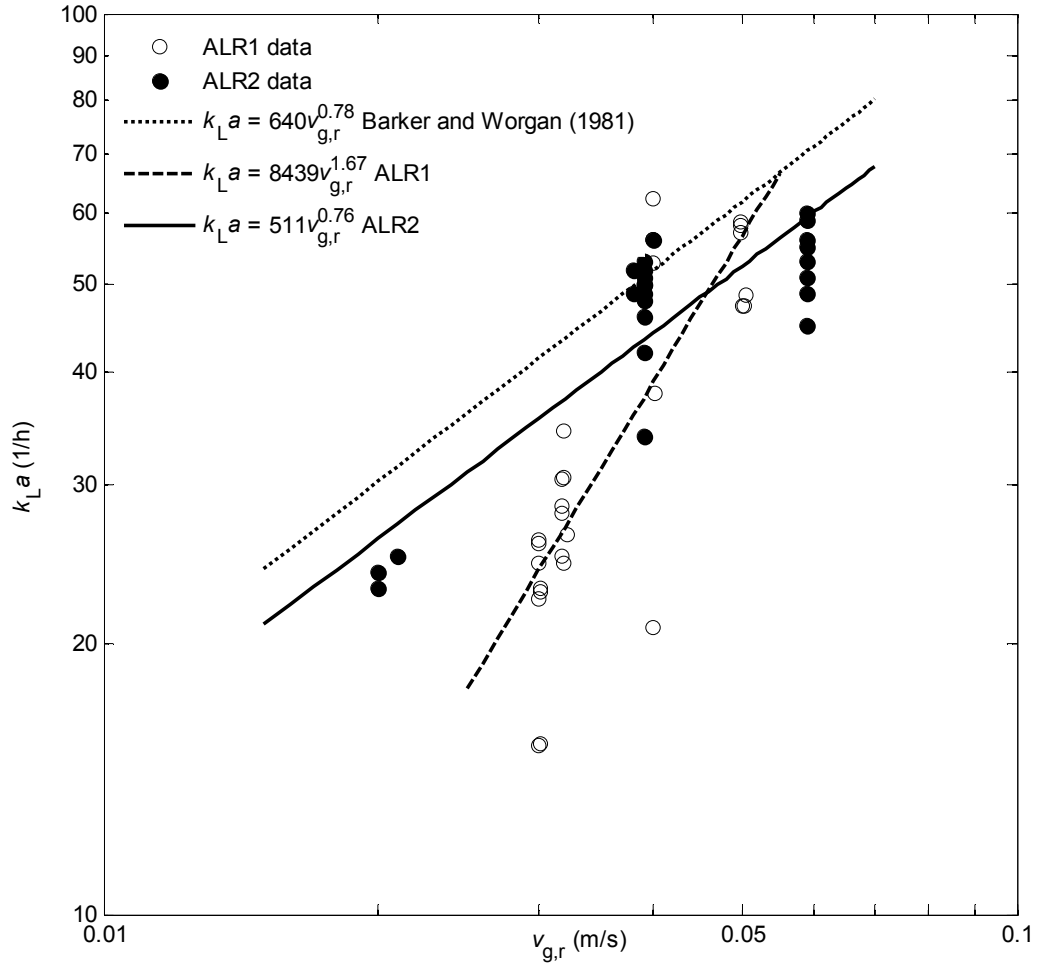

Figure 5.7. k_La in a log-log plot as function of riser zone superficial gas velocity for ALR1 and ALR2 fermentations. The relationship of Barker and Worgan (1981) is also shown as well as the least square regression of Eq. (5.4) to the ALR1 and ALR2 data, respectively.

By use of the ALR2 experimental data, the constants of Eq. (5.4) were estimated by least squares regression: C = 511 and a = 0.76. All experimental data are within ±30% of the model. Encouragingly, these constants were quite similar to the ones obtained from the literature and previously used where a = 0.78, however with C = 640 (Barker and Worgan, 1981). In their work Barker and Worgan (1981) determined C = 853 for water and recognized a certain influence of viscosity, but did not specify this influence quantitatively. In the technology screening of Chapter 4 the increased viscosity was assumed to reduce k_La by 25% yielding C = 640 (Barker and Worgan, 1981).

Eq. (5.5) includes a term for apparent viscosity by analogy to the empirical mass transfer correlation of the STR in Chapter 2. The term is included since biomass concentration and apparent viscosity were expected to increase during fermentation and affect the oxygen mass transfer negatively during the course of the fermentation. In Figure 5.8 the measured k_La data is shown in a log-log plot

versus Eq. (5.5) with constants estimated by least squares regression using the ALR2 data. For ALR2 which must be regarded as the most reliable data, the experimental data are always within ±30% of the model prediction, which is satisfactory for this type of measurements (e.g., Albaek et al., 2011, Cooke et al., 1988; Zhu et al., 2001).

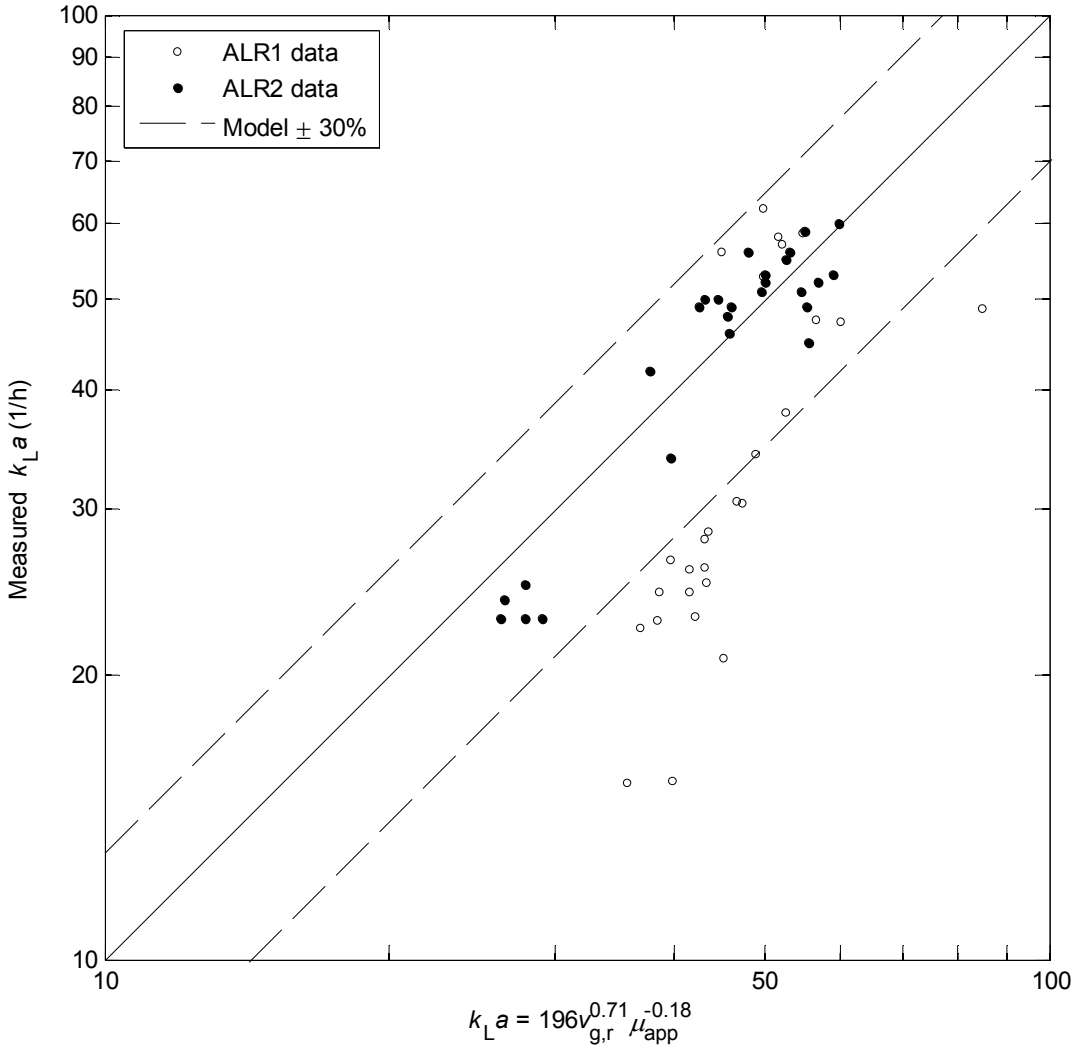

Figure 5.8. Log-log plot of the measured k_La values versus the modeled values using Eq. (5.5). By use of the ALR2 data, the exponents were estimated by least squares regression: a = 0.71 and b = -0.18. The ALR2 data are all within ±30% of the model prediction. The ALR1 data are generally overpredicted by the model indicating that mixing and mass transfer were better in the ALR2 configuration.

Both correlations Eq. (5.4) and (5.5) can be used to describe the experimental k_La data. In Eq. (5.4), the exponent a = 0.76 while due to the incorporation of the viscosity term, in Eq. (5.5) a = 0.71. The exponent of the viscosity term b was -0.18, which is numerically smaller than for the similar empirical mass transfer correlation for the STR, Eq. (2.30), where the exponent c was -0.50. This finding is in accordance with the previous study that found a seemingly less adverse effect of broth

viscosity in airlift fermentors than in the STR (Barker and Worgan, 1981). It was decided to use Eq. (5.5) and the corresponding constants (C = 196, a = 0.71, and b = -0.18) in the model based scale-up, since it allows the quantification of the effect of the viscosity increase during the course of fermentation.

5.3.5 Mixing time measurements

The results of the 90% mixing time measurements are shown in Figure 5.9, while the details of the measurements are provided in Appendix A. In general, mixing time decreased with superficial gas velocity and increased with the viscosity of the broth. The mixing times varied between 29 s (water and $v_{g,r}$ = 0.06) and 260 s (0.25% xanthan and $v_{g,r}$ = 0.02 m/s). The mixing time for the 0.125% xanthan solution was 57-87 s for both ALR1 and ALR2. For the xanthan solutions, ALR2 showed lower mixing times than the ALR1 while no difference was observed with water as the medium.

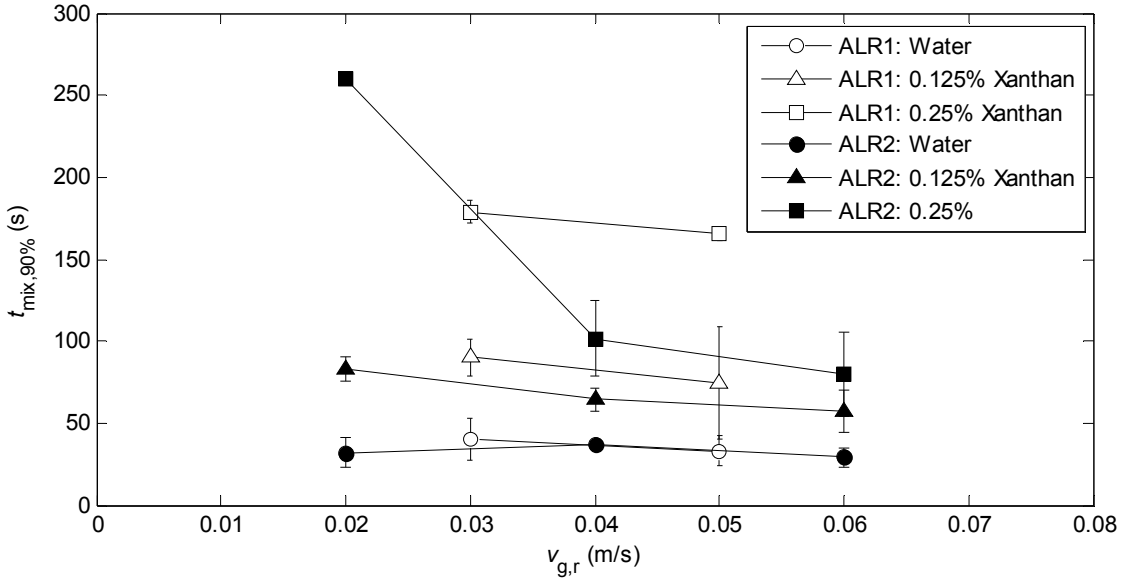

Figure 5.9. Mixing time versus $v_{g,r}$ for three different media in ALR1 and ALR2. 400 mL of 25% (w/v) NaCl were used as tracer. Injection time was 10 s and included in the mixing time. Experiments were done in triplicates; average values are shown and the standard deviation is shown with error bars.

The mixing times of the ALR were compared with the STR. Mixing times in the STR were measured with the agitation intensities used in Chapter 2 and otherwise the same procedure as described here. No aeration was included since this introduced too much noise for reasonable measurements of the conductivity. The measured mixing times are shown as function of the agitator power input in Figure 5.10. The mixing times for the STR including injection pulse time were below 35 s for all fluids and did not change much with power input. There was a difference between the fluids, but it is in the range of the injection time and the standard deviation of the measurements.

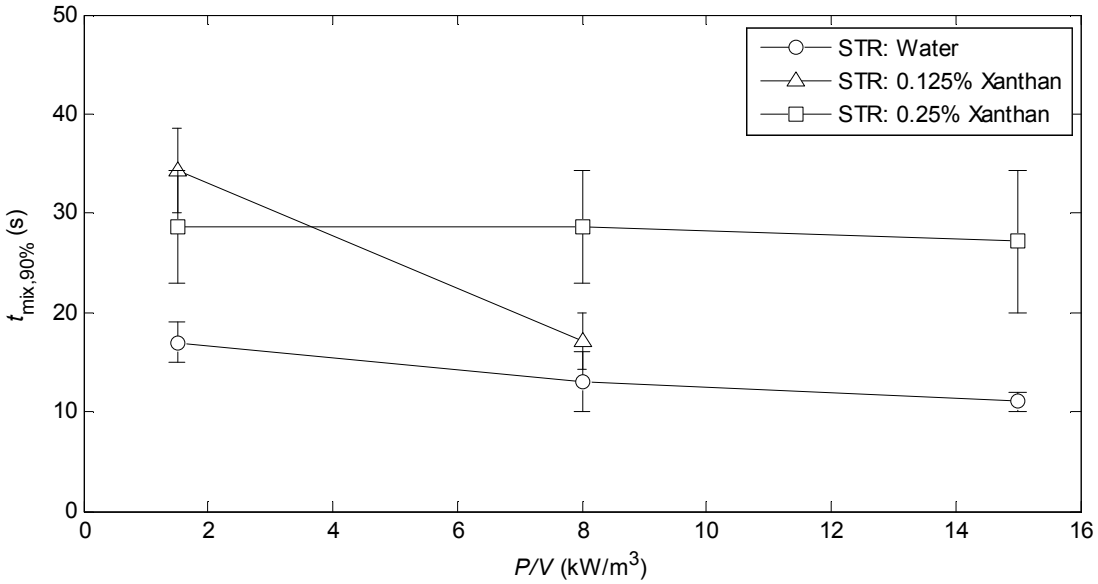

Figure 5.10. Mixing time measured for the STR with configuration as described in Chapter 2. No aeration was provided. 400 mL of 25% (w/v) NaCl were used as tracer. Injection time was 10 s and included in the mixing time. Experiments were done in triplicates; average values are shown and the standard deviation is shown with error bars.

A correlation for turbulent mixing in a STR with $H/T = 1$ was proposed (Nienow, 1997):

$$t_{\mathrm{m},95\%} = 5.9T^{2/3}\left(\frac{P}{V}\right)^{-1/3}\left(\frac{D}{T}\right)^{-1/3} \tag{5.6}$$

Eq. (5.6) predicts 95% mixing times at ~3-5 s for the agitation intensities used here.

The Reynolds number of the STR was calculated for each fluid and agitation intensity according to (Grenville and Nienow, 2004):

$$\mathrm{Re} = \frac{\sigma N D^2}{\mu_{\mathrm{app}}} \tag{5.7}$$

The Reynolds numbers for water were 272,000-726,000 and are thus clearly in the turbulent regime as expected at these high power inputs. For the 0.125% xanthan solution the apparent viscosity varied with N from 0.011-0.017 Pa.s, which yielded Reynolds numbers between 16,000-67,000. The apparent viscosities for the 0.25% xanthan solution varied from 0.029-0.056 Pa.s and the Reynolds numbers were between 4,900-25,000.

The transition from the turbulent region to the transitional region has been shown to occur at (Grenville and Nienow, 2004):

$$\mathrm{Re} = 6370\mathrm{Po}^{-1/3} \tag{5.8}$$

The power number determined for the D = 0.33 m B2 impeller was 2.69 and the transition to the transitional regime may therefore be estimated for this system at Re = 4580, which is slightly lower than the Reynolds numbers calculated for the 0.25% xanthan solution.

The data shown in Figure 5.10 seem to be in agreement with the literature correlation of Eq. (5.6) considering the injection time of ~10 s in these experiments. Eq. (5.6) states that the mixing time is independent of the fluid's physical properties in the turbulent regime. For the 0.25% xanthan solution the mixing time was longer which may be caused by the fact that the transitional regime is approached. The uncertainty of the measurement technique does not allow for more detailed conclusions.

5.3.6 Regime analysis

In order to evaluate the suitability of the liquid mixing times of the ALR, the additional characteristic times related to mass transfer were estimated. The aim of this analysis is to determine the ruling regime (or regimes) from a comparison of the characteristic times (or relaxation times) for the mechanisms involved in the process (Nielsen, 1997). In Table 5.5 the characteristic times necessary to compare the importance of oxygen mass transfer and mixing are given for two superficial gas velocities (Reuss, 1993).

Table 5.5. Characteristic times for mixing and oxygen mass transfer for low and high superficial gas velocity ALR fermentations.

	Definition[a]	$v_{g,r}$ = 0.02 m/s	$v_{g,r}$ = 0.06 m/s
Mixing, $t_{mix,95\%}$	empirical	83 s	57 s
Gas residence time	$t_{gas} = 3600\dfrac{(1-\varepsilon_g)V}{Q_1}$	85 s	43 s
Oxygen transfer	$t_{mt} = 3600\dfrac{1}{k_L a}$	156 s	72 s
Oxygen consumption	$t_{oc} = 3600\dfrac{DO}{OUR}$	40-60 s	40-60s

[a](Oosterhuis, 1984).

The characteristic time for oxygen transfer is the largest in both cases, which is quite obvious since this process is oxygen transfer limited. The characteristic time for gas hold up is in the same order of magnitude as that for oxygen transfer, and inhomogeneity in the gas phase is likely. The mixing times however approach the characteristic time for oxygen transfer, which indicates that mixing

might also be limiting the fermentation and it therefore cannot be ruled out that concentration gradients exist. It is important to keep this in mind if the process is further investigated in other scales.

The characteristic times for substrate addition and substrate consumption have not been included here, since the process is a fed-batch fermentation where the substrate concentration is not know. Intuitively, the substrate concentration must be very low and the substrate consumption must be in the same order of magnitude.

5.3.7 Simulations

All ALR fermentations were simulated using the process mode; the simulations utilized the yield and maintenance coefficients determined in Chapter 2, the rheological correlations for the ALR as shown in Figure 5.6, and the ALR mass transfer correlation shown in Figure 5.8. For comparison, simulations were also performed with the mass transfer correlation of Barker and Worgan (1981), while all other components of the model were unchanged.

An example of the simulation results is shown in Figure 5.11. The biomass concentration and product concentration of ALR2.3 increased steadily during the fermentation. Except for the last measurement, the specific growth rate in general decreased as expected for fed-batch fermentation. Furthermore, the apparent viscosity generally increased although with some fluctuation in the data. These trends were predicted quite well by both the simulation using the mass transfer correlation of Barker and Worgan (1981) and the correlation of this work. However, the mass transfer coefficient was overpredicted by the literature correlation. The literature prediction of k_La led then to an overestimation of the OTR and finally to an overestimation of the feed flow rate. The k_La prediction of this work led to a better estimation of OTR, feed flow rate, and ultimately a better estimation of biomass and protein concentration.

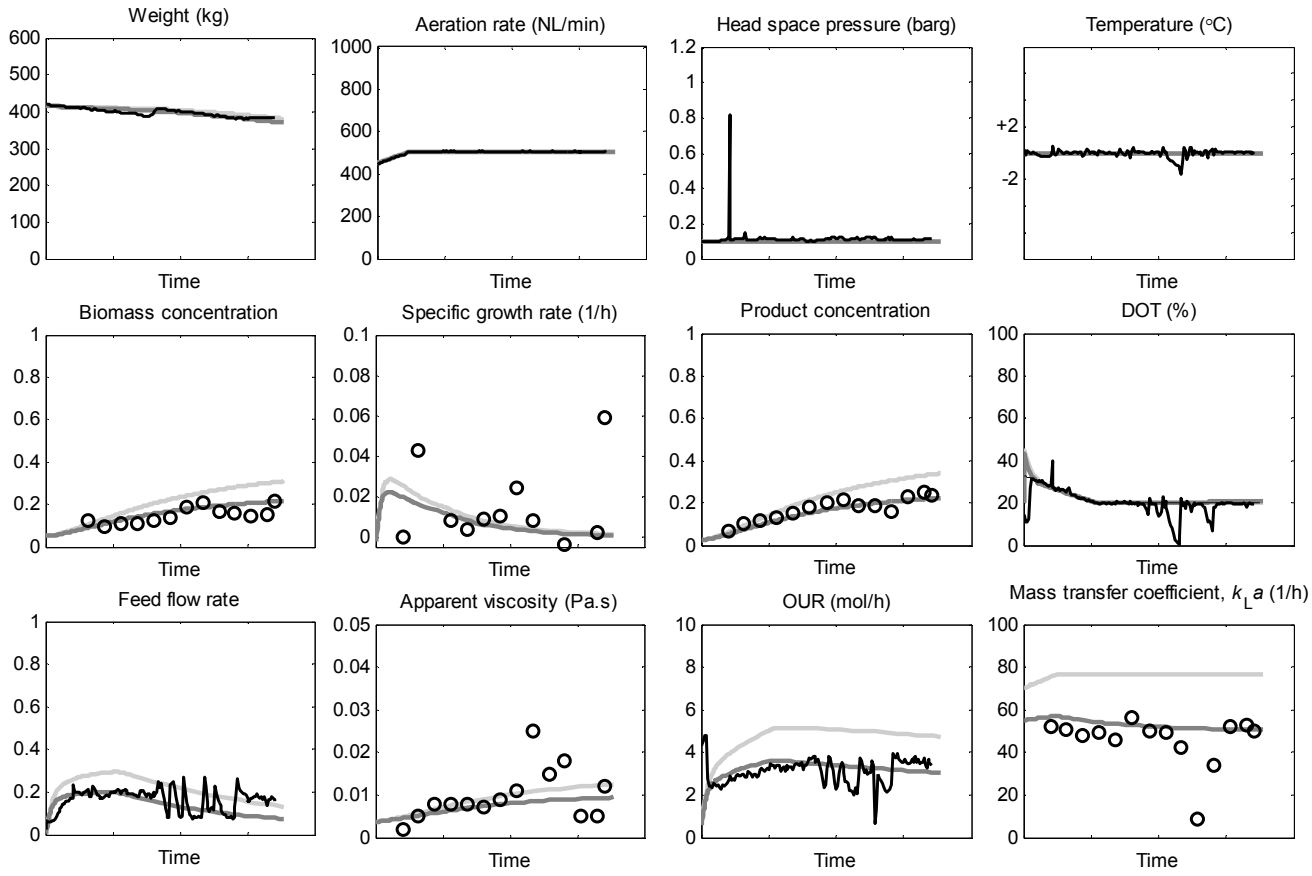

Figure 5.11. Fermentation profile and simulation predictions of ALR2.3. Two mass transfer models were used: Barker and Worgan (1981) $k_La = 853v_g^{0.78}$ (**light gray**) and the correlation of this work: $k_La = 196v_g^{0.7}\mu_{app}^{-0.18}$ (**dark gray**). The experimental data (**bold**) are also shown. The experimental data is described from the top left: The weight of the fermentation broth decreases due to evaporation. The aeration rate was controlled at the set point throughout the fermentation (505 NL/min). The headspace pressure was controlled at the set point (0.1 barg). The temperature was controlled at the set point throughout the fermentation. The biomass concentration increased slowly during the entire fermentation. The specific growth rate was below 0.045 1/h except for the last measurement. The product concentration increased steadily during the fermentation. The DOT is seen to follow the set point during the entire fermentation, expect for two short periods of time. This is probably due to fouling of the electrode, which was removed by blowing steam and condensate at the electrode. The feed flow rate varied during the fermentation as it was the control variable for the DOT. The viscosity was measured in the interval 0.002-0.025 Pa.s with an increasing trend as function of fermentation time. The OUR followed the profile of the feed flow rate. k_La was measured in the interval 40-60 1/h with only two exceptions. The k_La correlation of Barker and Worgan (1981) overpredicts the k_La. This means that the OUR is also overpredicted and hence the feed flow rate is also overpredicted. As a result the biomass concentration and product concentration are also overpredicted. The k_La correlation of this work is seen to successfully predict the OUR of the fermentation. Consequently the feed flow rate, biomass concentration, and product concentration are also predicted well. The apparent viscosity is estimated based on the biomass concentration and is also predicted well. As a result of the rising viscosity, k_La is predicted to decrease slightly during the fermentation.

In Figure 5.12 the measured EE_{O2} are shown versus the simulated EE_{O2} for all ALR fermentation using the mass transfer correlation of this work. Considering the better prediction of the k_La values in the ALR2 than the ALR1 as seen in Figure 5.8, it is unsurprising that the ALR2 fermentations

were in general simulated better than the ALR1 fermentations. Even so, in each end of the wide range of variation of the process parameters, the EE_{O2} is predicted with good accuracy for the ALR fermentations. The simulation error on average for the ALR1 and ALR2 fermentations was 18±16% and 9±5%, respectively.

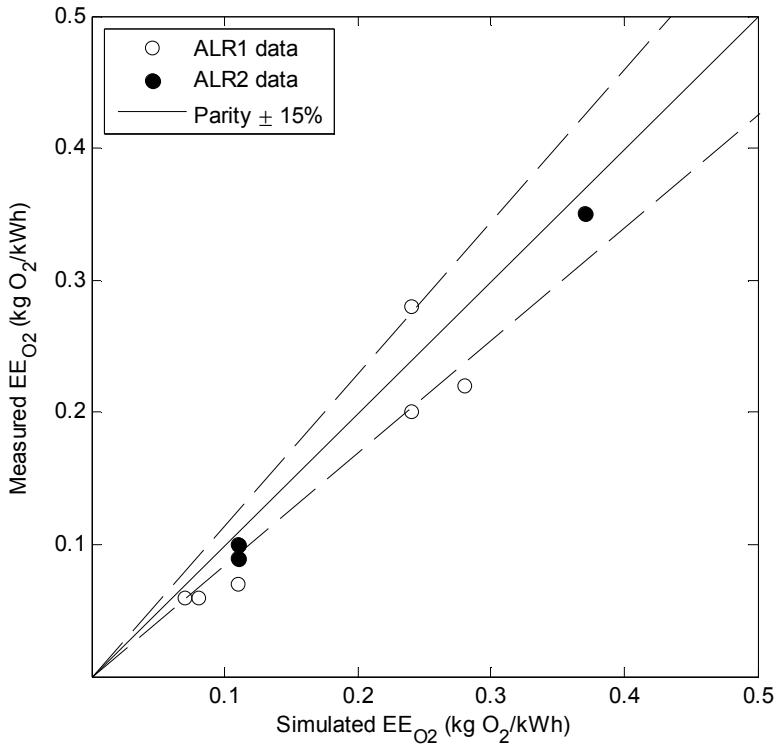

Figure 5.12. Parity plot of the measured EE_{O2} as function of the simulation EE_{O2} for the ALR fermentations using the mass transfer correlation of this work. The model covers well the entire range of fermentation conditions. The simulation error on average for the ALR1 and ALR2 fermentations is 18±16% and 9±5%, respectively. EE_{O2} was calculated including power consumption for air compression and cooling.

5.4 Conclusions

Nine fermentations of *T. reesei* were carried out in two different ALR configurations. In the ALR, the strain of *T. reesei* exhibited very similar yield coefficients and RQ as in the STR and the carbon mass balance was acceptable. The ALR configuration introduced some technical difficulties, which meant that the feed flow rate in some cases had to be adjusted manually. It was shown that the ALR technology could be used for fermentations of *T. reesei* even with lower aspect ratios than normally exploited for ALRs and possible improvements to the design of the reactor were discussed.

To estimate the viscosity of the fermentation broth the effective shear rate was based on the riser superficial gas velocity. A viscosity model was created which predicted the rheological properties of the fermentation broth as function of the biomass concentration. The accuracy of the viscosity model was within the uncertainty related to the assumed concept of an effective shear rate of the

vessel. The shear fields in any bioreactor are position dependent and the estimation of local or global shear rates are extremely complex and were not the subject of this work.

The correlations between the rheological parameters K and n and the biomass concentration were different from those observed for the STR. This could be due to the low biomass concentrations obtained in the ALR which meant that the comparison was not made over the same range of biomass concentrations. It could also be speculated that higher local mechanical forces in the STR influenced the morphology characteristics of the strain. More detailed studies would be needed to make certain conclusions on this matter.

Two mass transfer correlations were shown to predict the k_La with satisfactory accuracy. One was purely based on riser superficial gas velocity and was approximately 20% lower than the mass transfer correlation from the literature (Barker and Worgan, 1981). The second mass transfer correlation included a viscosity term to account for the decreasing k_La values that were observed as function of fermentation time. The apparent viscosity was shown to negatively impact k_La with an exponent of ~0.18. This means that a viscosity increase to 0.020 Pa.s leads to a reduction in mass transfer of ~40%. The ALR2 configuration had higher k_La values than the ALR1 configuration at least at low superficial gas velocities.

The mixing time of the ALR was measured by the conductivity method for three different media and compared to the STR. Mixing times in the ALR2 were lower than in the ALR1, but were in the range 57-87 s for both configurations with the 0.125% xanthan solution, which resembles the fermentation broth most closely. The mixing times were in the same order of magnitude as the characteristic time for oxygen transfer of the system, which indicates that mixing might also be limiting the fermentation. Finally the mixing times of the ALR were compared to those of the STR. For the STR mixing times were in the order of twice the salt tracer injection time (20 s).

The process model developed for the STR in Chapter 2 was also employed for prediction of the ALR fermentations. The viscosity model was revised using slightly different rheological correlations with the biomass concentration and the mass transfer correlation containing the riser superficial gas velocity and the apparent viscosity was inserted in the model. The nine ALR fermentations carried out were simulated well by the process model. The conditions covered were $0.02<v_{g,r}<0.06$ with headspace pressures from 0.1-1.1 barg.

Chapter 6

Objective comparison between airlift reactor and stirred tank reactor

In Chapter 4 the performance of the airlift reactor in relevant scale was estimated based on the literature data and correlations. The pilot scale trials described in Chapter 5 have provided detailed information about the level of mass transfer that can be expected in the medium used for *T. reesei* fermentations and how the fermentation broth viscosity differed from the STR fermentations. The process model was refined and proved to describe the ALR fermentations accurately too. In this chapter, the results obtained using the ALR and the STR at pilot scale will first be compared using two different estimations of the vessel power input. Finally and most importantly, the ALR and STR are evaluated at relevant scale using the revised process model.

6.1 Comparison of pilot scale experimental data

The power input of a fermentation vessel may be estimated in various ways. In this section, two different approaches for estimating the power input are employed. It will be clear that the choice of approach influences the results and might lead to very different conclusions.

Approach 1. The conventional approach: Power dissipated to the fermentation broth
The power input from mechanical agitation is the power actually dissipated to the fermentation broth determined by Eq. (2.22). The compression power input is estimated by the superficial gas velocity (Chisti, 1989). Specifically, in bubble columns and airlift reactors this is calculated by

$$\frac{P}{V_{\mathrm{L}}} = \frac{\rho g v_{\mathrm{g,r}}}{1 + \frac{A_{\mathrm{d}}}{A_{\mathrm{r}}}} \tag{6.1}$$

In the literature, this is the commonly used approach for fermentor comparison (Gasner, 1974; Schügerl, 1990; Schügerl, 1991; Schügerl, 1993).

Approach 2. An integrated approach: The total power consumption of the fermentor
The total power consumption of the fermentation vessel considers that of agitation (the

power consumption of the motor), aeration (the power consumption of the compressor), and cooling, following Eq. (2.22) - (2.28) of Chapter 2. The energy that is to be removed by cooling consists of metabolic heat and the energy dissipated by the stirrer. The possible energy loss due to evaporation depends on the fermentation temperature and humidity of the air and only plays a minor role compared to the metabolic heat development (Soderberg, 1997).

6.1.1 Distribution of the power consumption

The respective contributions to the power consumption of agitation, aeration, and cooling (only in approach 2) are shown in Figure 6.1 for all pilot scale fermentations. The power consumption for agitation of the STR fermentations was designed to be 1.5, 9, or 15 kW/m^3; here the realized values as average of the entire fermentations are shown. For approach 1, the energy dissipated in the STR is almost completely from agitation. The energy dissipated by aeration in the ALR was always below 1 kW/m^3.

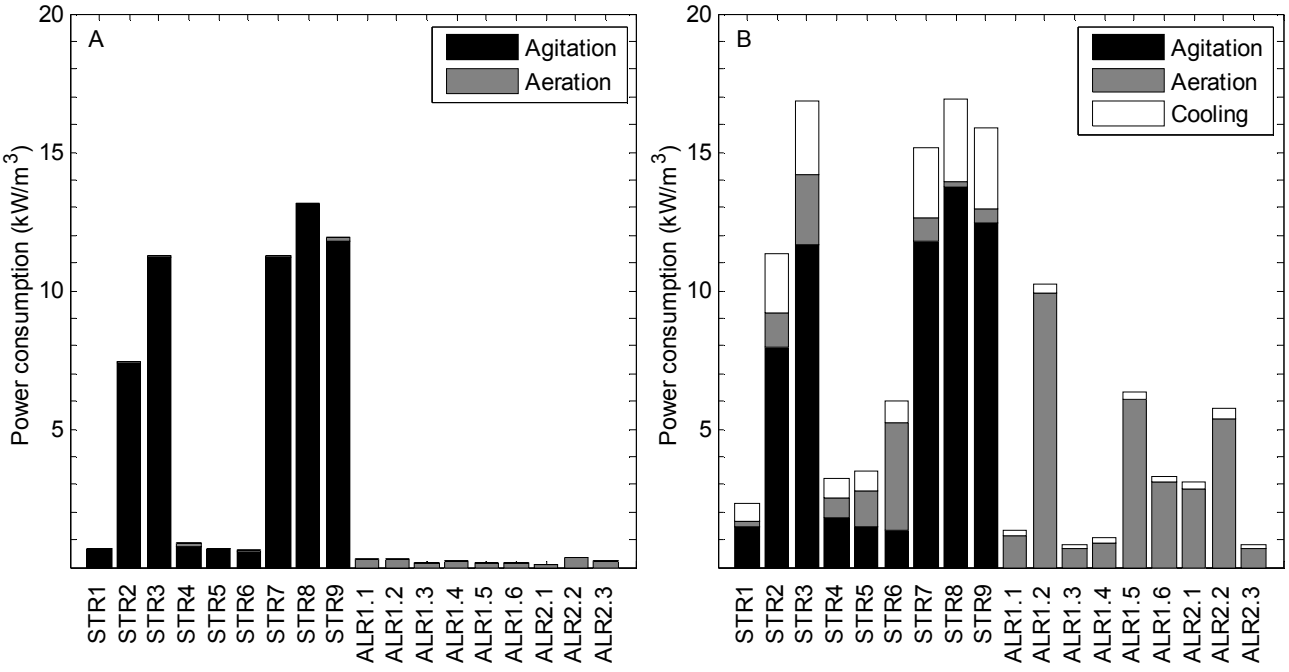

Figure 6.1. Two approaches for the estimation of the power consumption of STR and ALR fermentations in pilot scale. **A:** Approach 1: Power dissipation to the liquid broth from agitation and aeration. **B:** Approach 2: Total power consumption of the fermentation vessel with contributions from agitation, aeration (compressor power consumption) and cooling.

For approach 2, agitation on average accounted for 62% of the total STR power consumption, while cooling contributed with up to 25% of the total power consumption. For the ALR, cooling on average only contributed 11% of the total power consumption. Notably also is the large influence of

the headspace pressure on the power consumption for aeration. In ALR2.3 the low headspace pressure of 0.10 barg and 505 NL/min aeration rate required a power consumption of 0.65 kW/m^3, while the lower aeration rate of ALR2.1 of 475 NL/min with 1.10 barg headspace pressure required a power consumption of 2.8 kW/m^3. The power consumption of the ALR fermentations was in general lower than for the STR. Four ALR fermentations were carried out with 0.1 barg headspace pressure and the power consumption of those fermentations was around 1 kW/m^3. It is clear that the power dissipated by the air (approach 1) was much smaller than the power consumed by the compressor in order to deliver the air.

6.1.2 Key performance indicators

The key performance indicators have been calculated for all fermentations using both approach 1 and approach 2. The oxygen transfer rates and EE_{O2} for approach 1 are shown as function of the total power consumption in Figure 6.2A+B, respectively. The ALR fermentations had much lower power inputs than the STR fermentations. As expected, the STR fermentations also had the highest oxygen transfer rates. The estimated values of EE_{O2} were up to 2.3 kg O_2/kWh for the ALR and up to 1.3 kg O_2/kWh for the STR; however this was only achieved at the lowest power inputs.

For approach 2, the oxygen transfer rates and EE_{O2} are shown in Figure 6.2C+D. While the measured OTR obviously was not changed compared to approach 1, the calculated power consumption for all fermentations was higher compared with approach 1. For similar power consumption, the OTR was lower in the ALR than the STR, and EE_{O2} was higher for the STR at similar power consumption. In a single case was the EE_{O2} higher for the ALR, and this was achieved at the lowest power input, which was lower than the STR power inputs of this study. Approach 1 and 2 give significantly different values of EE_{O2}, especially for the ALR where the difference between the energy input by aeration and the actual energy consumption by the compressor is large.

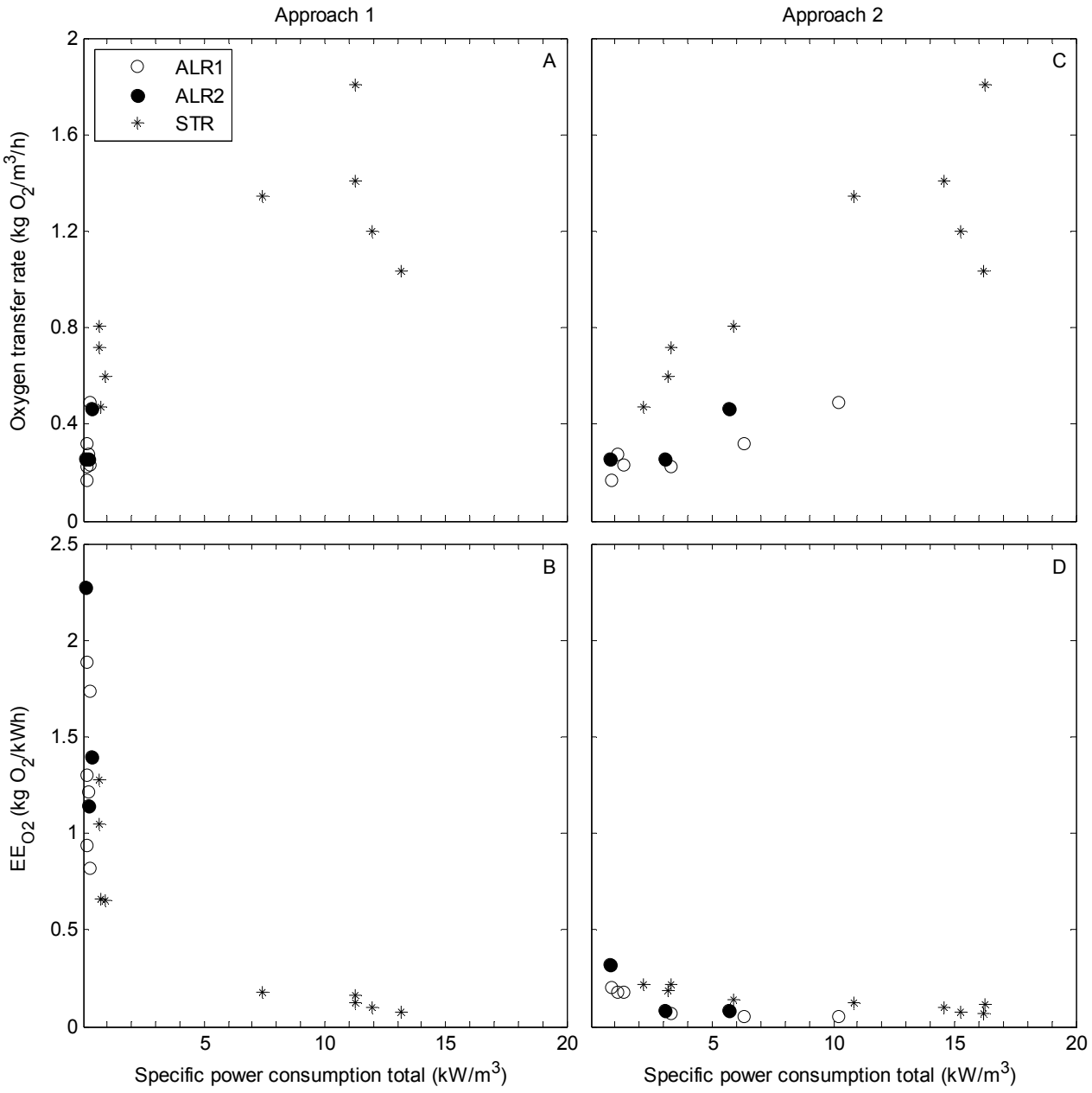

Figure 6.2. Oxygen transfer rate and EE_{O2} for all pilot scale STR and ALR fermentations as function of the total power input. **A:** OTR for approach 1. **B:** EE_{O2} for approach 1. **C:** OTR for approach 2. **D:** EE_{O2} for approach 2. For approach 1, less power was dissipated in the ALR fermentations, and the OTR and EE_{O2} cannot be compared at equal power consumption for the two fermentation technologies. EE_{O2} was estimated around 2 kg O_2/kWh or higher for some ALR fermentations, while the highest EE_{O2} for the STR was 1.3 kg O_2/kWh. For approach 2, at similar power consumption the oxygen transfer rate was lower in the ALR than the STR. For similar power consumption, EE_{O2} was higher for the STR. At low power consumption, the highest achieved EE_{O2} was 0.32 for the ALR at 1 kW/m^3, while an EE_{O2} of 0.22 was achieved in the STR with a power consumption of around 3 kW/m^3.

In Figure 6.3 EE_{O2} is shown as function of oxygen transfer rate for all fermentations for approach 1 and approach 2, respectively. For approach 1, the ALR1.2 and ALR2.2 fermentations had similar

oxygen transfer rates as the low power STR fermentation and had higher values of EE_{O2}. Even higher values of EE_{O2} were observed for ALR2.1 and ALR1.5 (2.3 and 1.9 kg O_2/kWh, respectively), though at lower oxygen transfer rates. The ALR fermentations with the highest values of EE_{O2} were carried out with the highest headspace pressures. For approach 2, the ALR fermentations in general provided a lower oxygen transfer rate; only in two cases were the ALR oxygen transfer rates as high as the lowest STR oxygen transfer rates. Five ALR fermentations had both low oxygen transfer rates and low EE_{O2}. Those five ALR fermentations were carried out with headspace pressure higher than 0.10 barg. This shows that increased headspace pressure in the ALR is not economical at pilot scale.

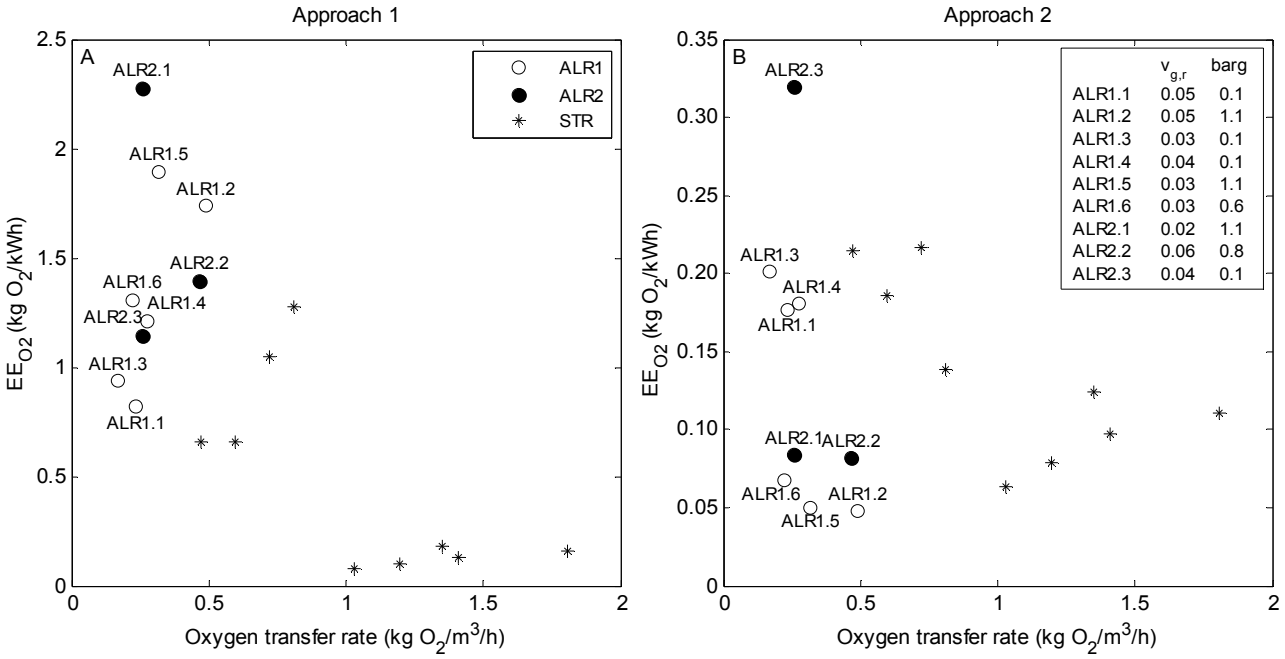

Figure 6.3. EE_{O2} as function of oxygen transfer rate for all STR and ALR fermentations. **A:** Approach 1. The ALR fermentations reached values up to 2.3 kg O_2/kWh, while the STR reached up to 1.3 kg O_2/kWh. The highest EE_{O2} were obtained with the highest head space pressure. At similar oxygen transfer rates, the ALR1.2 and ALR2.2 fermentations had a considerably higher EE_{O2} than the low power STR fermentations **B:** Approach 2: The STR generally achieves the same EE_{O2} as the ALR but at a higher OTR. Five ALR fermentations were characterized with both low oxygen transfer rates and EE_{O2}: ALR1.2, ALR1.5, ALR1.6, ALR2.1, and ALR2.2. These were the ALR fermentations carried out with headspace pressures higher than 0.10 barg. ALR2.3 had the highest EE_{O2} of 0.32 kg/kWh. Note that ALR2.3 was carried out with identical conditions as ALR1.4. Also note that **A** and **B** have different axes.

ALR2.3 was carried out with $v_{g,r} = 0.04$ and a headspace pressure of 0.10 barg. Following approach 2, the average OTR was 0.25 kg O_2/m^3/h while the EE_{O2} was 0.32 kg O_2/kWh. This EE_{O2} was 50% higher than observed for the low power STR. The low power STR however was operated at oxygen transfer rates around 0.6 kg O_2/m^3/h, which means that in order to achieve the same quantitative oxygen transfer the ALR must be operated with a larger volume than the STR.

Interestingly, ALR1.4 was operated with the same fermentation conditions as ALR2.3, but EE_{O2} for

the ALR2.3 was almost twice as high. There are a number of possible reasons for the better performance of the ALR2.3. First, it is likely that the design of the ALR2 is superior to the ALR1 in terms of mixing and mass transfer. The ALR2 had a larger volume and thus a higher aspect ratio, which can have improved the liquid circulation and led to the decrease in mixing time measured in Chapter 5. Secondly, the higher volume of the ALR2 led to a better utilization of the compressed air and allowed for a longer time of oxygen exchange between the air bubbles and the fermentation broth. Finally, as shown in Figure 5.4 the carbon substrate feed rate was manually adjusted in the last half of the fermentation when the DOT signal was missing. It is therefore quite likely that ALR1.4 was not limited by the oxygen transfer rate as the DOT controlled substrate feeding of ALR2.3.

6.1.3 Discussion of calculation method of power consumption

In this section, two different approaches of estimating the power consumption of fermentation vessels have been utilized. The results have shown that depending on the method, very different conclusions may be made.

Approach 1 may be grasped as the theoretical and strictly correct approach of investigating the effect of the dissipated power on mass transfer and mass transfer efficiency. Approach 2 attempts to evaluate the entire power consumption of the fermentation vessel. It is used in order to evaluate the total power consumption of the system, imitating the value of an imaginary energy meter of the system.

For the industrial manufacturer of a biotechnological product, approach 2 seems to be the most objective way to compare technologies. If approach 1 is used, some unpleasant and surprising energy bills will surely result from the vast underestimation of the cooling demand and the compressor power consumption. Approach 1 is however widely used in the literature and if comparison with literature data is needed, taking this approach is necessary.

6.2 Comparison at industrial scale

6.2.1 Evaluation of cost efficiency

The scope of this work has until now been to investigate the energy and substrate efficiencies of fermentation technologies. It has been shown that the substrate yield coefficients and thus also the substrate efficiency are independent on the fermentation technology. The experimental data have confirmed that the energy efficiency of each technology depends on the process conditions, and a mechanistic model has been shown to describe the experimental data well.

The comparison at pilot scale showed that at equal oxygen transfer rate, less energy was consumed per oxygen transfer in the STR reactor than in the ALR. The ALR is however usually operated at low oxygen transfer rates, where the efficiency (of both technologies) is higher. In order for the

ALR to have the same total oxygen transfer as the STR a larger fermentation volume is thus needed. This can be achieved by having a larger numbers of fermentors or by increasing the vessel size.

This section has a dual purpose. First, based on the process model the optimal reactor specification and process conditions for the ALR and the STR are sought. Secondly, with this knowledge the two technologies should be objectively compared. In other words, the problem can be defined as the search for optimum design of oxygen transfer in the ALR and the STR for the *T. reesei* fermentation process. Following the principles of engineering process design, the criteria for optimality can ultimately be reduced to a consideration of costs (Peters et al., 2003). The development of an optimum design usually involves the following phases which will be covered in this section:

- Determination of the objective function that is to be minimized or maximized

- Determination of the design process variables and the process constraints

- Identification of optimum conditions

6.2.1.1 *Determination of the objective function*

The objective function in this case is the total cost of oxygen transfer, which should be minimized for the optimal fermentation design. The cost of oxygen transfer, C_{O2} (\$/kg O_2), can be estimated by the relation between the sum of the equipment investment cost, $C_{\text{investment}}$ (\$/h) and the running cost, RC (\$/h), and the time specific oxygen transfer

$$C_{O2} = \frac{C_{\text{investment}} + \text{RC}}{\text{OTR} \cdot V_L} \tag{6.2}$$

where the time specific oxygen transfer is easily found as the OTR (kg O_2/m^3/h) multiplied with the volume (m^3).

To simplify the estimation of the cost efficiency, only the reactor, the compressor, and the cooling system are taken into account for the investment cost. Humbird et al. (2011) have collected vendor quotes for fermentors (303 m^3, internal cooling coils), fermentor agitators (800 horse power), and air compressors (225 Nm^3/min at 3 atm) for their detailed lignocellulosic ethanol plant (Humbird et al., 2011). In this work, the cooling system is including the agitator cost as 40% of the agitator price (Peters et al., 2003). In Table 6.1 the costs of the equipment are summarized as well as the scaling exponent and the installation cost factors used. A number of costs including piping, instrumentation and controls, as well as electrical systems are assumed to be constant and are therefore not considered.

Table 6.1. Scaled installed costs of the mechanical equipment considered for the cost function. Adopted from Humbird et al. (2011). Prices are in 2007$.

Equipment	Size	Cost ($)	Scaling exp.[a]	Inst. Factor
Fermentor (internal cooling coils)	303 m^3	400,000	Eq. (6.3) - (6.5)	2
Agitator, motor, and cooling system	588 kW	812,000	0.4	1.5
Air compressor	225 (Nm^3/min)	350,000	0.6	1.6

[a](Peters et al., 2003)

The fermentor cost is estimated by calculating the total weight of the vessel following the procedure of Peters et al. (2003). The weight of the fermentor specified above was estimated, and the cost factor is then applied to the other fermentor geometries and sizes explored here.

The maximal internal pressure of the vessel is then calculated as the headspace pressure plus the liquid pressure of a completely filled tank plus 2.5 bar for safety. The minimum wall thickness for cylindrical shells is (Peters et al., 2003)

$$t = \frac{P_i r}{SE_J - 0.6P_i} + C_c \tag{6.3}$$

where t is the wall thickness, P_i is the maximum allowable internal pressure, r is the reactor radius, S is the maximum allowable working stress, E_J is the efficiency of joints, and C_c is the allowance for corrosion. For stainless steel 316, S =79,300 kPa, and the joint efficiency E_J = 0.85 assuming spot-examined double welded butt joints. The corrosion allowance was assumed to be 3.8 mm (Peters et al., 2003). The heads of the fermentors were assumed to be torispherical and their weight was estimated by (Peters et al., 2003)

$$\rho_{SS316} \frac{\pi(T + T/24 + 3t)^2 t}{4} \tag{6.4}$$

The weight of the fermentor specified by Humbird et al. (2011) was estimated to be 37,993 kg using Eq. (6.3) and (6.4) and assuming 20% weight increase for nozzles, manholes, and saddles (Peters et al., 2003).

The cost of pressure vessels as price per kilogram weight of the fabricated unit is given by (Peters et al., 2003)

$$\text{Cost} = C_p \left(W_v\right)^{-0.34} \tag{6.5}$$

where C_p is the cost factor and W_v is the total calculated weight of the vessel (kg). Using the cost of 400,000$ for the 37,993 kg reactor, the specific cost of the vessel including internal cooling coils is

10.52 \$/kg. The cost factor is therefore estimated as $C_p = 230$. Using this procedure and cost factor, the cost of all fermentor configurations can be estimated.

For the estimation of the compressor cost, the dependence of pressure is neglected since compressors are usually designed to have a working overpressure higher than needed here; thus only the volumetric flow rate is considered to be cost related (Knoll et al., 2005). For the estimate of the specific investment cost, a lifetime of ten years is used. The specific investment cost for the ALR is given by

$$C_{\text{investment,ALR}} = \frac{C_{\text{reactor}} + C_{\text{compressor}}}{10 \cdot 8760\text{h}} = \frac{C_{\text{reactor}} + 1.6\left(\frac{Q_N}{225}\right)^{0.6} 350{,}000\$}{87600\text{h}} \tag{6.6}$$

Similarly, the specific investment cost for the STR is given by

$$C_{\text{investment,STR}} = \frac{C_{\text{reactor}} + C_{\text{agitator}} + C_{\text{compressor}}}{10 \cdot 8760\text{h}}$$

$$= \frac{C_{\text{reactor}} + 1.5\left(\frac{P_a}{558}\right)^{0.6} 580{,}000 + 1.6\left(\frac{Q_N}{225}\right)^{0.6} 350{,}000\$}{87600\text{h}} \tag{6.7}$$

For example, the specific investment cost of a 200 m^3 ALR with an aspect ratio of 7 that requires an aeration rate of 50 Nm^3/min is estimated below with the fermentor weight estimated at 40,750 kg

$$C_{\text{investment}} = \frac{2 \cdot 380\$/\text{kg}\left(40{,}750\right)^{-0.34} \cdot 40{,}750\text{kg} + 1.6\left(\frac{50}{225}\right)^{0.6} 350{,}000\$}{87{,}600\text{h}} = 12.16\$/\text{h} \tag{6.8}$$

The running cost is estimated by the power consumption for agitation, aeration, and cooling as well as the cost of nutrients. The annual average utilization ratio was set to 0.7 and the electricity cost, EC, was set to 0.05717 \$/kWh (Humbird et al., 2011). The cost of nutrients is assumed to equal the cost of the carbon source. The carbon source requirement per oxygen transfer, $Y_{OC} = 1.47$ g/g, and its cost, $C_{carbon} = 0.526$ \$/kg, were adopted from Humbird et al. (2011)

$$\text{RC} = \left(P_a + P_c + P_w\right) \cdot \text{UR} \cdot \text{EC} + V_L \cdot \text{OTR} \cdot Y_{OC} \cdot C_{\text{carbon}} \tag{6.9}$$

6.2.1.2 *Determination of design process variable and process constraints*

Different fermentor geometries and process conditions were investigated for each technology. The

intervals for these process variables are given in Table 6.2. The intervals were chosen based on rule of thumb values obtained from the available literature about the respective technologies.

Table 6.2. Process variables for each fermentation technology

Process variable	Airlift reactor	Stirred tank reactor
Fermentor size (m^3)	100-1000[d]	100-400[c]
Fermentor aspect ratio (-)	1.5-25[d]	2-5[a,b]
Agitation intensity (kW/m^3)	-	0.5-7[c]
Superficial gas velocity (v_g or $v_{g,r}$, m/s)	0.069-0.2[d]	0.05-0.2[c]
Headspace pressure (barg)	0-2[a]	0-2[a]

[a](Chisti, 2003), [b](Humbird et al., 2011), [c](Middleton, 1997), [d](Moresi, 1981)

The developed process model contains the desired DOT set point which determined the substrate feed flow rate. In that regard the process model is inherently constrained. A physical constraint was however included since the partial pressure of CO_2 seemingly impacts product formation negatively at certain levels. For the strain investigated in this work, there seemed to be a threshold level around 40-60 mbar, but the constraint was set here to pCO_2>200 mbar since it has not been determined for other strains and it is also expected to depend on pH and other medium properties.

6.2.1.3 *Identification of optimum conditions*

The enzyme production considered here is a fed-batch fermentation. This implies that the liquid volume during fermentation will almost never be constant; this would only be the case when the evaporation rate of water equals the carbon and ammonium feed flow rate. Therefore the following procedure was followed for the application of the process model to each fermentation technology:

1. A set of process variables were assumed (fermentor size, aspect ratio, agitation intensity, superficial gas velocity, and head space pressure). The initial filling was set to 60% of the fermentor size.
2. The process model was run and the final filling and average liquid volume were calculated.
3. The final filling was compared with the fermentor volume. The final filling target was 80% of the fermentor volume. The initial filling was adjusted (step 1) and the procedure was repeated until the target of 80±2% final filling target was reached.
4. The operating and investment cost were evaluated as shown above.

Identification of the optimum reactor design and operation conditions is a multivariable task. Therefore, the response surface methodology – a statistical tool known from design of experiments – was used in order to explore the relationship between the process variables with the ranges

specified in Table 6.2 (in statistical language termed the explanatory variables) and the cost efficiency evaluation (termed the response variable) (Montgomery, 1997). The statistical design was a central composite design enabling the determination of interaction and squared terms. A central composite design of the process variables was constructed for each technology, fermentation simulations were performed using the process model, and the cost efficiency was evaluated in each case. The design and simulation results are given in the appendix (Table B.1 and B.2).

Second-degree polynomial models were then approximated for the cost efficiency and the pCO_2 of fermentation for each technology. The design and data analysis were carried out in the software JMP 8.0.1. Non-significant effects were removed successively (highest p-values first), until only effects with $p<0.05$ remained.

6.2.2 Airlift reactor

The constraint of $pCO_2<200$ was reached at aspect ratios above ~15 for almost any combination of the remaining variables. Therefore in the following a maximum aspect ratio of 13.2 is assumed. The results of the statistical models for C_{O2} and pCO_2 are shown as function of the four process variables for the ALR in Figure 6.4. The following key observations can be made: 1) combinations of headspace pressure and high aspect ratios often lead to inacceptable levels of pCO_2, 2) large vessel volumes combined with low riser superficial gas velocity lead to the most favorable operation, 3) there seems to be optimum levels of headspace pressure and aspect ratio. The optimal conditions of the airlift reactor within the biological constraint were predicted at the maximum fermentor volume (1000 m^3), the minimum riser superficial gas velocity $v_{g,r}$ = 0.069 m/s, and a headspace pressure of 1 barg. It was not possible to determine the exact optimal aspect ratio. The minimum cost of oxygen transfer at these conditions was predicted at ~0.95$/kg O_2, see Figure 6.4.

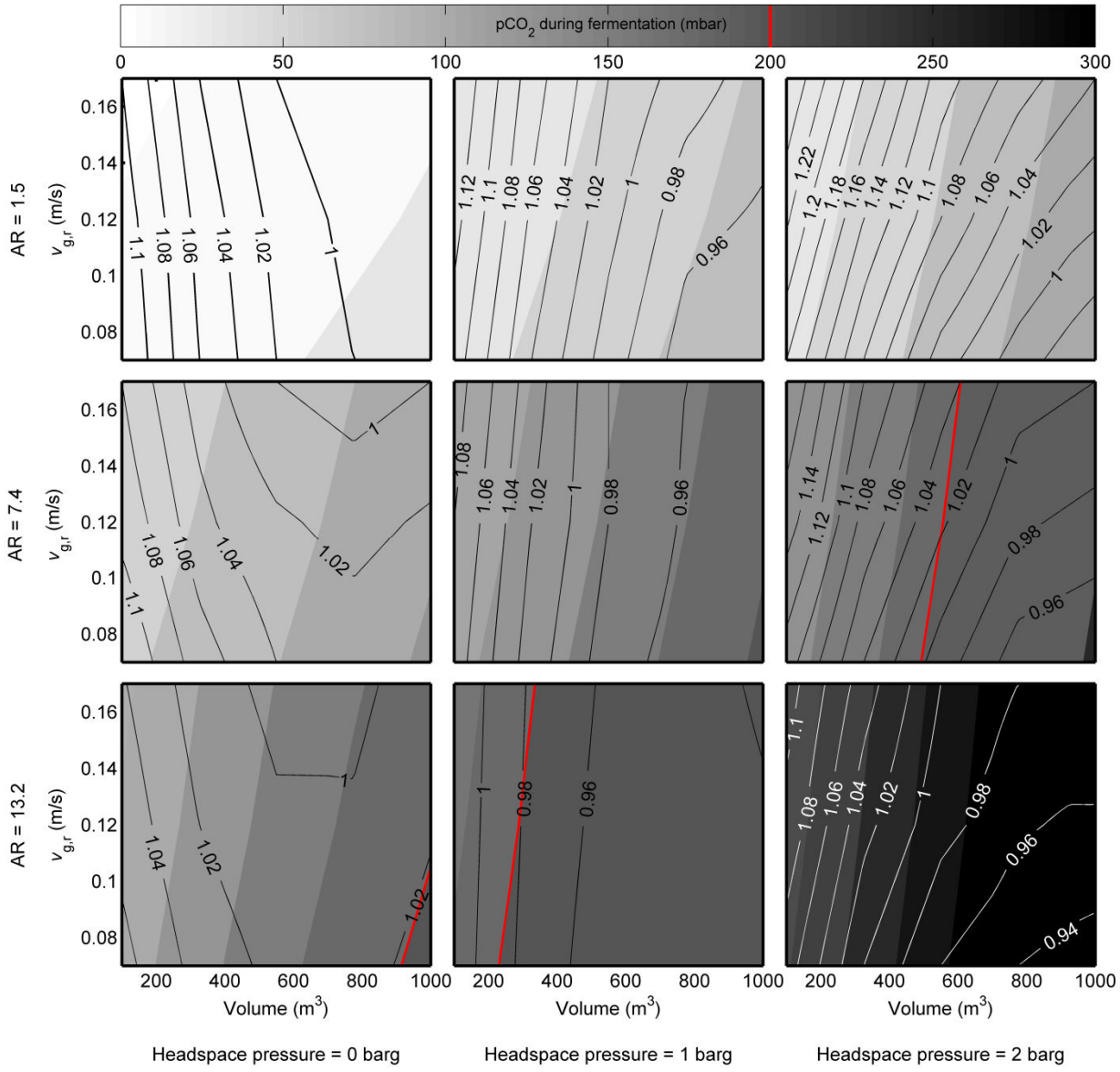

Figure 6.4. Statistical model of the airlift reactor: Cost of oxygen transfer (contours, \$/kg O_2) and corresponding carbon dioxide partial pressure (shading, mbar) as function of aspect ratio (from top to bottom: 1.5, 7.4, or 13.2, respectively), riser superficial gas velocity (y-axis), headspace pressure (from left: 0, 1, or 2 barg, respectively), and fermentor volume (x-axis). The prediction of the lowest cost (within the biological limit) is with aspect ratios between 1.5 and 7.4, headspace pressure of 1 barg, minimum riser superficial gas velocity and the maximum volume.

The statistical model was used to predict the approximate optimal conditions. This reduced the number of simulations needed to be run. It was decided to investigate in detail the operational space around the optimum identified by the statistical model. The aspect ratio and the headspace pressure were varied while the volume was set to 1000 m^3 and the riser superficial gas velocity was set to 0.069 m/s. The results of these simulations are shown in Figure 6.5. The lowest cost was achieved with a headspace pressure of 1 barg and aspect ratio ~5. The optimum aspect ratio with no

headspace pressure seems to be lower. Aspect ratios in the range 2-6 only changed the cost of oxygen transfer within 3% for a headspace pressure of 1 barg. At an aspect ratio of 5, a headspace pressure of 2 exceeds the biological constraint of the system, and the optimal headspace pressure is close to 1 barg. The simulation results are very similar to the predictions of the statistical model shown in Figure 6.4.

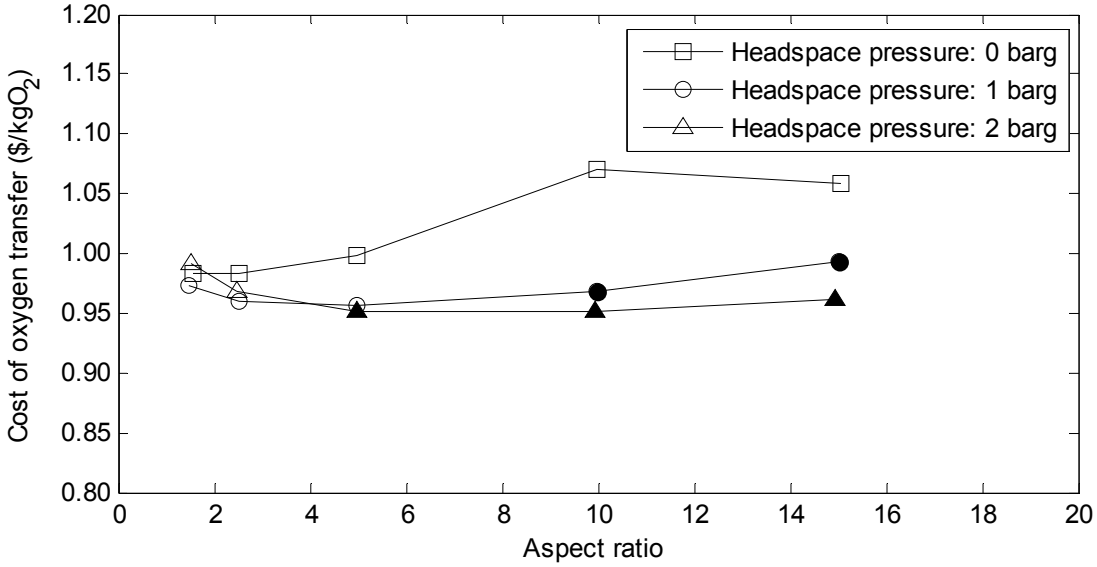

Figure 6.5. Simulation-based estimations of the cost of oxygen transfer as function of headspace pressure and aspect ratio for the airlift reactor. The fermentor volume was 1000 m^3 and the riser superficial gas velocity was 0.069 m/s. The filled symbols represent conditions where pCO_2>200 mbar and were thus not considered. The lowest cost was achieved with a headspace pressure of 1 barg and aspect ratio ~5. The cost difference between different levels of headspace pressure was clearly low. Also, in this operating region, aspect ratios between 1.5 and 10 only changed the cost within 10%.

6.2.3 Stirred tank reactor

The design space of the STR in this work has an additional variable, the agitation intensity (P/V). Therefore, the results of the statistical model for the STR are shown in three separate figures with headspace pressures of 0, 1, and 2 barg. The results shown in Figure 6.6 were obtained with a headspace pressure of 1 barg, while the remaining predictions are found in the appendix. The following key observations can be made for the STR: 1) large vessel volumes give lower cost, 2) low agitation intensities give lower cost, 3) low superficial gas velocities give lower cost, 4) high aspect ratios seem to give lower cost. The cost of oxygen transfer is predicted to be in the range ~1.05-1.45 $/kg for the STR.

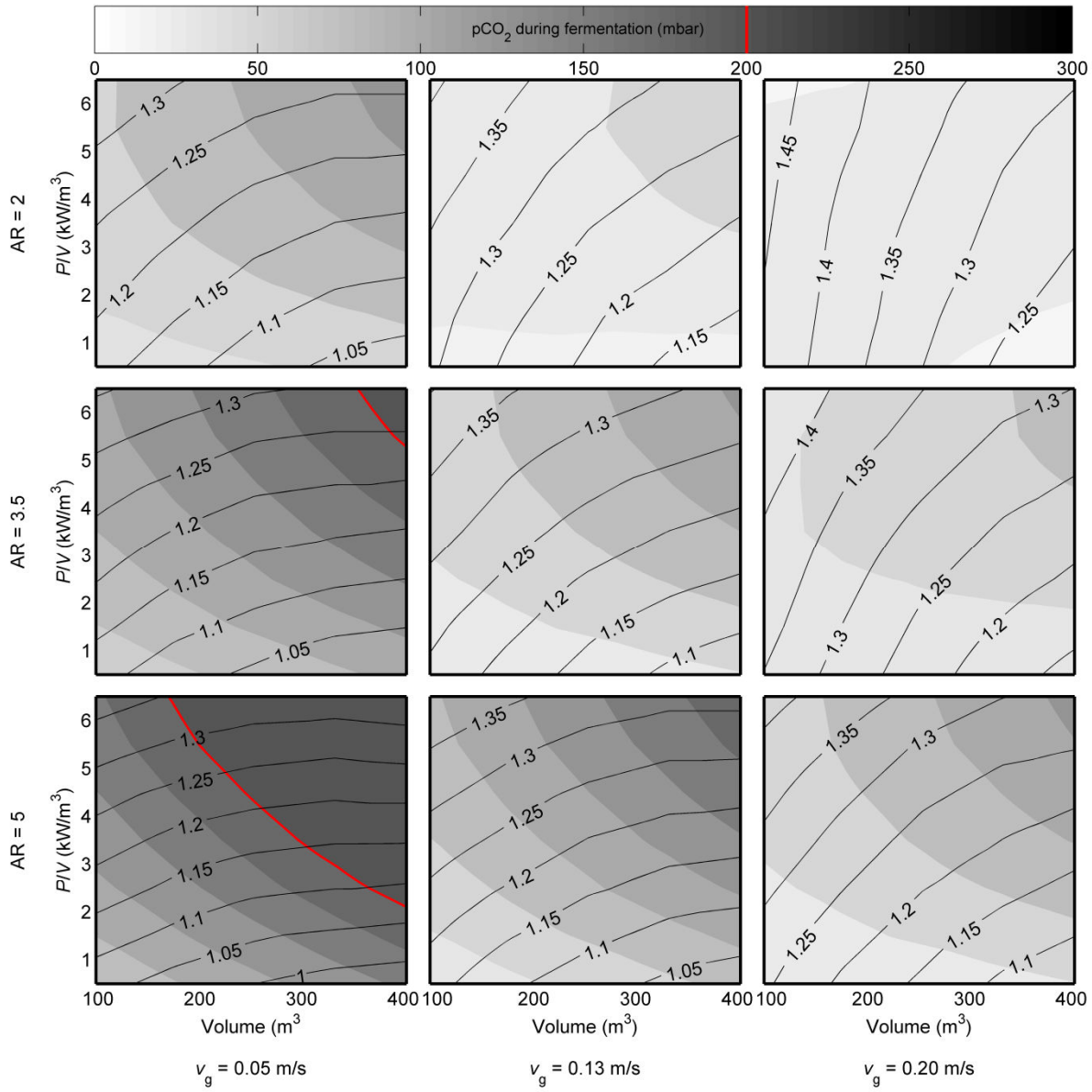

Figure 6.6. Statistical model of the stirred tank reactor: Cost of oxygen transfer (contours, \$/kg O_2) and corresponding carbon dioxide partial pressure (shading, mbar) as function of aspect ratio (from top to bottom: 2, 3.5, or 5, respectively), agitator power input (y-axis), superficial gas velocity (from left: 0.05, 0.13, or 0.20 m/s, respectively), and fermentor volume (x-axis). The head space pressure was 1 barg. The optimum conditions seem to be large volume, low agitation power input, and low superficial gas velocity.

In order to identify the optimal conditions for the STR, the volume was set to the maximum of 400 m^3, the superficial gas velocity was set to the minimum of 0.05 m/s, the agitation intensity was set to the minimum of 0.5 kW/m^3, while three different aspects ratios were tested and the headspace pressure was varied between 0-2 barg. The results of these simulations are given in Figure 6.7. From this figure it can be seen that higher aspect ratios give lower oxygen transfer costs, even though the difference between aspect ratios of 2 and 5 is below 6%. Furthermore there seems to be

an optimum headspace pressure between 0.5 and 1 barg depending on the aspect ratio.

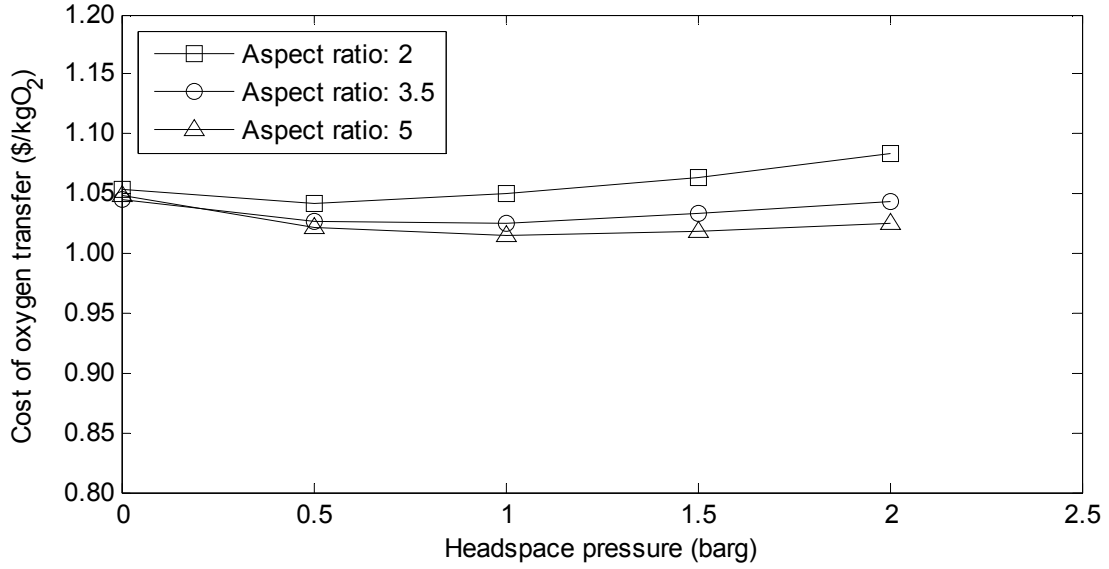

Figure 6.7. Simulation-based estimations of the cost of oxygen transfer as function of aspect ratio and headspace pressure for the STR. The fermentor volume was 400 m^3 and the riser superficial gas velocity was 0.05 m/s. High aspect ratios give lower costs, while there seems to be an optimum headspace pressure between 0.5 and 1.5 barg depending on the aspect ratio. The cost of oxygen transfer with an aspect ratio of 5 and a headspace pressure of 1 barg was 1.015$/kg O_2, however the cost changes within 3% for headspace pressures between 0-2 barg (aspect ratio of 5).

6.2.4 Comparison

The analyses summarized in this chapter have led to a prediction of the most desirable configurations for the industrial scale airlift reactor and the stirred tank reactor. It is important to remember that the fermentor design and operating conditions have been selected simultaneously. This means that for example a higher headspace pressure increased the oxygen transfer driving force but also increased the fermentor and compressor costs since a higher pressure should be accommodated for in the fermentor design and more aeration was needed to maintain the same superficial gas velocity at higher pressure. Therefore the differences between similar configurations are not very big (see Figure 6.7).

In Table 6.3 three reactor designs are presented. The optimal configuration of the ALR identified in this chapter has a large volume, aspect ratio of 5, relatively low aeration, and headspace pressure of 1 barg. The STR1 configuration was identified as the optimal STR configuration. It has a large volume, high aspect ratio of 5, low agitation intensity, and headspace pressure of 1 barg. The STR2 configuration included in this comparison is identical to STR1 except for the headspace pressure, which is equal to zero for the STR2. It is not surprising that for a number of the reactor variables, the optimum is one of the extreme values of the conditions specified in Table 6.2.

It is seen that the ALR is ideally operated with an OTR of 0.75, which is similar to the STR2 with no headspace pressure. The STR1 is operated with an OTR of 1.15 because of the increased driving force, which however also increases the aeration need. The energy efficiencies of the reactors are also provided. The EE_{O2} for the optimum ALR is estimated at 0.336 kg O2/kWh, which is the highest of the three compared configurations. The efficiency is lower than predicted in the technology screening of Chapter 4 (EE_{O2} = 0.40), since the experimental mass transfer rate was lower than the literature data used for the screening. The EE_{O2} of the two STR configurations are around 0.29 kg/kWh. The efficiency is lower than that of the ALR, but higher than predicted in the literature screening (EE_{O2} = 0.13), since the configuration has now been optimized.

Table 6.3. Reactor design and process variables for the optimum design for the ALR and two STR configurations within the biological constraint of the process model.

	Optimum ALR	STR1	STR2
Fermentor design			
Volume (m^3)	1000	400	400
Aspect ratio	5	5	5
Fermentor height (m)	36	26	26
Diameter (m)	5.85	4.34	4.34
Agitator capacity(kW/m^3)[a]	0	0.5	0.5
Aeration (Nm^3/min)	187	114	93
NVVM ($Nm^3/m^3/min$)	0.19	0.29	0.23
Headspace pressure (barg)	1	1	0
Oxygen transfer rate (kg $O_2/m^3/h$)[b]	0.75	1.15	0.74
EE_{O2} (kg O_2/kWh)	0.336	0.290	0.283

[a]The specified agitator capacity is the maximum installed agitator in relation to the total fermentor volume. *P*/*V* during fermentation is higher since the start filling is approximately 50% of the fermentor volume. [b]OTR is the average data obtained by the process model from this work.

The energy efficiency as predicted by simulation is shown as function of the predicted oxygen transfer rate for both technologies in Figure 6.8. These were the simulations used for constructing the statistical models shown in Figure 6.4 and Figure 6.6, and simulations with pCO_2>200 mbar have been removed. Interestingly, the two technologies cannot be distinguished in this representation. The ALR does not seem to deliver higher energy efficiency at equal oxygen transfer rate. It is also seen that the results of the technology screening of Chapter 4 are covered quite well by the simulations of this chapter. The trend observed in Figure 6.8 is similar to what was seen in Figure 2.7, which is an inverse relationship between oxygen transfer efficiency and the productivity

of the process. The influence of viscosity is again worth remembering, since a high power input or OTR leads to higher biomass concentration and eventually higher viscosity. This mechanism favors low energy systems.

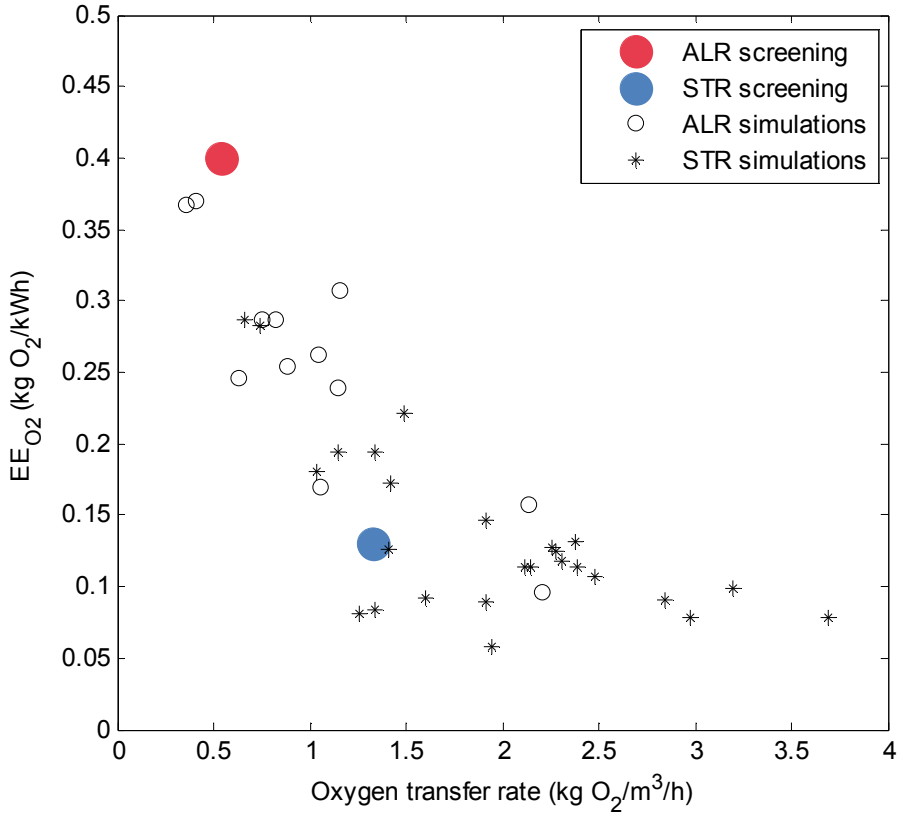

Figure 6.8. Simulated energy efficiency shown as function of oxygen transfer rate for the ALR and the STR. The data from the technology screening of Chapter 4 are shown for comparison. The simulation details are seen in Table B.1 and B.2.

The total costs of oxygen transfer are summarized in Table 6.4 for the three reactor configurations. The total cost ranges from 0.949 \$/kg O_2 for the ALR to 1.042 \$/kg O_2 for the STR2 configuration. The largest contributor to the total cost is the cost of nutrients. In this analysis only the carbon substrate is considered, but the cost of nutrients is 5-7 times larger than the electricity cost. The nutrients cost is the same for all technologies, since identical yield coefficients of substrate on oxygen consumption were assumed in the analysis.

Assuming identical volumes, the fermentor cost is lower for fermentors with high aspect ratios than fermentors with low aspect ratios, since the cost is related to fermentor weight and the fermentor wall thickness. The fermentor wall thickness is not dependent on fermentor height, only the fermentor diameter. Furthermore, the specific fermentor cost is assumed to decrease with the fermentor weight (with a negative exponent of 0.4). This explains why all configurations have high aspect ratios. The agitator cost also influences the total cost significantly.

Table 6.4. Cost of oxygen transfer ($/kg O_2) of three reactor configurations

	Optimum ALR	STR1	STR2
Capital cost			
Fermentor cost	0.053	0.049	0.061
Agitator and cooling system	-	0.033	0.045
Compressor cost	0.012	0.015	0.019
Total capital cost	**0.065**	**0.097**	**0.125**
Electricity cost			
Agitation	-	0.029	0.040
Aeration	0.081	0.076	0.066
Cooling	0.030	0.035	0.037
Total electricity cost	**0.111**	**0.139**	**0.143**
Nutrients cost (carbon substrate)	**0.773**	**0.773**	**0.773**
Total cost of oxygen transfer($/kg O_2)	0.949	1.010	1.042

The electricity cost of the STR is estimated between 0.139-0.143 $/kg O_2. The contribution from cooling is higher or similar to the contribution from agitation. Interestingly, the total electricity cost for the ALR is up to 22% lower than that of the STR, even though the ALR requires more electricity for aeration.

The comparison between STR1 and STR2 indicate that increased headspace pressure can be a way to increased oxygen transfer rate *and* higher energy efficiency. This comparison is valid for a future enzyme production facility where the operation pressure of the compressor can be matched exactly to the requirements (the minimum pressure to sparge the air into the bottom of the fermentor). For an existing facility (where a compressor system is already installed) it could be most optimal to run the process with as high headspace pressure as possible.

6.2.5 Uncertainties of the comparison

6.2.5.1 *Mixing at large scale*

The comparison of this section has relied on a process model with the oxygen mass transfer model as the governing equation. Thus it has been assumed, that the oxygen mass transfer is the limiting rate. It was shown in Chapter 5 that the mixing times of the ALR in pilot scale were in the same order of magnitude as the characteristic time for oxygen transfer. Mixing therefore could also be

limiting the ALR. However, for the ALR it has been shown that liquid velocity and thus mixing is generally improved upon scale-up as function of the liquid height (Chisti et al., 1988)

$$v_{l,r} \propto Z^{0.5} \tag{6.10}$$

where $v_{l,r}$ is the liquid velocity in the riser. A tall ALR presumably leads to a more defined liquid circulation flow and lower circulation times. Mixing of the large scale ALR may therefore prove to be better than observed in the pilot scale experiments and not impose a greater challenge at scale-up.

Mixing times in industrial scale STRs are much longer than in laboratory or pilot scale. Mixing times might be in the range 150-250 s, and the mixing time is certainly a function of agitation intensity (Li et al., 2002). Furthermore it is well known that increasing aspect ratio leads to longer mixing times and the following relation has been suggested for both radial and axial flow impellers (which have approximately half the mixing time of radial impellers) (Cooke et al., 1988)

$$t_{\text{mix}} \propto \left(H / T\right)^{2.43} \tag{6.11}$$

Eq. (6.11) clearly shows that mixing should be considered if the aspect ratio of the STR is increased in the effort to increase energy efficiency of the fermentor system. The effect of longer mixing times could be studied using a scale-down model like described in the literature (Enfors et al., 2001)

6.2.5.2 *Capital cost estimations*

It is quite clear that the total capital costs of an actual enzyme production facility are larger than estimated here. It has been estimated that the purchased and installed equipment (as considered here) constitutes 30% of the total capital investment of a new facility (Peters et al., 2003). Therefore the absolute numbers in this work cannot be used for direct comparison.

The specific cost of fermentation vessels is assumed to decrease with a negative exponent of 0.4 of the fermentor weight. There are however upper limits to the size and thickness of fermentors that can be constructed. These limits include practical issues such as the feasibility of transporting the fermentors, physical limits of steel rolling mills, and the limits of the thickness of steel that is to be welded. The cost of fermentors therefore might not decrease with scale as assumed in Eq. (6.5) and some fermentor configurations may not be possible to construct at all. The cost of fermentors is furthermore not only a function of the fermentor weight. For very tall fermentors, custom-made support for the fermentor and i.e. enforced foundations are likely to add significantly to the cost.

The cost of the cooling system is here included in the agitator cost price and therefore not included in the ALR capital costs. However it might not be very large due to the cooling effect of the evaporation of water and the possible co-location with other facilities.

In this analysis a default fermentation time was specified and used for all cases. To complete the analysis, the optimal fermentation time (including down time) should be determined for each fermentor configuration and considered in the analysis.

Finally, in this analysis the economy of scale is considered in the scaling exponents of Table 6.1. However, the cost function does not include construction expenses and the cost for engineering and supervision. These expenses decrease with the number of fermentors being installed and create a benefit of multiple units instead of a single larger volume.

Chapter 7

Overall conclusions and suggestions for future work

7.1 Overall conclusions

The production of cellulases in submerged fermentations of *Trichoderma reesei* has been studied in pilot scale. Fed-batch fermentations were carried out in the traditional STR and in one alternative configuration, the ALR. A mechanistic model has been developed to describe the process of the fed batch fermentation. The model consists of four interchangeable parts: 1) the reaction equation, 2) a mass transfer correlation, 3) a viscosity prediction, and 4) a mathematical description of the process including the process control variables.

For the STR, the model proved to describe the fermentation process well for a range of conditions applied including agitation intensity from 1.5-15 kW/m^3, aeration rates from 96-320 NL/min, and headspace pressure from 0.1-1.3 barg. In the ALR, the model covers superficial gas velocities in the riser from 0.02-0.06 m/s and a headspace pressure from 0.1-1.1 barg. For both technologies it was shown that the energy efficiency of the fermentation process is a function of the process conditions. In general, the efficiency of the process is inversely proportional to the productivity. This relation was predicted successfully by the process model.

Nine fermentations were carried out using the ALR technology. The strain of *T. reesei* exhibited the same yield coefficients in the ALR as measured in the STR. The rheological properties however were shown to be slightly different functions of the biomass concentration than in the STR. The viscosity model for the ALR model was revised based on this new knowledge. The mass transfer correlation for the ALR was approximately 20% lower than the corresponding literature correlation. A viscosity term was incorporated in the mass transfer correlation with an exponent of -0.18, indicating a less adverse effect of viscosity than in the STR. An increase of viscosity of e.g. 0.020 Pa.s “only” results in a mass transfer reduction of 40%. The mixing time for the ALR configurations tested in pilot scale was measured in viscous fluids with properties resembling those of the fermentation broth. The mixing time was estimated in the range 40-60 s.

When different fermentation technologies are compared, it is of great importance to consider the total power consumption of the system. The approach often used in the literature is based on the power dissipated to the fermentation broth. If a technology is selected on these grounds, the energy consumption at large scale might be underestimated considerably.

The process model was used to identify the optimal reactor design and process conditions for the ALR and the STR based on oxygen transfer. The cost function included capital costs for the fermentor, agitator, and compressor and running costs for electricity and nutrients. Large volumes combined with low power inputs lead to lower overall cost of oxygen transfer. It was shown that depending on the design and process conditions up to 22% of the electricity cost may be saved, while the cost for nutrients remains the largest contributor to the overall cost. Mixing was not considered in the comparison but mixing may be improved upon scale-up in the ALR, while for the STR mixing is impaired at lower energy inputs and larger scale.

7.2 Suggestions for future work

7.2.1 Focus on energy efficiency

The comparison between the two technologies investigated in this thesis suggests that the energy consumption might be reduced up to 22% by a change in technology from the optimal STR configuration to the optimal ALR configuration. The ALR has a lower specific productivity and thus demands a larger total vessel volume to maintain the same enzyme production rate.

However, the energy consumption at present represents a relatively minor part of the total cost of enzyme production so a fiscal motive for technology chance is missing. A large part of the total cost is constituted by nutrients, and the studies performed in the frame of this thesis have shown that the consumption of nutrients is independent of process conditions and fermentation technology. Development of even more efficient strains might however lead to improved yield coefficients in the future.

The future electricity price and the increasing focus on energy efficiency might lead to changes in the enzyme production. The development in average US electricity price is shown in Figure 7.1. In the 1970s much work around optimization of bioreactor operation and design was carried out, and there again seems to be focus on this area. If energy costs increase, it would raise the incentive to converge to less energy consuming technologies and processes.

The increased focus on energy efficiency could also play a role in the future choice of technologies. For example, the European Commission has set a target for 2020 of saving 20% of its primary energy consumption compared to the projections (European Commision, 2011). Higher energy efficiency is claimed to enhance security of energy supply and to reduce emissions of greenhouse gas and other pollutants. Furthermore, a number of companies now openly report their energy consumption and CO_2 emissions (e.g., Wall-Mart: http://walmartstores.com/sustainability/ and Novozymes: http://report2011.novozymes.com/). It is not unlikely that factors such as energy efficiency and energy savings can be competitive parameters that some companies can use to increase market shares.

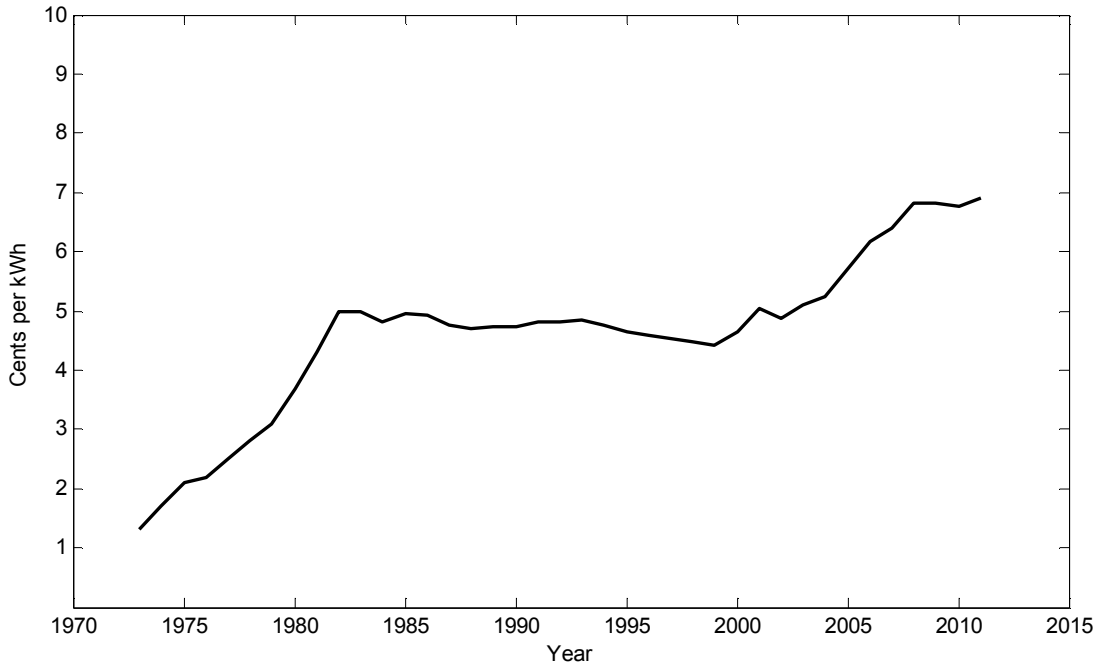

Figure 7.1. Development in US electricity price since 1973 (cents per kWh including taxes). The price is the annually average retail price of electricity for the industrial sector. Prices vary over time and by locality due to the availability of power plants and fuels, local fuels costs, and pricing regulation and structures. Source: U.S. Energy Information Administration, www.eia.gov/energyexplained/index.cfm?page=electricity_factors_affecting_prices (accessed March 4th 2012)

7.2.2 Development of a detailed airlift reactor process design

This thesis contains a preliminary process design of cellulase production in the ALR. Compared with the STR, the total cost efficiency of the ALR was found to be lower based on capital costs and electricity costs, while the nutrient costs were the same. Any commercial producer must develop a detailed process design for a plant, which involves many other factors such as plant location, downstream operations, and waste management systems. Those factors depend on the business strategy and possible co-location with customers and suppliers. All of the above considerations may influence the choice of technology.

It is assumed here that a change in technology would only be considered for the construction of future enzyme production facilities. In the development of a detailed process design, a number of refinements to the cost estimation must be considered. The estimation of the capital investment must include direct costs such as land, buildings, piping, electrical systems, and instrumentation as well as indirect costs such as engineering and supervision, construction expenses, and contingency (Peters et al., 2003). The estimation of the manufacturing costs must furthermore include all raw material costs, operating labor, and maintenance (Peters et al., 2003).

Of the abovementioned factors, it is likely that there are differences between the STR and the ALR

which have not been included in this work. For example the labor requirements for the larger ALRs might be bigger. It should be the task of experienced project planners and plant engineers to estimate these costs and provide a more detailed process design.

Finally it will be the task of the managements of the companies or collaborative consortia of companies to decide upon the future enzyme production technology. The STR is very well known and used from laboratory scale through pilot plant scale to production scale. The ALR has been - and is currently - used in production scale of various biotechnological processes, but some uncertainty is definitely involved with regard to its introduction as the main production technology for industrial enzymes. The ALR has a lower probability of mechanical failure and likelihood of loss of sterility. The ALR is less flexible than the STR in the sense, that power input is constrained by the aeration capacity of the fermentor.

7.2.3 Airlift reactor scale up

If decision should be taken to explore the use of the ALR in production scale, an approach to maximizing the probability of a successful result is proposed here. It seems that the development within computational fluid dynamics (CFD) has now reached a level of maturity that makes it useful for bioreactor design and optimization. CFD utilizes computer power to make numerical simulations and predictions of fluid flow, heat, mass, species concentration, and momentum transfer in a model system (Revstedt et al., 1998). CFD models are based on the conservation statements for each quantity transported with the flow, and this is calculated for the whole volume of the fluid which is subdivided into small control volumes (Brown, 2009). While the use of CFD is certainly a task of experienced analysts, it seems that much useful work can be done with CFD now. A recent article describes for example how a CFD model of an ALR can be coupled with a growth model of *Trichoderma reesei* using the open-source CPD package OpenFOAM (Bannari et al., 2012). However, a major concern surrounding the use of CFD should be validation of the computer simulations, which is not always easy.

Based on the data collected in this thesis, it could be possible to validate a CFD model for the current ALR configuration including the non-Newtonian rheology of the fermentation broth (ANSYS Inc., 2011). The obtained data for mixing time and oxygen mass transfer could serve as basis for this validation (see Figure 7.2 for an example of a CFD model). Next, a CFD simulation of the production scale ALR could be created as well. The CFD model could serve as a tool in determining the optimal engineering design of the production scale ALR by prediction of various scale-up effects. The technical problems to be overcome also include the design and position of the draft tube or split baffle, and the design of the sparger. The development of reliable CFD model requires appropriate software and expertise.

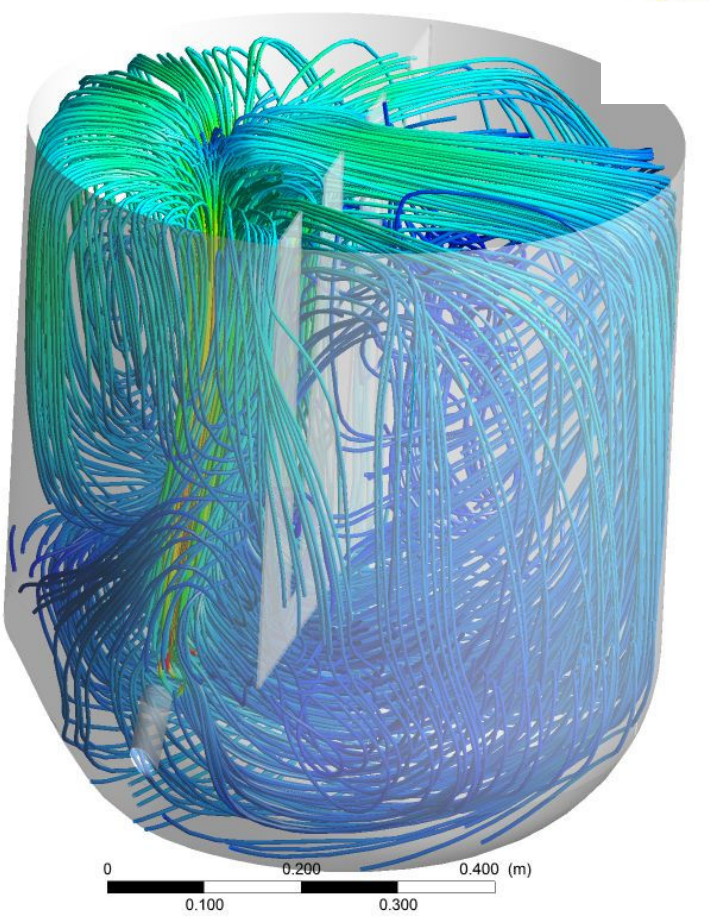

Figure 7.2. Example of CFD interpretation of the liquid flow pattern in the ALR1 configuration using the software ANSYS. CFD model kindly provided by Ulrich Krühne, Department of Chemical and Biochemical Engineering at the Technical University of Denmark.

Finally, it is advised to construct a demonstration ALR that can serve as validation of the models. Such a vessel should have a relevant geometry and size representative of the hydrodynamics of the proposed final design. Experiments with production strains should be carried out in order to investigate the possible sensitivity to pCO_2.

7.2.4 Optimization of the stirred tank reactor

If the STR is used as the future enzyme production technology, this work has proven that the STR can be operated with varying efficiency and productivity. While it is certain that mixing is impaired at lower agitation intensities, energy efficiency is increased as long as mass transfer of oxygen is the limiting rate. Considering the scale of operation, it is worthwhile to consider the design and process conditions of future facilities using process models like the ones shown in this work.

The analysis suggests that the fermentor volume could be increased for lower overall costs, while

the agitation intensity could be decreased. In addition to the effect on mixing performance, higher fermentor volumes also decrease the flexibility of the production facility and impact the design of the recovery process. All of such diverted effects must also be considered before taking a decision on changing the current enzyme production technology.

Appendix

Appendix A: Supplementary data for chapter 5

Rheological characterization

A number of different proportionality constants for Eq. (5.2) have been suggested in the literature as shown in Table A.1, the disparity among the constants is large. It is generally agreed that the correct solution is still to be found (Chisti, 1989; Merchuk and Gluz, 2002). Here, the different proportionality constants will be compared in the presentation of the rheological characterization of the fermentation broth.

Table A.1. Effective (average) shear rate in bubble columns as a function of superficial gas velocity for three studies.

Reference	Correlation	Variation of n	Equation	Derivation
Nishikawa et al (1977)	$\dot{\gamma}_{\text{eff}} = 5000 v_{\text{g}}$	1-0.72	(5.2a)	Heat transfer
Henzler (1980)	$\dot{\gamma}_{\text{eff}} = 1500 v_{\text{g}}$	0.82-0.38	(5.2b)	Lit. $k_{\text{L}}a$ data
Schumpe and Deckwer (1987)	$\dot{\gamma}_{\text{eff}} = 2800 v_{\text{g}}$	1-0.18	(5.2c)	Own $k_{\text{L}}a$ data

Combination of the three different riser superficial gas velocities and the three proportionality constants reveals that the effective shear rates of this study are estimated between 45 and 250 1/s. The rheological characterization was performed in the span 10-300 1/s which thus covers the expected shear rate range. In Figure A.1 the measured shear stress is shown as a function of shear rate for an arbitrarily chosen fermentation sample. Also the calculated apparent viscosity is shown. The broth shows shear thinning behavior as the apparent viscosity decreases with the shear rate. The apparent viscosity in the range of 45-250 1/s decreases from 0.023 Pa.s to 0.013 Pa.s.

The power law model

$$\tau = K\dot{\gamma}^{n} \tag{A.1}$$

and the Herchel-Bulkley model (Nienow, 1998)

$$\tau = \tau_{\text{y}} + K_{\text{HB}}\dot{\gamma}^{n_{\text{HB}}} \tag{A.2}$$

were tested for their ability to describe the rheological properties of the fermentation broth. The rheological parameters K, n, τ_{y}, K_{HB}, and n_{HB} were estimated using least squares regression. Both models proved to describe the observed rheological behavior with high values of R^2 (0.9942 and 0.9991, respectively). In the shear rate range 45-250 1/s there is little difference between the two models. For example, assuming an effective shear rate of 168 1/s the difference between the models is less than 2%. It should be remembered that the parameters K and n of Eq. (A.1) are highly correlated and so are τ_{y}, K_{HB}, and n_{HB} of Eq. (A.2) and therefore direct comparison between the parameters obtained for each model does not seem reasonable (Petersen et al., 2008).

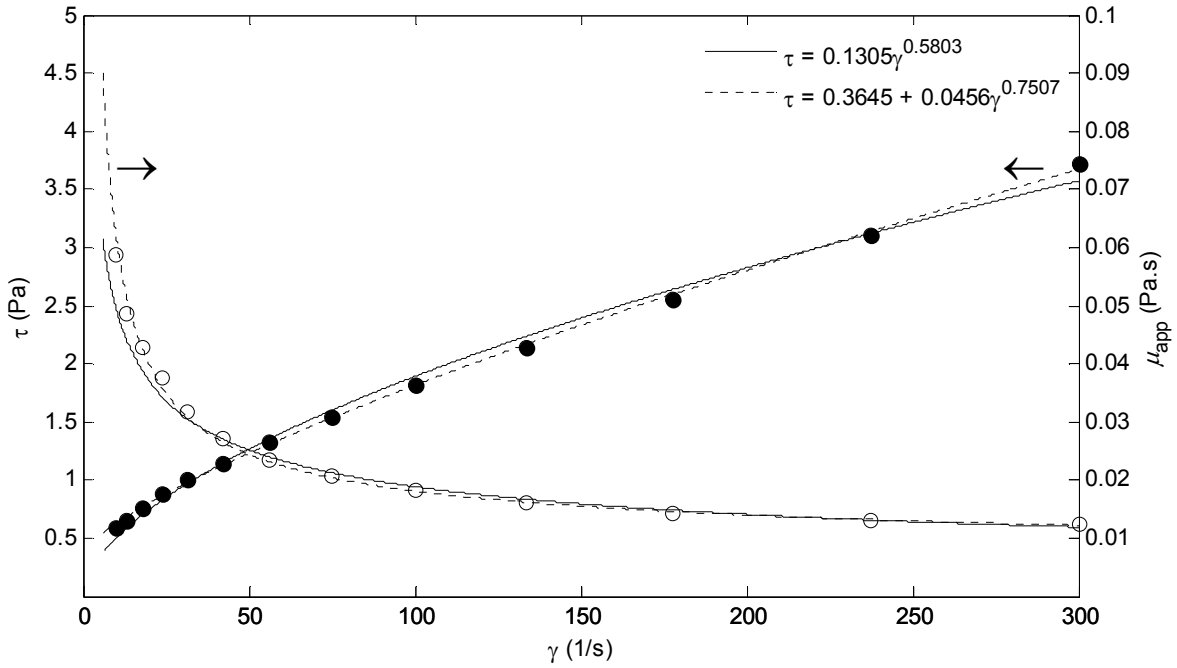

Figure A.1. Example of the rheological characterization of the fermentation broth (ALR2.2). 14 steady state measurements of the shear stress (left axis) were made within the shear rate range of 10-300 1/s. The calculated apparent viscosity is also shown (right axis). Two rheological models were tested for their ability to describe the observed shear thinning behavior: the power law and the Herschel-Bulkley model (R^2 = 0.9942 and R^2 = 0.9991, respectively). Assuming an effective shear rate of 168 1/s ($v_{g,r}$ = 0.06 m/s and Eq. (5.2c)) the model predicted effective viscosity is 0.0152 and 0.0149, respectively (<2% difference).

The apparent viscosity calculated by both models for all measurements for ALR2.2 is shown as function of fermentation time in Figure A.2. The difference between the two models was always below 5% and on average the difference was 3.1%. Since it can be seen from Figure A.1 that the yield stress of the fermentation broth is quite small (<0.5 Pa.s), it seems reasonable therefore to use the power law model. The power law has one parameter less than the Herschel-Bulkley model but describes the rheological behavior in the relevant shear rate range equally well. The important parameter here is the apparent viscosity and not the actual rheological parameters.

The result of the differences between the proportionality coefficients in Eq. (5.2A-C) can be seen in Figure A.3.. The size of the proportionality constant primarily impacts the relative position of the viscosity curve. The difference between the apparent viscosities can be up to 0.010 Pa.s. It was decided to use Eq. (5.2C), the least radical of the three relations, in this work.

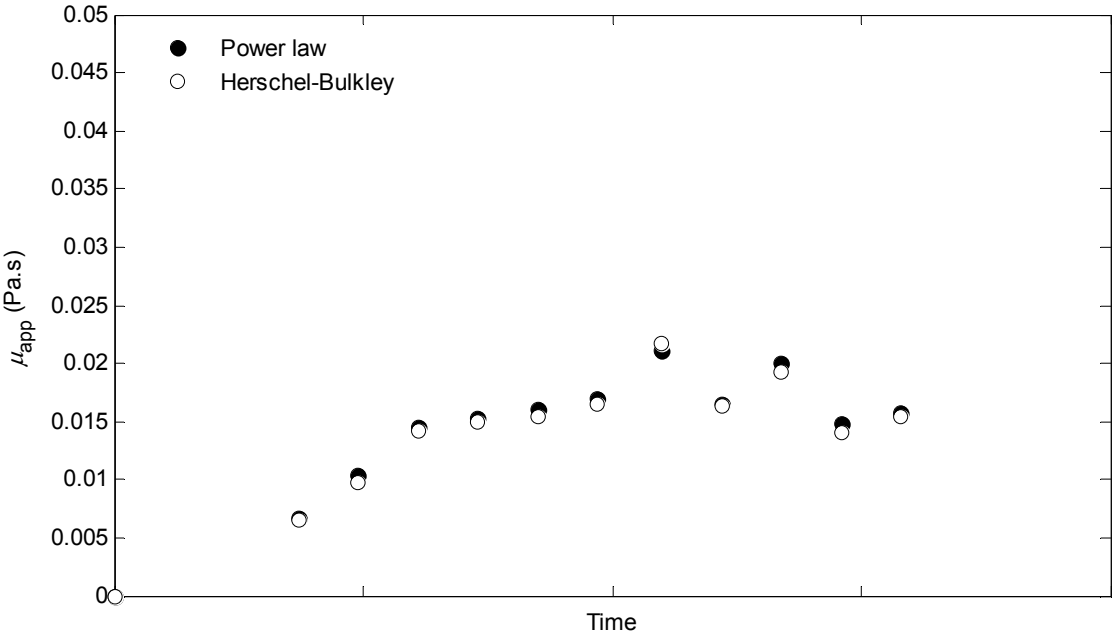

Figure A.2. Apparent viscosity determined by regression of the rheological measurements by the power law and the Herschel-Bulkley model shown as function of time for ALR2.2 ($\dot{\gamma}_{eff}$ = 168 1/s). The average difference between the predictions is 3.1%.

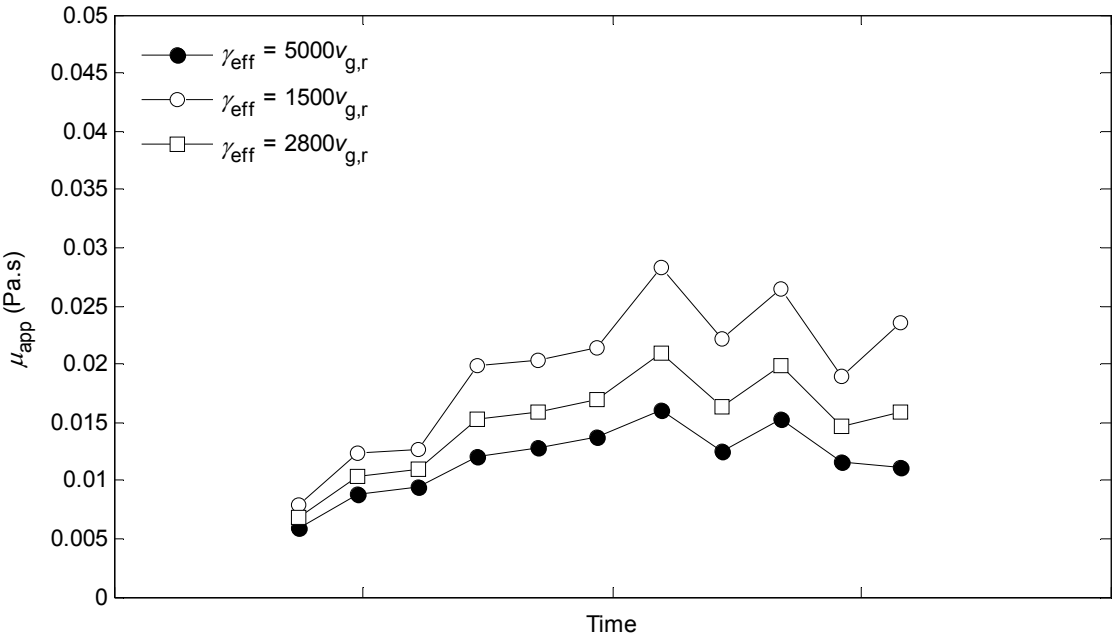

Figure A.3. Apparent viscosity determined by use of three different proportionality coefficients in Eq. (5.3). The fermentation is ALR2.2 and the power law model is used.

Rheological measurements during fermentation

The power law model was applied to all rheological measurements. The rheological development during the fermentation is shown in Figure A.4-Figure A.6. The consistency index varies quite significantly between the fermentations and it also appears in some fermentations that K fluctuates quite a lot (Figure A.4). Generally K increases during the course of fermentation to values up to 0.4 Pa.s^n. The flow behavior index development with fermentation time is depicted in Figure A.5. At the fermentation start n is close to 1 and decreases to values between 0.4 and 0.8 towards the end of the fermentations. Also n seems to fluctuate for some fermentations; note however that as K and n are highly correlated, the values of each of the parameters are not as important as the apparent viscosity calculated based on both of these. The apparent viscosity is shown as function of fermentation time for all ALR fermentations in Figure A.6. $v_{g,r}$ ranged from 0.02-0.06 m/s and the effective shear rate was calculated based on Eq. (5.2C). The apparent viscosity ranged during the course of fermentation from values around 0.001 Pa.s at the fermentation start up to values of 0.030 Pa.s.

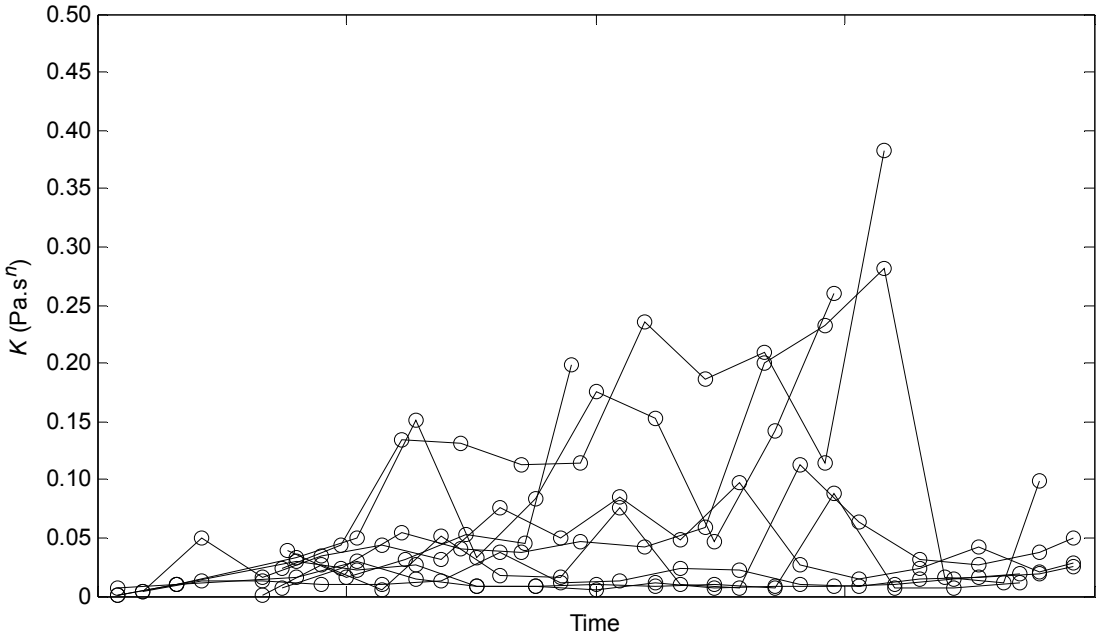

Figure A.4. Measurements of the consistency index K as function of fermentation time for all ALR fermentations.

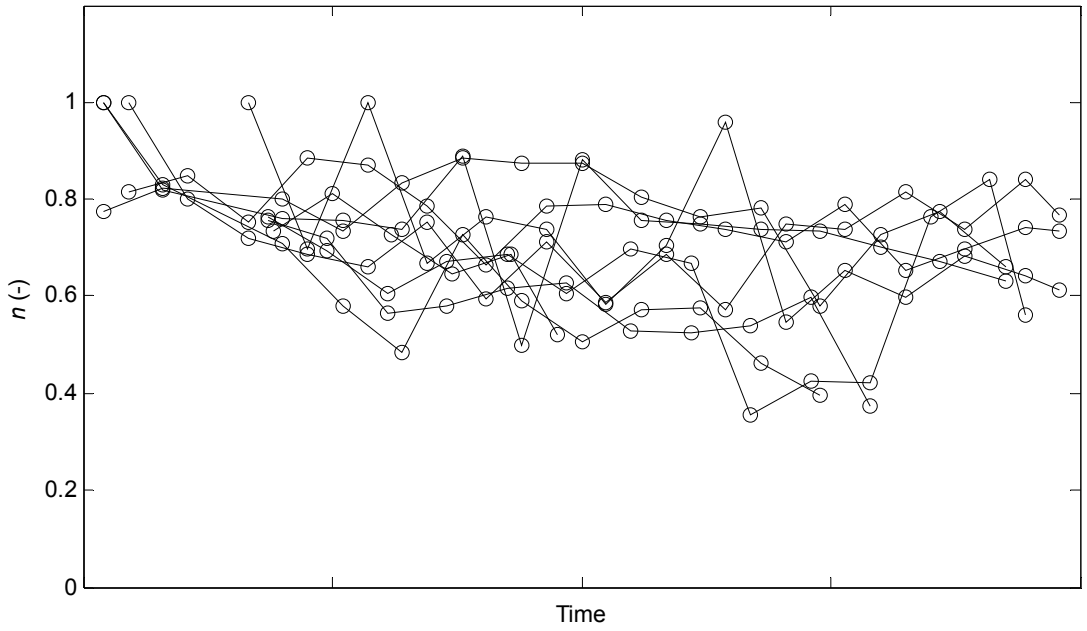

Figure A.5. Measurements of the flow behavior index *n* as function of fermentation time for all ALR fermentations.

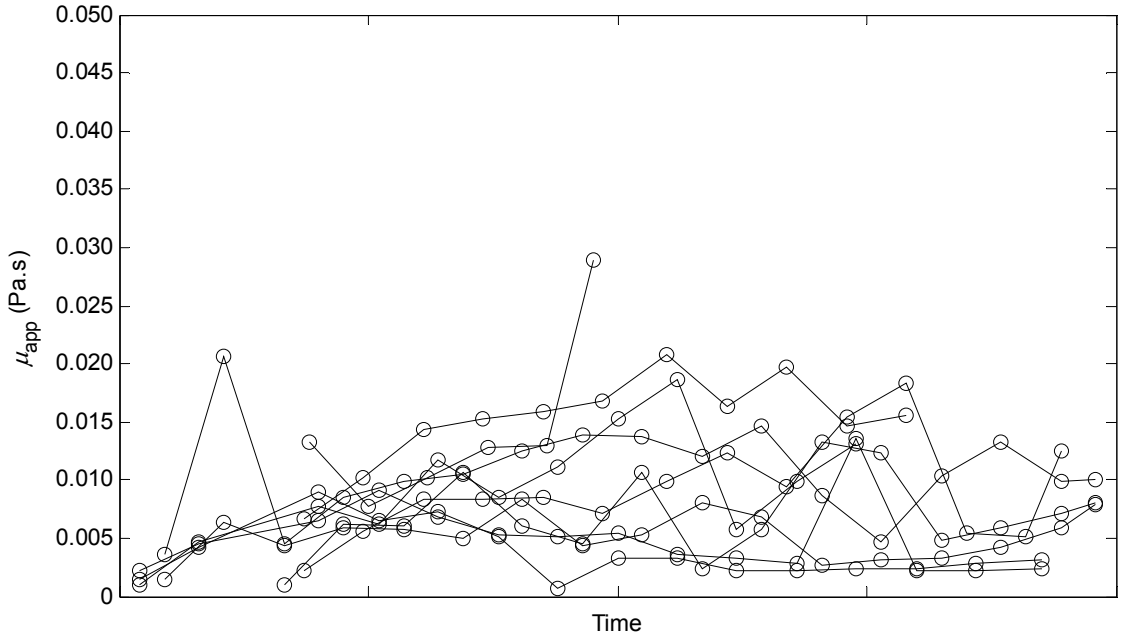

Figure A.6. Measurements of the apparent viscosity as function of fermentation time for all ALR fermentations. Note that the effective shear rates varied and were calculated based on Eq. (5.2C).

The observed rheological behavior with increasing non-Newtonian properties (decreasing *n*) and increasing apparent viscosity is similar to other data from filamentous fungi in the literature (Marten et al., 1997; Wang et al., 1979). Compared to the industrial strain of *A. oryzae* previously studied in a similar approach (using the STR), the increase in apparent viscosity and *K* for this strain of *T.*

reesei is considerably smaller (Albaek et al., 2011).

A viscosity model

It has previously been shown that various rheological parameters can be correlated with biomass concentration (Albaek et al., 2011; Petersen et al., 2008). The development of biomass concentration as function of fermentation time is shown in Figure A.7. The biomass concentration is rather low at the fermentation start as the seed material constitutes only about 10% of the broth volume. During the course of fermentation the biomass concentration increases manyfold although to quite different levels for the different fermentations. The different levels of biomass concentration are also expected since very different process conditions were applied. As seen from Table 5.4 the biomass formation (on average) followed the amount of carbon substrate fed to the fermentation.

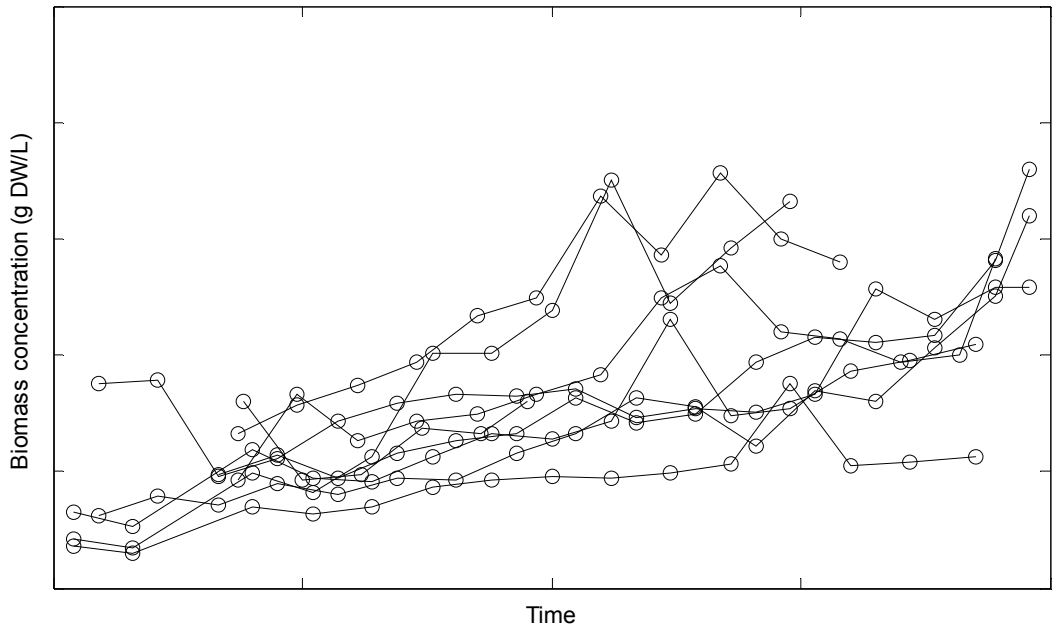

Figure A.7. Biomass concentration shown as function of fermentation time. Note that the units are not shown for proprietary reasons.

The consistency index K and the flow behavior index n are shown as function of biomass concentration in Figure A.8(A+B). As K tends to increase rapidly with biomass concentration, X, the power function of Eq. (2.10) has been widely used to describe the relationship between K and X for a range of fermentations with filamentous fungi (Olsvik and Kristiansen, 1994). A logistic equation for the dependence of K on biomass concentration has been proposed by Goudar et al. (1999)

$$K = \frac{K_0 e^{cX}}{1 - \frac{K_0}{K_f}\left(1 - e^{cX}\right)} \tag{A.3}$$

where K_0 and K_f can be considered representative of the initial and final values of K, and c is a constant (Goudar et al., 1999).

Both Eq. (2.10) and (A.3) with parameters estimated by least squares regression using the experimental values are shown in Figure A.8(A). At low biomass concentrations the experimental K values are <0.05. At higher biomass concentrations some low K values are still observed while $K_f \sim$ 0.25. Naturally, neither Eq. (2.10) nor (A.3) are able to describe all of the data, since the data are quite scattered.

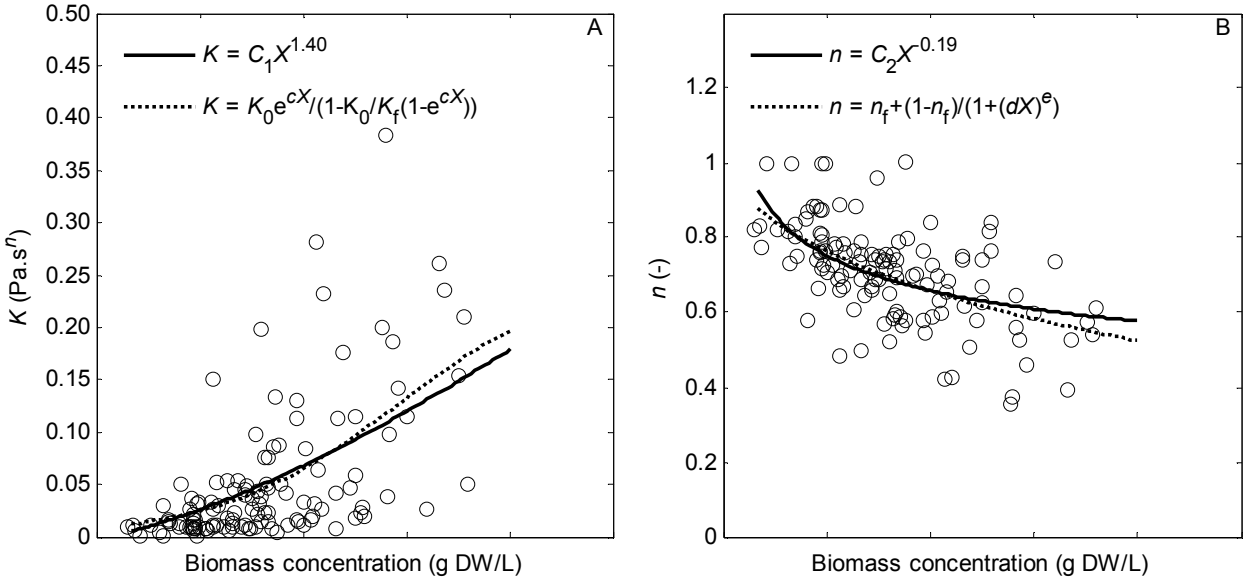

Figure A.0.1. A: K as function of biomass concentration for all ALR fermentations Eq. (2.10) and (A.3) with parameters estimated by least squares regression are both shown. **B:** n as function of biomass concentration for all ALR fermentations. Eq. (2.11) and (A.4) with parameters estimated by least squares regression are both shown. n_f was determined to be -0.37.

For n, Eq. (2.11) was used in Chapter 2 to describe the dependence of n on biomass concentration. Goudar et al. (1999) proposed an equation with a final value of n

$$n = n_f + \frac{1 - n_f}{1 + \left(dX\right)^e} \tag{A.4}$$

where d and e are constants and n_f is representative of the final value of n (Goudar et al., 1999). Eq. (A.4) proved to fit well to a range of literature data collected by Goudar et al. (1999).

In Figure A.8(B), Eq. (2.11) and (A.4) with parameters estimated by least squares regression are shown as well as the experimental data. n seems to decrease with increasing biomass concentration, but the data are quite scattered. The two equations predict a very similar trend for n, but none of them describes all the experimental data. It should be noted that the final value of n, n_f, predicted by Eq. (A.4) was -0.37, which does not make sense from a rheological point of view.

In order to compare the prediction power of Eq. (2.10)/(2.11) with Eq. (A.3)/(A.4) the two parity plots of the experimental data versus the model prediction are shown in Figure A.9(A) and Figure A.9(B), respectively. Both models generally overpredict the apparent viscosity in the low-viscosity region, and about 45% of the experimental data are within ±25% of either model. The mean square error was calculated in order to compare the predictive power of each model and it was found to be $3.17 \cdot 10^{-5}$ and $3.00 \cdot 10^{-5}$, respectively. The mean absolute error of the viscosity models are 0.0056 and 0.0055 Pa.s, respectively. To put the difference between the model prediction and the measured viscosity in perspective it is worth remembering, that the effective shear rate in this section has been estimated using Eq. (5.2C). The difference in the proportionality constants can be up to 0.010 Pa.s. The models thus seem to describe the experimental data reasonably well considering the uncertainty that exist around μ_{app}.

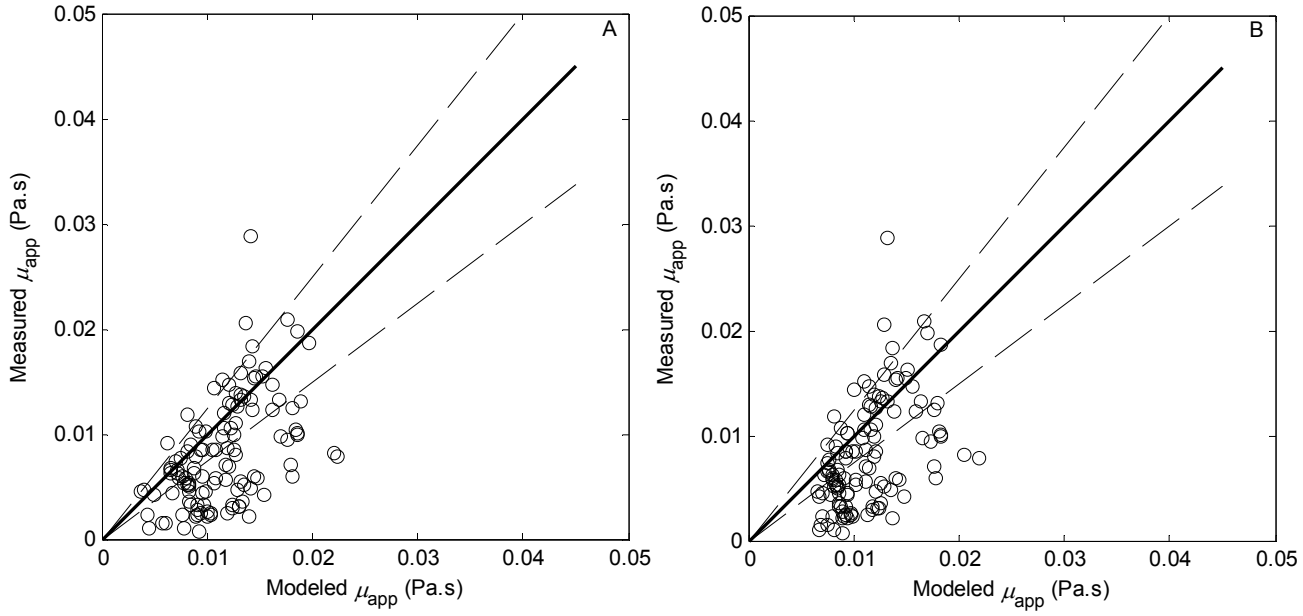

Figure A.9. Parity plots for two proposed viscosity models. The parity line (bold) is shown ± 25%. **A:** Measured apparent viscosity versus modeled apparent viscosity using Eq. (2.10) and (2.11). Mean square error: $3.17 \cdot 10^{-5}$ **B:** Measured apparent viscosity versus modeled apparent viscosity using Eq. (A.3) and (A.4). Mean square error: $3.00 \cdot 10^{-5}$.

As the mean square error for the two models are very similar, it was decided to use the simpler model described by Eq. (2.10) and (2.11), mainly for two reasons: it contains only four constants in contrast to six variables and the constants of the second model do not make sense in a rheological context as intended. The exponents of Eq. (2.10) and (2.11) (α, β) were 1.40 and -0.19, respectively,

while the constants C_1 and C_2 are not given for proprietary reasons. α has previously been shown vary within the range 0.7-3.3 dependent on the type of strain and the mycelial morphology (Olsvik and Kristiansen, 1994; Petersen et al., 2008).

Additional data for the mass transfer correlation

It was shown in the section on rheological characterization that the use of different proportionality constants in Eq. (5.3) could lead to quite different apparent viscosities. In Figure A.10 the measured k_La values are shown as function of three different sets of constants of Eq. (5.5) corresponding to the different proportionality constants. For all three proportionality constants it is seen that the correlation of Eq. (5.5) is able to describe the experimental k_La values with satisfactory accuracy.

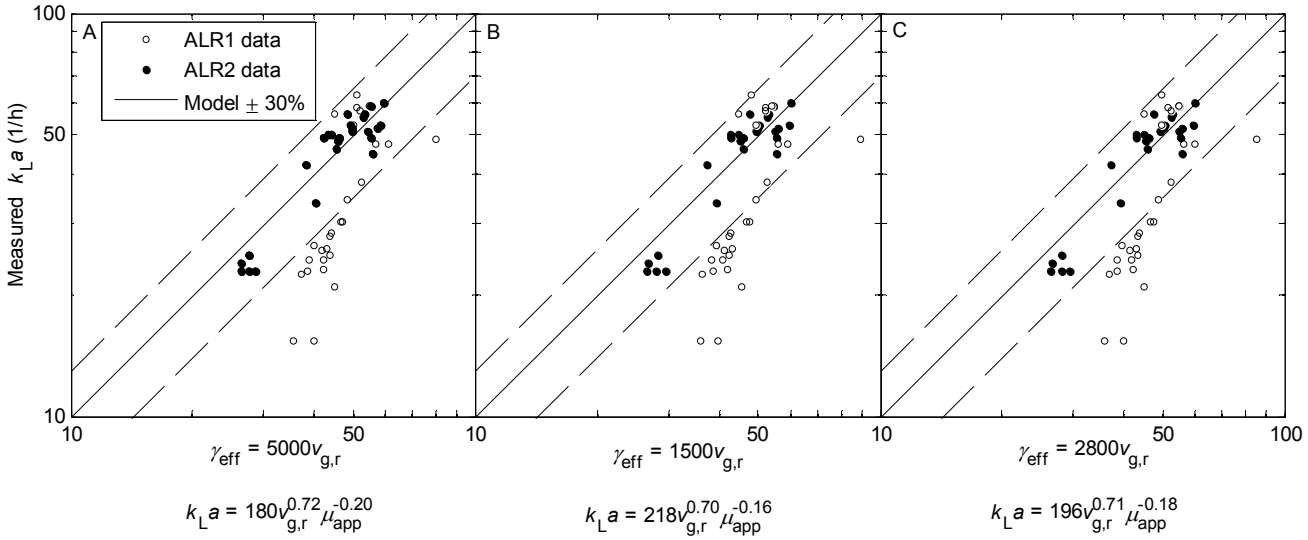

Figure A.10. Impact of three proportionality constants on Eq. (5.5). In each case the experimental k_La is shown as function of Eq. (5.5) with constants estimated by least squares regression. **A:** C_s =5000, Eq. (5.2A). Regression curve slope: 1.04 (R^2 = 0.83). **B:** C_s =1500, Eq. (5.2B). Regression curve slope: 1.04 (R^2 = 0.82).**C:** C_s =2800, Eq. (5.2C). Regression curve slope: 1.04 (R^2 = 0.83).

The exponents (*a, b*) of Eq. (5.5) were estimated to be in the narrow ranges 0.70-0.72 and (-0.20)-(-0.16), respectively, for the three proportionality constants investigated. As expected from Eq. (2.3) and Eq. (5.2A-C), the larger the proportionality constant, the smaller difference in apparent viscosities is expected at different superficial gas velocities. This was confirmed in Figure A.3.. The numerically larger exponent *a* (-0.20) for C_s = 5000 is thus explained since the differences in apparent viscosities were smaller for this proportionality constant (compared e.g. with C_s = 1500 where the viscosity varied to a larger degree and *a* = -0.16).

It was decided to continue the use of C_s = 2800 from Eq. (5.2C) in the further investigations, and the corresponding constants 196, 0.71, and -0.18 in the mass transfer correlation Eq. (5.5). The effect of the viscosity increase during the course of fermentation can thereby easily be quantified.

Use of the other proportionality constants proposed in the literature yields the same information.

Mixing Time Measurements

In order to ensure that the addition of the tracer did not damage the rheological properties of the xanthan gum solutions, rheological characterizations were performed similarly to the characterizations of the fermentation broth. The results of these measurements are shown in Figure A.11. The xanthan gum solutions were shear thinning with rheological properties as shown in Table A.2. The 0.125% xanthan solution resembled the properties of the fermentation broth closest. During the mixing time measurements up to 2% (v/v) of the concentrated NaCl tracer was injected, but even addition of 5% (v/v) does not significantly alter the rheology of the xanthan gum solution.

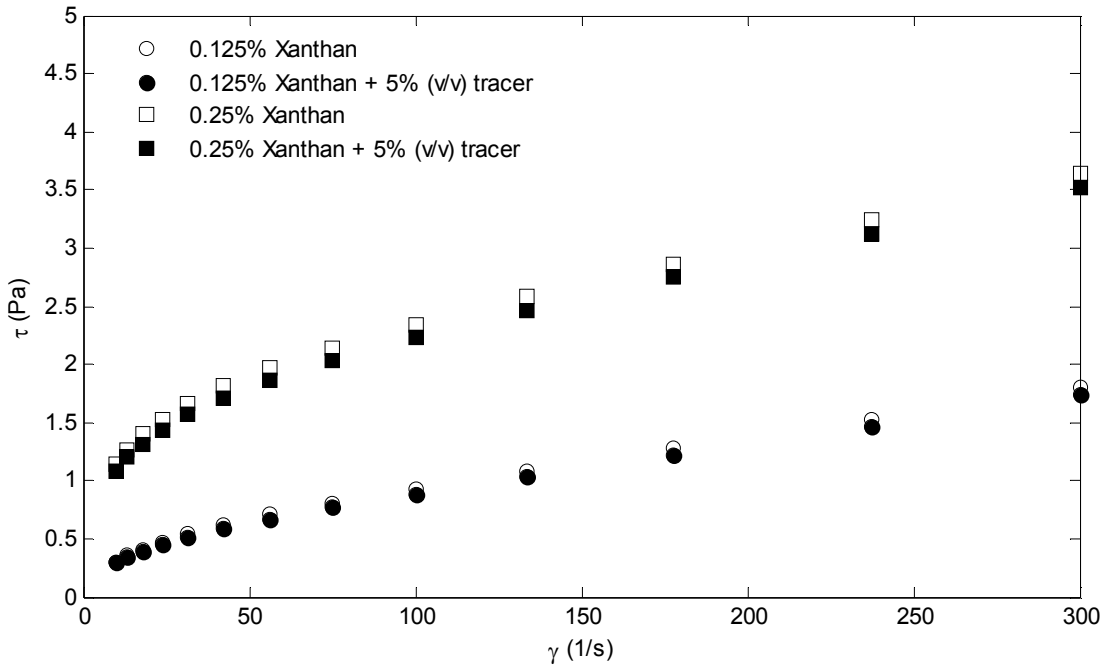

Figure A.11. Rheological characterization of the shear thinning xanthan gum solutions used for mixing time measurements. In the experiments <2% (v/v) of the NaCl tracer was injected. Addition of 5% (v/v) of the tracer does not significantly alter the rheology of xanthan gum solutions.

Table A.2. Rheological characterization of the xanthan gum solutions used for mixing time measurements. The power law is used to describe the rheological behavior.

Medium	K	n
0.125% (v/v) xanthan gum solution	0.083	0.53
0.125% (v/v) xanthan gum solution + 5% (v/v) tracer	0.077	0.54
0.25% (v/v) xanthan gum solution	0.51	0.34
0.25% (v/v) xanthan gum solution + 5% (v/v) tracer	0.47	0.35

The conductivity readings were normalized between the initial zero value, C_0, measured before the addition and the final stable value measured after the test is complete, C_∞ (Brown et al., 2004)

$$C_\mathrm{i}' = \frac{C_\mathrm{i} - C_0}{C_\infty - C_0} \tag{A.5}$$

where C_i' is the normalized conductivity. The data was finally also plotted in terms of a log variance as a function of time (Brown et al., 2004)

$$\log\sigma^2 = \log\left(C_\mathrm{t}' - 1\right)^2 \tag{A.6}$$

An example of the data and flow of data processing described here is shown in Figure A.12 for the ALR2 configuration with water as medium and $v_{\mathrm{g,r}}$ = 0.02 m/s. The conductivity raw data are shown in Figura A.12(A), the normalized probe output is shown in Figure A.12(B), and the log variance is shown in Figure A.12(C). The mixing time was determined as the time to achieve 90% mixing. Thus the lines representing ±10% are shown with the normalized output and the line representing 90% mixedness is shown with the log variance. The 90% mixing time in this case was determined to be 39s.

The measurement of mixing time was complicated with the presence of the non-conductive air bubbles, which resulted in a rather low signal to noise ratio for the viscous xanthan gum solutions. This is an inherent disadvantage of the conductivity method when used for aerated systems (Nordkvist, 2005). The noise caused by the air bubbles increased with the apparent viscosity. An example is shown in Figure A.13, where the degree of mixing apparently only surpasses 80% and the normalized probe output thus only remains within ±20%. If it assumed that mixing is a first order process, the 90% mixing time can be calculated as

$$t_{\mathrm{mix},90\%} = \frac{\ln(1-0.90)}{\ln(1-0.80)} t_{\mathrm{mix},80\%} = 1.43 t_{\mathrm{mix},80\%} \tag{A.7}$$

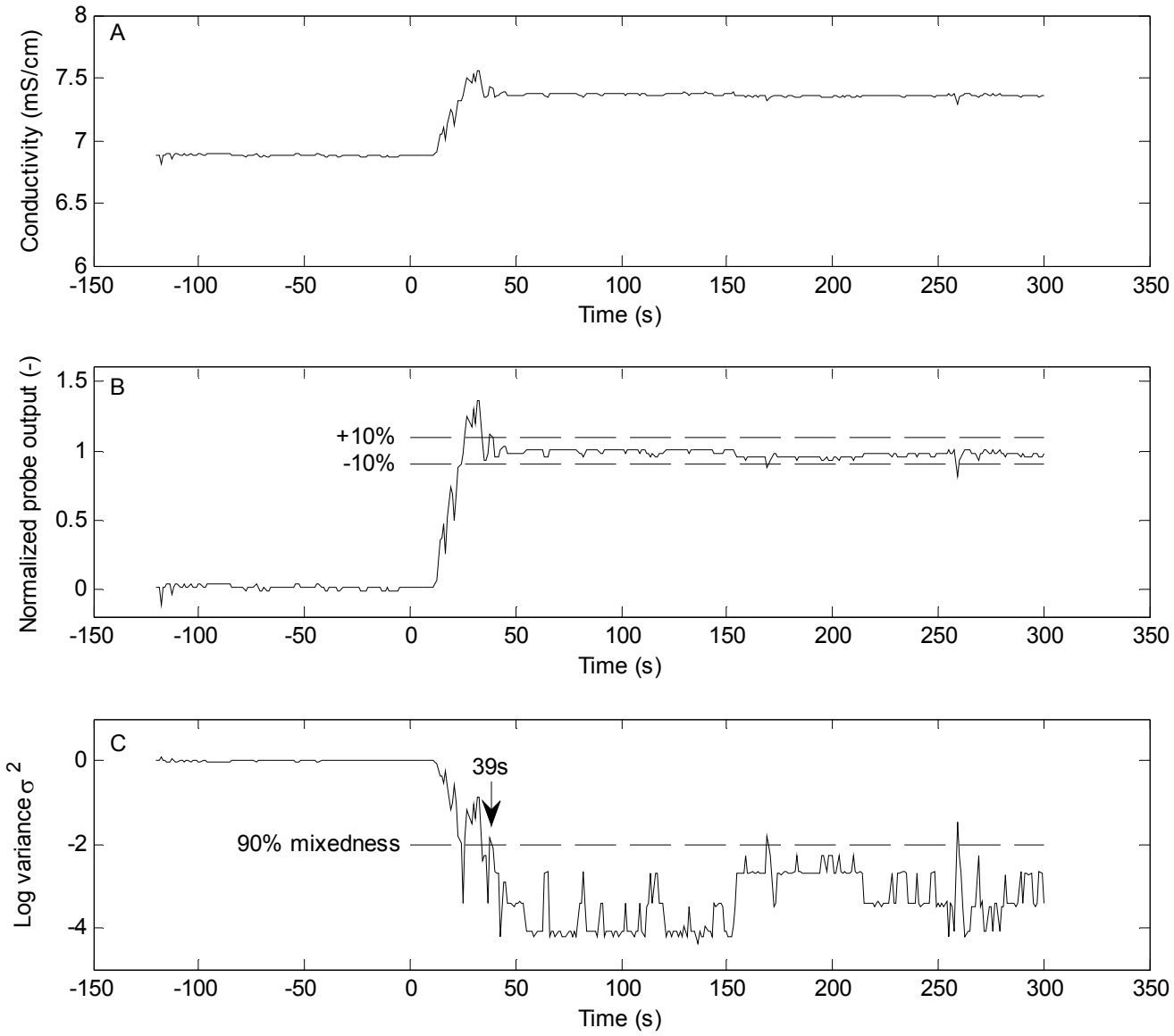

Figure A.12. Mixing time measurement with water as the medium for ALR2 ($v_{g,r}$ = 0.02m/s) **A**: Conductivity. **B** Normalized probe output with lines representing ±10%. **C**: Log variance σ^2 with line representing 90% mixedness. 90% mixing time determined to be 39 s.

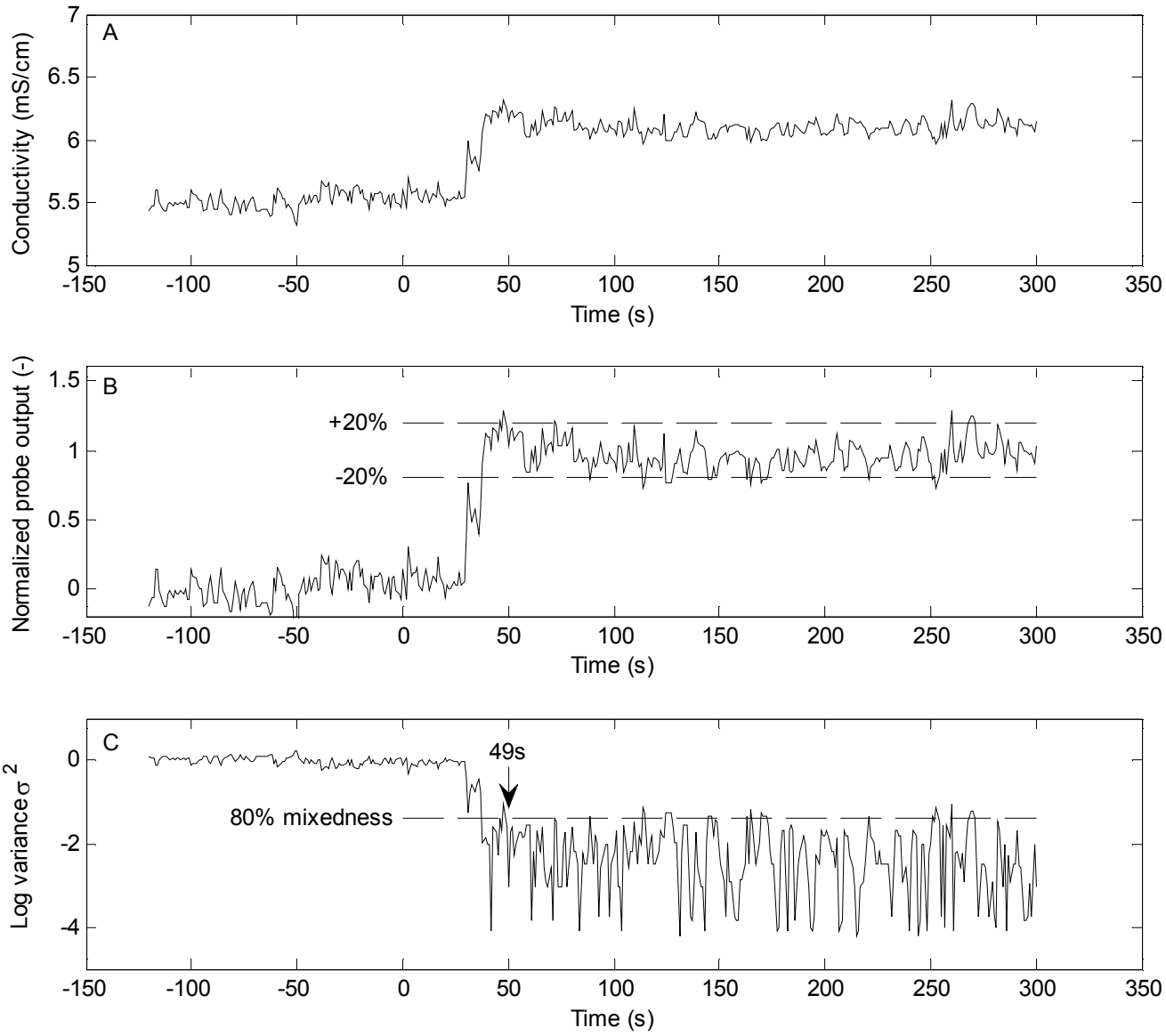

Figure A.13. Mixing time determination with 0.125% xanthan as the medium for ALR2 ($v_{g,r}$ = 0.04m/s) **A**: Conductivity. **B** Normalized probe output with lines representing ±20%. **C**: Log variance σ^2 with line representing 80% mixedness, $t_{mix,80\%}$ = 49 s. The 90% mixing time was calculated using Eq. (A.7), $t_{mix,90\%}$ = 70 s.

Appendix B: Supplementary data for chapter 6

Table B.1. Cost efficiency of simulated ALR fermentations

Run nr	Volume	Aspect ratio	$v_{g,r}$	Headspace pressure	Maximum pCO_2	Energy cost	Capital cost	Nutrients cost	Cost efficiency
	m^3	-	m/s	barg	mbar	$/kg O2	$/kg O2	$/kg O2	$/kg O2
1	101	1.5	0.069	0	16	0.11	0.24	0.77	1.13
2	100	1.5	0.069	2	46	0.24	0.15	0.77	1.16
3	99	1.5	0.200	0	11	0.14	0.16	0.77	1.07
4	100	1.5	0.200	2	35	0.42	0.13	0.77	1.33
5	101	25.0	0.069	0	212	0.14	0.27	0.77	1.19
6	99	25.0	0.069	2	344	0.11	0.15	0.77	1.03
7	100	25.1	0.200	0	112	0.16	0.15	0.77	1.08
8	99	25.0	0.200	2	294	0.15	0.11	0.77	1.04
9	995	1.5	0.069	0	40	0.11	0.09	0.77	0.98
10	1001	1.5	0.069	2	107	0.15	0.06	0.77	0.99
11	1003	1.5	0.200	0	31	0.14	0.06	0.77	0.97
12	997	1.5	0.200	2	83	0.26	0.05	0.77	1.08
13	1000	25.0	0.069	0	412	0.14	0.11	0.77	1.03
14	1005	25.0	0.069	2	543	0.13	0.09	0.77	0.99
15	1018	21.9	0.200	0	282	0.26	0.09	0.77	1.12
16	998	25.0	0.200	2	528	0.14	0.05	0.77	0.97
17	100	13.2	0.135	1	143	0.13	0.12	0.77	1.03
18	1001	13.3	0.135	1	298	0.13	0.06	0.77	0.96
19	549	1.5	0.135	1	50	0.17	0.07	0.77	1.01
20	551	25.0	0.135	1	329	0.14	0.08	0.77	0.98
21	555	13.2	0.069	1	278	0.11	0.09	0.77	0.96
22	552	13.2	0.200	1	246	0.14	0.06	0.77	0.96
23	552	13.2	0.135	0	126	0.16	0.10	0.77	1.02

continues on next page

continued from previous page

Run nr	Volume	Aspect ratio	$v_{g,r}$	Headspace pressure	Maximum pCO_2	Energy cost	Capital cost	Nutrients cost	Cost efficiency
	m^3	-	m/s	barg	mbar	$/kg O2	$/kg O2	$/kg O2	$/kg O2
24	550	13.3	0.135	2	360	0.13	0.06	0.77	0.96
25	554	13.3	0.135	1	257	0.13	0.07	0.77	0.97
26	554	13.3	0.135	1	257	0.13	0.07	0.77	0.97

Table B.2. Cost efficiency of simulated ALR fermentations

Run nr	Volume	Aspect ratio	P/V	v_g	Headspace pressure	Maximum pCO_2	Energy cost	Capital cost	Nutrients cost	Cost efficiency
	m^3	-	kW/m3	m/s	barg	mbar	$/kg O2	$/kg O2	$/kg O2	$/kg O2
1	102	2.0	0.50	0.05	0	26	0.14	0.25	0.77	1.17
2	101	2.0	0.50	0.20	2	17	0.69	0.20	0.77	1.67
3	102	2.0	5.00	0.05	1	81	0.36	0.21	0.77	1.34
4	101	2.0	7.00	0.20	0	14	0.44	0.23	0.77	1.45
5	101	5.0	0.50	0.05	2	116	0.18	0.17	0.77	1.12
6	102	5.0	0.50	0.20	0	21	0.21	0.18	0.77	1.16
7	100	5.0	7.00	0.05	0	105	0.48	0.28	0.77	1.53
8	96	5.1	5.00	0.20	1	72	0.52	0.23	0.77	1.52
9	400	2.0	0.50	0.05	2	90	0.21	0.10	0.77	1.08
10	399	2.0	0.50	0.20	0	17	0.22	0.10	0.77	1.10
11	403	2.0	7.00	0.05	0	82	0.50	0.14	0.77	1.41
12	408	2.1	6.00	0.20	1	50	0.52	0.11	0.77	1.41
13	398	5.0	0.50	0.05	0	87	0.14	0.13	0.77	1.04
14	397	5.0	0.50	0.20	2	75	0.35	0.09	0.77	1.22
15	411	5.0	7.00	0.05	2	388	0.41	0.11	0.77	1.29
16	402	5.0	7.00	0.20	0	80	0.45	0.11	0.77	1.34
17	101	3.5	3.75	0.13	1	54	0.34	0.20	0.77	1.32
18	406	3.5	3.75	0.13	1	97	0.32	0.10	0.77	1.19
19	253	2.0	3.75	0.13	1	44	0.36	0.13	0.77	1.26
20	253	5.0	3.75	0.13	1	116	0.31	0.12	0.77	1.21
21	249	3.5	0.50	0.13	1	45	0.24	0.12	0.77	1.12
22	256	3.5	7.00	0.13	1	102	0.45	0.14	0.77	1.36
23	246	3.5	3.75	0.05	1	154	0.28	0.13	0.77	1.18
24	255	3.5	3.75	0.20	1	56	0.38	0.13	0.77	1.28

continues on next page

continued from previous page

Run nr	Volume	Aspect ratio	P/V	v_g	Headspace pressure	Maximum pCO_2	Energy cost	Capital cost	Nutrients cost	Cost efficiency
	m^3	-	kW/m3	m/s	barg	mbar	$/kg O2	$/kg O2	$/kg O2	$/kg O2
25	246	3.5	3.75	0.13	0	49	0.32	0.15	0.77	1.24
26	251	3.5	3.75	0.13	2	101	0.41	0.13	0.77	1.32
27	253	3.5	3.75	0.13	1	80	0.32	0.13	0.77	1.22
28	253	3.5	3.75	0.13	1	80	0.32	0.13	0.77	1.22

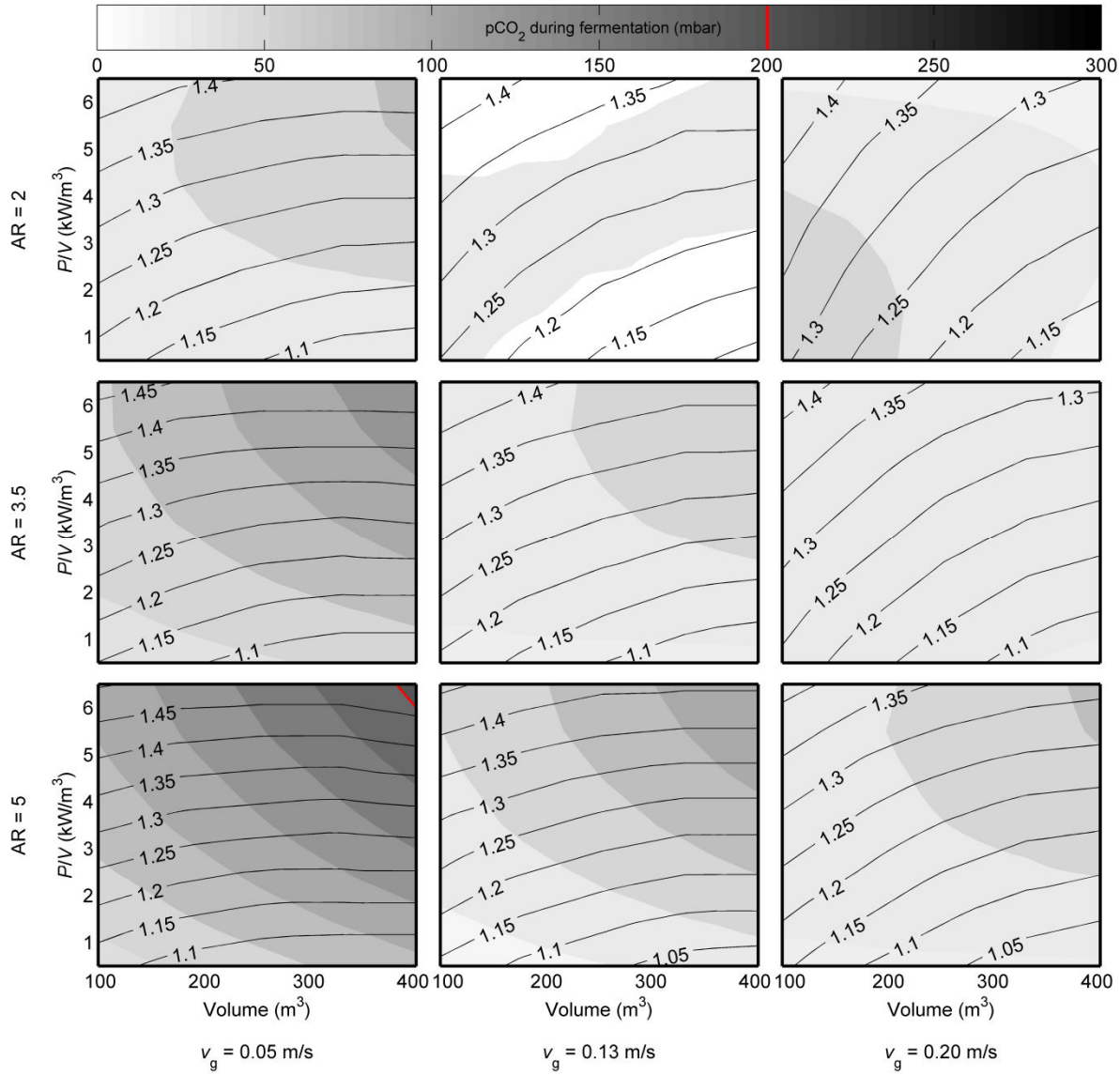

Figure B.1. Stirred tank reactor: Cost of oxygen transfer (contours, \$/kg O_2) and corresponding carbon dioxide partial pressure (shading, mbar) as function of aspect ratio (from top to bottom: 2, 3.5, or 5, respectively), agitator power input (y-axis), superficial gas velocity (from left: 0.05, 0.13, or 0.20 m/s, respectively), and fermentor volume (x-axis). The head space pressure was 0 barg.

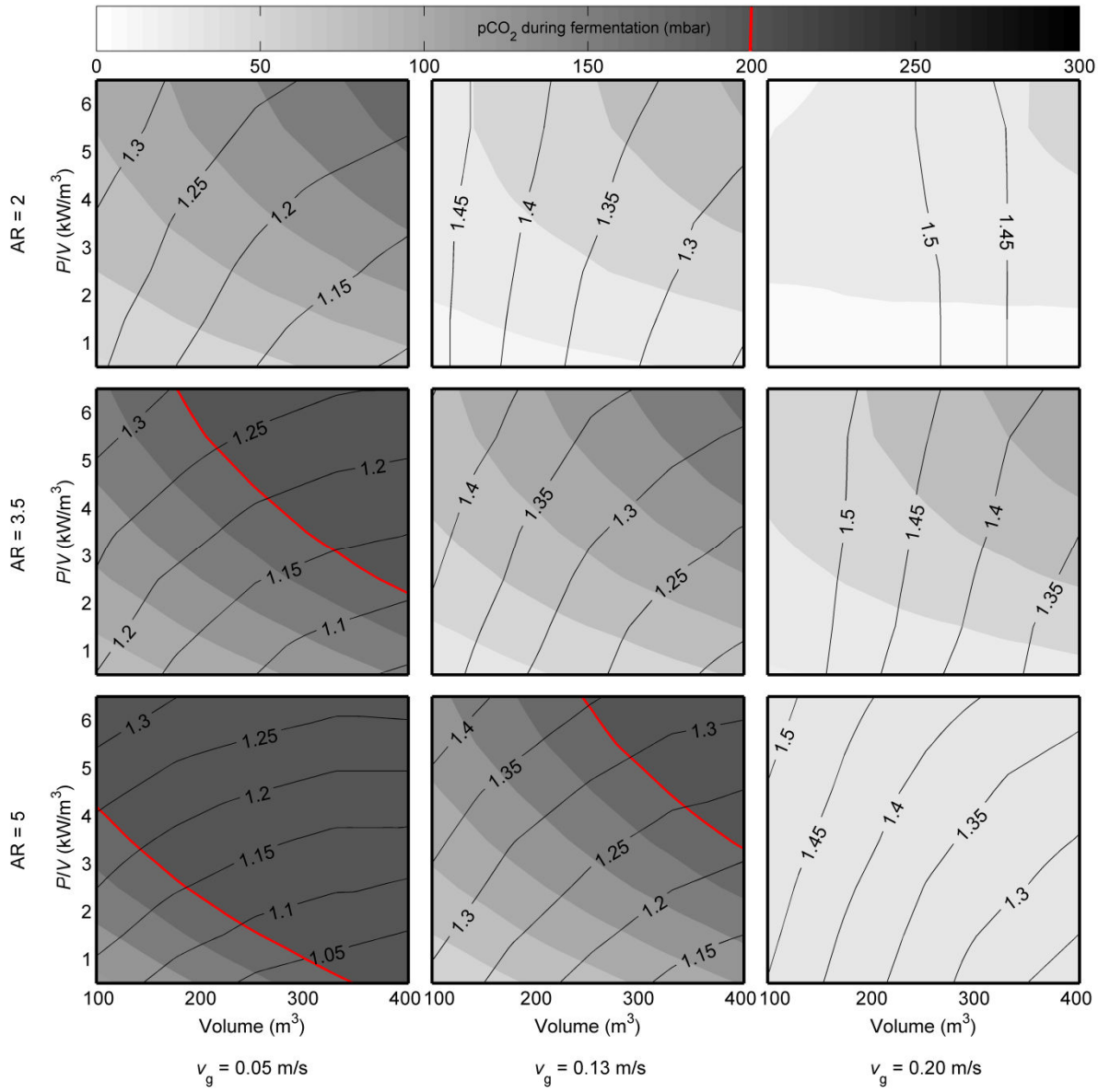

Figure B.2. Stirred tank reactor: Cost of oxygen transfer (contours, \$/kg O_2) and corresponding carbon dioxide partial pressure (shading, mbar) as function of aspect ratio (from top to bottom: 2, 3.5, or 5, respectively), agitator power input (y-axis), superficial gas velocity (from left: 0.05, 0.13, or 0.20 m/s, respectively), and fermentor volume (x-axis). The head space pressure was 2 barg.

Bibliography

Adler I, Fiechter A. 1986. Valuation of bioreactors for low viscous media and high oxygen transfer demand. Bioprocess Biosyst Eng 1:51-59.

Agger T, Spohr AB, Carlsen M, Nielsen J. 1998. Growth and product formation of *Aspergillus oryzae* during submerged cultivations: verification of a morphologically structured model using fluorescent probes. Biotechnol Bioeng 57:322-329.

Albaek MO, Gernaey KV, Stocks SM. 2008. Gassed and ungassed power draw in a pilot scale 550 litre fermentor retrofitted with up-pumping hydrofoil B2 impellers in media of different viscosity and with very high power draw. Chem Eng Sci 63:5813-5820.

Albaek MO, Gernaey KV, Hansen MS, Stocks SM. 2011. Modeling enzyme production with *Aspergillus oryzae* in pilot scale vessels with different agitation, aeration and agitator types. Biotechnol Bioeng 108:1828-1840.

Albaek MO, Gernaey KV, Hansen MS, Stocks SM. 2012. Evaluation of the energy efficiency of enzyme fermentation by mechanistic modeling. Biotechnol Bioeng 109:950-961.

Allen DG, Robinson CW. 1989. Hydrodynamics and mass transfer in *Aspergillus niger* fermentations in bubble column and loop bioreactors. Biotechnol Bioeng 34:731-740.

Allen DG, Robinson CW. 1991. Comments on the communication: On the calculation of shear rate and apparent viscosity in airlift and bubble column bioreactors. Biotechnol Bioeng 38:212-216.

Amanullah A, Blair R, Nienow AW, Thomas CR. 1999. Effects of agitation intensity on mycelial morphology and protein production in chemostat cultures of recombinant *Aspergillus oryzae*. Biotechnol Bioeng 62:434-446.

Amanullah A, Christensen LH, Hansen K, Nienow AW, Thomas CR. 2002. Dependence of morphology on agitation intensity in fed-batch cultures of *Aspergillus oryzae* and its implications for recombinant protein production. Biotechnol Bioeng 77:815-826.

ANSYS Inc. 2011. ANSYS 14.0 Capabilities Chart. www ansys com.

Atkinson B, Mavituna F. 1991. Biochemical engineering and biotechnology handbook. 2nd ed. New York: Macmillan Publishers Ltd.

Audet J, Thibault J, LeDuy A. 1996. Polysaccharide concentration and molecular weight effects on the oxygen mass transfer in a reciprocating plate bioreactor. Biotechnol Bioeng 52:507-517.

Bailey JE. 1980. Biochemical reaction engineering and biochemical reactors. Chem Eng Sci 35:1854-1886.

Bannari R, Bannari A, Vermette P, Proulx P. 2012. A model for cellulase production from *Trichoderma reesei* in an airlift reactor. Biotechnol Bioeng Accepted article, doi: 10 1002/bit 24473.

Barker T, Worgan J. 1981. The application of air-lift fermenters to the cultivation of filamentous

fungi. Appl Microbiol Biotechnol 13:77-83.

Bartholomew WH. 1960. Scale-up of submerged fermentations. Adv Appl Microbiol 2:289-300.

Berka RM, Cherry JR. 2006. Enzyme biotechnology, In: Ratledge C, Kristiansen B, editors. Basic Biotechnology. Cambridge: Cambridge University Press. p 477-498.

Berka RM, Grigoriev IV, Otillar R, Salamov A, Grimwood J, Reid I, Ishmael N, John T, Darmond C, Moisan MC, Henrissat B, Coutinho PM, Lombard V, Natvig DO, Lindquist E, Schmutz J, Lucas S, Harris P, Powlowski J, Bellemare A, Taylor D, Butler G, de Vries RP, Allijn IE, van den Brink J, Ushinsky S, Storms R, Powell AJ, Paulsen IT, Elbourne LDH, Baker SE, Magnuson J, LaBoissiere S, Clutterbuck AJ, Martinez D, Wogulis M, de Leon AL, Rey MW, Tsang A. 2011. Comparative genomic analysis of the thermophilic biomass-degrading fungi *Myceliophthora thermophila* and *Thielavia terrestris*. Nat Biotech 29:922-927.

Bevan MW, Franssen MCR. 2006. Investing in green and white biotech. Nat Biotech 24:765-767.

Blenke H. 1979. Loop reactors, In: Ghose T, Blakebrough N, Fiechter A, editors. Advances in Biochemical Engineering, Volume 13. Berlin/Heidelberg: Springer. p 121-214.

Brauner N, Barnea D. 1986. Slug/Churn transition in upward gas-liquid flow. Chem Eng Sci 41:159-163.

Brown DAR. 2009. Computational Fluid Dynamics. Course materials: Improving Mixing Processes. BHR Group Limited.

Brown DAR, Jones PN, Middleton JC, Papadopoulus G, Arik EB. 2004. Experimental Methods, In: Paul EL, Atiemo-Obeng V, Kresta SM, editors. Handbook of Industrial Mixing: Science and Practice. Hoboken: John Wiley & Sons, Inc. p 145-201.

Charles M. 1985. Fermentation scale-up: problems and possibilities. Trends Biotechnol 3:134-139.

Chen JH, Hsu YC, Chen YF, Lin CC. 2003. Application of gas-inducing reactor to obtain high oxygen dissolution in aeration process. Water res 37:2919-2928.

Chisti Y. 1989. Airlift bioreactors. London: Elsevier.

Chisti Y, Halard B, Moo-Young M. 1988. Liquid circulation in airlift reactors. Chem Eng Sci 43:451-457.

Chisti Y, Moo-Young M. 1987. Airlift reactors: characteristics, applications and design considerations. Chem Eng Commun 60:195-242.

Chisti Y. 2003. Bioreactor design, In: Ratledge C, Kristiansen B, editors. Basic biotechnology. Cambridge: Cambridge University Press. p 181-200.

Chisti Y, Jauregui-Haza UJ. 2002. Oxygen transfer and mixing in mechanically agitated airlift bioreactors. Biochem Eng J 10:143-153.

Chisti Y, Kasper M, Moo-Young M. 1990. Mass transfer in external-loop airlift bioreactors using static mixers. Can J Chem Eng 68:45-50.

Chisti Y, Moo-Young M. 1989. On the calculation of shear rate and apparent viscosity in airlift and bubble column bioreactors. Biotechnol Bioeng 34:1391-1392.

Cooke, M., Middleton, J. C., and Bush, J. R. 1988. Mixing and mass transfer in filamentous fermentations. 2nd International conference on bioreactors. Cambridge, UK.p. 37-64.

Cooney CL, Wang DIC, Mateles RI. 1969. Measurement of heat evolution and correlation with oxygen consumption during microbial growth. Biotechnol Bioeng 11:269-281.

Curran JS, Smith J, Holms W. 1989. Heat-and-power in industrial fermentation processes. Appl Energy 34:9-20.

Danish AgriFish Agency (former Direktoratet for FødevareErhverv). 2006. Biotechnology strategy for non-food and feed. Copenhagen, Denmark

Dashtban M, Schraft H, Qin WS. 2009. Fungal bioconversion of lignocellulosic residues; opportunities & perspectives. Int J Biol Sci 5:578-595.

Davenport R. 2008. Chemicals & polymers from biomass. Ind biotechnol 4:59-63.

Deckwer WD, Nguyen-Tien K, Schumpe A, Serpemen Y. 1982. Oxygen mass transfer into aerated CMC solutions in a bubble column. Biotechnol Bioeng 24:461-481.

Dodge T. 2009. Production of industrial enzymes, In: Whitehurst RJ, van Oort M, editors. Enzymes in Food Technology, 2nd edition. Oxford, UK: Wiley-Blackwell. p 44-58.

Enfors O, Jahic M, Rozkov A, Xu B, Hecker M, Jürgen B, Krüger E, Schweder T, Hamer G, O'Beirne D, Noisommit-Rizzi N, Reuss M, Boone L, Hewitt C, McFarlane C, Nienow A, Kovacs T, Trägårdh C, Fuchs L, Revstedt J, Friberg PC, Hjertager B, Blomsten G, Skogman H, Hjort S, Hoeks F, Lin Y, Neubauer P, der Lans Rv, Luyben K, Vrabel P, Manelius Å. 2001. Physiological responses to mixing in large scale bioreactors. J Biotechnol 85:175-185.

European Commision. 2011. Energy efficiency plan 2011 (http://ec.europa.eu/energy/efficiency/action_plan/action_plan_en.htm).

Fukuda H, Shiotani T, Okada W, Morikawa H. 1978. Oxygen transfer in a new tower bioreactor containing a draft tube and perforated plates. J Ferment Technol 56:619-625.

Garcia-Ochoa F, Gomez E. 2009. Bioreactor scale-up and oxygen transfer rate in microbial processes: An overview. Biotechnol Adv 27:153-176.

Gasner LL. 1974. Development and application of the thin channel rectangular air lift mass transfer reactor to fermentation and waste-water treatment systems. Biotechnol Bioeng 16:1179-1195.

Godbole SP, Schumpe A, Shah YT, Carr NL. 1984. Hydrodynamics and mass transfer in non-

Newtonian solutions in a bubble column. AIChE J 30:213-220.

Goudar CT, Strevett KA, Shah SN. 1999. Influence of microbial concentration on the rheology of non-Newtonian fermentation broths. Appl Microbiol Biotechnol 51:310-315.

Gow JS, Littlehailes JD, Smith SRL, Walter RB. 1975. SCP production from methanol: bacteria, In: Tannenbaum SR, Wang DIC, editors. Single-cell protein II. Cambridge: MIT Press. p 370-384.

Grajek W. 1987. Comparative studies on the production of cellulases by thermophilic fungi in submerged and solid-state fermentation. Appl Microbiol Biotechnol 26:126.

Green DW, Perry RH. 2008. Perry's Chemical Engineers' Handbook. 8th Edition. New York, USA: McGraw-Hill.

Grenville RK, Nienow AW. 2004. Blending of Miscible Liquids, In: Paul EL, Atiemo-Obeng V, Kresta SM, editors. Handbook of Industrial Mixing: Science and Practice. Hoboken: John Wiley & Sons, Inc. p 507-539.

Grima EM, Fernández JMS, Fernández FGA. 2009. Microalgae, mass culture methods, In: Flickinger MC, editor. Encyclopedia of Industrial Biotechnology. John Wiley & Sons, Inc.

Gschwend K, Fiechter A, Widmer F. 1983. Oxygen transfer in a loop reactor for viscous non-Newtonian biosystems. J Ferment Technol 61:491-498.

Hari-Prajitno D, Mishra VP, Takenaka K, Bujalski W, Nienow AW, McKemmie J. 1998. Gas-liquid mixing studies with multiple up- and down-pumping hydrofoil impellers: Power characteristics and mixing time. Can J Chem Eng 76:1056-1068.

Harris PV, Welner D, McFarland KC, Re E, Navarro Poulsen JC, Brown K, Salbo R, Ding H, Vlasenko E, Merino S, Xu F, Cherry J, Larsen S, Lo Leggio L. 2010. Stimulation of lignocellulosic biomass hydrolysis by proteins of glycoside hydrolase family 61: structure and function of a large, enigmatic family. Biochemistry 49:3305-3316.

Hatch RT. 1975. Fermentor design, In: Tannenbaum SR, Wang DIC, editors. Single cell protein II. Cambridge, MA: MIT Press. p 46-68.

Heim A, Rzyski E, Stelmach J, Kraslawski A. 1995. Aeration of bioreactors by self-aspirating impellers. Chem Eng J Biochem Eng J 58:59-63.

Heinzle E, Biwer AP, Cooney CL. 2006. Development of Sustainable Bioprocesses. Hoboken: John Wiley & Sons, Inc.

Herbst H, Schumpe A, Deckwer WD. 1992. Xanthan production in stirred tank fermenters: Oxygen transfer and scale-up. Chem Eng Technol 15:425-434.

Hewitt CJ, Nienow AW. 2007. The scale-up of microbial batch and fed-batch fermentation processes. Adv Appl Microbiol 62:105-135.

Heyouni A, Roustan M, Do-Quang Z. 2002. Hydrodynamics and mass transfer in gas-liquid flow through static mixers. Chem Eng Sci 57:3325-3333.

Hines DA, Bailey M, Ousby JC, Roesler FC. 1975. The ICI deep shaft aeration process for effluent treatment. Inst Chem Engng Symp Ser 41:D1-D10.

Hölker U, Höfer M, Lenz J. 2004. Biotechnological advantages of laboratory-scale solid-state fermentation with fungi. Appl Microbiol Biotechnol 64:175-186.

Hölker U, Lenz J. 2005. Solid-state fermentation - are there any biotechnological advantages? Curr Opin Microbiol 8:301-306.

Hua L, Nordkvist M, Nielsen PM, Villadsen J. 2007. Scale-up of enzymatic production of lactobionic acid using the rotary jet head system. Biotechnol Bioeng 97:842-849.

Hui JPM, Lanthier P, White TC, McHugh SG, Yaguchi M, Roy R, Thibault P. 2001. Characterization of cellobiohydrolase I (Cel7A) glycoforms from extracts of *Trichoderma reesei* using capillary isoelectric focusing and electrospray mass spectrometry. J Chromotogr B 752:349-368.

Hui JPM, White TC, Thibault P. 2002. Identification of glycan structure and glycosylation sites in cellobiohydrolase II and endoglucanases I and II from *Trichoderma reesei*. Glycobiology 12:837-849.

Humbird, D, Davis, R, Tao, L, Kinchin, C, Hsu, D., Aden, A, Schoen, P, Lukas, J, Olthof, B, Worley, M, Sexton, D, and Dudgeon, D. 2011. Process design and economics for biochemical conversion of lignocellulosic biomass to ethanol; dilute-acid pretreatment and enzymatic hydrolysis of corn stover. Technical Report NREL/TP-5100-47764

Jahic M, Wallberg F, Bollok M, Garcia P, Enfors SO. 2003. Temperature limited fed-batch technique for control of proteolysis in *Pichia pastoris* bioreactor cultures. Microb cell fact 2:1-11.

Jüsten P, Paul GC, Nienow AW, Thomas CR. 1998. Dependence of *Penicillium chrysogenum* growth, morphology, vacuolation, and productivity in fed-batch fermentations on impeller type and agitation intensity. Biotechnol Bioeng 59:762-775.

Kawase Y, Moo-Young M. 1988. Volumetric mass transfer coefficients in aerated stirred tank reactors with Newtonian and non-Newtonian media. Chem Eng Res Des 66:284-288.

Knoll A, Maier B, Tscherrig H, Buchs J. 2005. The oxygen mass transfer, carbon dioxide inhibition, heat removal, and the energy and cost efficiencies of high pressure fermentation. Adv Biochem Eng Biotechnol 92:77-99.

Kold, David. Study of mass transfer in viscous fermentations. 2010. PhD thesis. Technical University of Denmark.

Kouremenos D, Antonopoulos K. 1987. Isentropic exponents of real gases and application for the

air at temperatures from 150 K to 450 K. Acta Mech 65:81-99.

Krebser U, Meyer HP, Fiechter A. 1988. A comparison between the performance of continuously stirred-tank bioreactors and a TORUS bioreactor with respect to highly viscous culture broths. J Chem Technol Biotechnol 43:107-116.

Kubicek CP, Mikus M, Schuster A, Schmoll M, Seiboth B. 2009. Metabolic engineering strategies for the improvement of cellulase production by *Hypocrea jecorina*. Biotechnology for Biofuel 2.

Kura S, Nishiumi H, Kawase Y. 1993. Oxygen transfer in a stirred loop fermentor with dilute polymer solutions. Bioprocess Biosyst Eng 8:223-228.

Lehman, L. Physiological characterization of enzyme production in *Trichoderma reesei*. 2011. PhD thesis. Technical University of Denmark.

Li ZJ, Shukla V, Fordyce AP, Pedersen AG, Wenger KS, Marten MR. 2000. Fungal morphology and fragmentation behavior in a fed-batch *Aspergillus oryzae* fermentation at the production scale. Biotechnol Bioeng 70:300-312.

Li ZJ, Shukla V, Wenger KS, Fordyce AP, Pedersen AG, Marten MR. 2002. Effects of Increased Impeller Power in a Production-Scale *Aspergillus oryzae* Fermentation. Biotechnol Prog 18:437-444.

Lounes M, Audet J, Thibault J, LeDuy A. 1995. Description and evaluation of reciprocating plate bioreactors. Bioprocess Biosyst Eng 13:1-11.

Lübbert A. 2010. Bubble columns and airlift loop bioreactors, In: Berovic M, Enfors S-O, editors. Comprehensive bioprocess engineering. Ljubljana: University of Ljubljana. p 160-178.

Lynd LR, Weimer PJ, van Zyl WH, Pretorius IS. 2002. Microbial cellulose utilization: Fundamentals and biotechnology. Microbiol Mol Biol R 66:506-577.

Mach RS, Zeilinger S. 2003. Regulation of gene expression in industrial fungi: *Trichoderma*. Appl Microbiol Biotechnol 60:515-522.

Marten MR, Wenger KS, Khan SA. 1997. Rheology, mixing time, and regime analysis for a production-scale *Aspergillus oryzae* fermentation. BHR Group Conference Series 25:295-316.

Martinez D, Berka RM, Henrissat B, Saloheimo M, Arvas M, Baker SE, Chapman J, Chertkov O, Coutinho PM, Cullen D, Danchin EGJ, Grigoriev IV, Harris P, Jackson M, Kubicek CP, Han CS, Ho I, Larrondo LF, de Leon AL, Magnuson JK, Merino S, Misra M, Nelson B, Putnam N, Robbertse B, Salamov AA, Schmoll M, Terry A, Thayer N, Westerholm-Parvinen A, Schoch CL, Yao J, Barbote R, Nelson MA, Detter C, Bruce D, Kuske CR, Xie G, Richardson P, Rokhsar DS, Lucas SM, Rubin EM, Dunn-Coleman N, Ward M, Brettin TS. 2008. Genome sequencing and analysis of the biomass-degrading fungus *Trichoderma reesei* (syn. *Hypocrea jecorina*). Nat Biotechnol 26:553-560.

McIntyre M, Müller C, Dynesen J, Nielsen J. 2001. Metabolic engineering of the morphology of *Aspergillus*. Adv Biochem Eng Biotechnol 73:103-128.

Mcneil B, Harvey LM. 1993. Viscous fermentation products. Crit Rev Biotechnol 13:275-304.

Meesters PAEP, Wal H, Weusthuis R, Eggink G. 1996. Cultivation of the oleaginous yeast *Cryptococcus curvatus* in a new reactor with improved mixing and mass transfer characteristics (Surer). Biotechnol Tech 10:277-282.

Meister D, Post T, Dunn IJ, Bourne JR. 1979. Design and characterization of a multistage, mechanically stirred column absorber. Chem Eng Sci 34:1367-1374.

Merchuk JC, Gluz M. 2002. Bioreactors, air-lift reactors.Encyclopedia of Bioprocess Technology. Hoboken: John Wiley & Sons, Inc.

Merino ST, Cherry J. 2007. Progress and challenges in enzyme development for biomass utilization. Biofuels 108:95-120.

Middleton JC. 1997. Gas-liquid dispersion and mixing, In: Harnby N, Edwards MF, Nienow AW, editors. Mixing in the Process Industries. Oxford: Butterworth-Heinemann. p 322-363.

Miller CE. 2007. Chemometrics in process analytical chemistry, In: Bakeev KA, editor. Process Analytical Technology. Oxford, UK: Blackwell Publishing Ltd. p 226-328.

Ministry of Foreign Affairs of Denmark, Ministry of Transport of Denmark Danish Ministry of the Environment. 2006. Export promotion of energy and environmental technologies.

Mishra IM, El-Temtamy SA, Schügerl K. 1982. Growth of *Saccharomyces cerevisiae* in gaseous fluidized beds. Appl Microbiol Biotechnol 16:197-203.

Mitchell DA, Krieger N, Berovic M. 2006. Solid-State fermentation bioreactors: fundamentals of design and operation. Berlin: Springer.

Moebus O, Teuber M. 1979. Herstellung von single cell protein mit *Saccharomyces cerevisiae* in einer tauchstrahlbegasungsanlage. Kieler milchwirtsschaftliche Forschungsberichte 31:297-361.

Montenecourt BS, Eveleigh DE. 1977a. Preparation of mutants of *Trichoderma reesei* with enhanced cellulase production. Appl Environ Microbiol 34:777-782.

Montenecourt BS, Eveleigh DE. 1977b. Semiquantitative plate assay for determination of cellulase production by *Trichoderma viride*. Appl Environ Microbiol 33:178-183.

Montgomery D. 1997. Response surface methods and other approaches to process optimization. In: Design and analysis of experiment. New York: John Wiley & Sons, Inc. p 427-510.

Moresi M. 1981. Optimal design of airlift fermenters. Biotechnol Bioeng 23:2537-2560.

Morris MD. 1991. Factorial sampling plans for preliminary computational experiments 1.

Technometrics 33:161-174.

National Academy of Sciences, National Academy of Engineering National Research Counsil. 2009. Liquid transportation fuels from coal and biomass: technological status, costs, and environmental impacts. Washington, DC: National Academy of Sciences

Nevalainen H, Suominen P, Taimisto K. 1994. On the safety of *Trichoderma reesei*. J Biotechnol 37:193-200.

Ni X, Gao S, Cumming RH, Pritchard DW. 1995a. A comparative study of mass transfer in yeast for a batch pulsed baffled bioreactor and a stirred tank fermenter. Chem Eng Sci 50:2127-2136.

Ni X, Gao S, Pritchard DW. 1995b. A study of mass transfer in yeast in a pulsed baffled bioreactor. Biotechnol Bioeng 45:165-175.

Nielsen J. 1997. Physiological engineering aspects of *Penicillium chrysogenum*. Singapore: World Scientific.

Nielsen J. 1993. A simple morphologically structured model describing the growth of filamentous microorganisms. Biotechnol Bioeng 41:715-727.

Nielsen J, Villadsen J, Lidén G. 2003. Bioreaction engineering principles. New York: Kluwer Academic/Plenum Publishers.

Nienow AW. 1990. Agitators for mycelial fermentations. Trends Biotechnol 8:224-233.

Nienow AW. 1996. Gas-liquid mixing studies: A comparison of Rushton turbines with some modern impellers. Trans IChemE 74:417-423.

Nienow AW. 1997. On impeller circulation and mixing effectiveness in the turbulent flow regime. Chem Eng Sci 52:2557-2565.

Nienow AW. 1998. Hydrodynamics of stirred bioreactors. Appl Mech Rev 51:3-32.

Nishikawa M. 1991. On the estimation of average shear rate in bubble columns. Biotechnol Bioeng 37:691-692.

Nordkvist, Mikkel. Mixing and mass transfer by rotating jets: fundamentals and applications. 2005. PhD thesis. Technical University of Denmark.

Nordkvist M, Grotkjær T, Lazar JÅ, Hummer JS, Villadsen J. 2003. Hiv røreværket op, sænk jetten ned. Dansk Kemi 84:18-21.

Nordkvist M, Vognsen M, Nienow AW, Villadsen J, Gernaey KV. 2008. Mixing by rotary jet heads: Indications of the benefits of head rotation under turbulent and transitional flow conditions. Chem Eng Res Des 86:1454-1461.

Novozymes A/S. 2007. The Novozymes Report 2007. Bagsvaerd, Denmark

Olivier APC, Oosterhuis NMG. 1988. Oxygen mass transfer in non-Newtonian fermentation systems, In: Durant G, Robichon L, Florent J, editors. Proceedings 8th International Biotechnology Symposium. Paris: Société francaise de microbiologie. p 389-409.

Olsen, HS. 2008. Enzymes at work. Novozymes A/S. www.novozymes.com

Olsvik E, Kristiansen B. 1994. Rheology of filamentous fermentations. Biotechnol Adv 12:1-39.

Onken U, Liefke E. 1989. Effect of total and partial pressure (oxygen and carbon dioxide) on aerobic microbial processes. Adv Biochem Eng Biotechnol 40:137-169.

Oosterhuis, N. M. G. Scale-up of bioreactors. A scale-down approach. 1984. PhD thesis. Delft University of Technology.

Pandey A. 2003. Solid-state fermentation. Biochem Eng J 13:81-84.

Papagianni M. 2004. Fungal morphology and metabolite production in submerged mycelial processes. Biotechnol Adv 22:189-259.

Pazouki M, Panda T. 2000. Understanding the morphology of fungi. Bioprocess Eng 22:127-143.

Pedersen, A. G. 1997. $k_l a$ characterization of industrial fermentors. Proceedings of the forth international conference on bioreactor and bioprocess fluid dynamics. Edinburgh, UK: 263-276.

Peri S, Steen H, Pandey A. 2001. GPMAW - a software tool for analyzing proteins and peptides. Trends Biochem Sci 26:687-689.

Perlack, R., Wright, L, Turhollow, A., Graham, R., Stokes, B., and Erbach, D. 2005. Biomass as feedstock for a bioenergy and bioproducts industry: The technical feasibility of a billion-ton annual supply (U.S. Department of Energy and U.S. Department of Agriculture, Eds.). Washington, DC: U.S. Department of Energy

Persson I, Tjerneld F, Hahn-Hägerdal B. 1991. Fungal cellulolytic enzyme production: A review. Process Biochem 26:65-74.

Peters MS, Timmerhaus KD, West RE. 2003. Plant design and economics for chemical engineers. New York, USA: McGraw-Hill.

Petersen N, Stocks S, Gernaey KV. 2008. Multivariate models for prediction of rheological characteristics of filamentous fermentation broth from the size distribution. Biotechnol Bioeng 100:61-71.

Pirt SJ. 1965. The maintenance energy of bacteria in growing cultures. Proceedings of the Royal Society of London Series B, Biological Sciences 163:224-231.

Poncin S, Nguyen C, Midoux N, Breysse J. 2002. Hydrodynamics and volumetric gas-liquid mass transfer coefficient of a stirred vessel equipped with a gas-inducing impeller. Chem Eng Sci 57:3299-3306.

Popovic MK, Robinson CW. 1989. Mass transfer studies of external-loop airlifts and a bubble column. AIChE J 35:393-405.

Renewable Fuels Association. 2011. 2011 Ethanol Industry Outlook. Washington, DC

Rettich TR, Battino R, Wilhelm E. 2000. Solubility of gases in liquids. 22. High-precision determination of Henry's law constants of oxygen in liquid water from T = 274 K to T = 328 K. J Chem Thermodyn 32:1145-1156.

Reuss M. 1993. Oxygen transfer and mixing: scale-up implications, In: Rehm H-J, Reed G, editors. Biotechnology: Bioprocessing. Weinheim, Germany: Wiley-VCH Verlag GmbH. p 185-217.

Revill BK. 1985. Jet mixing, In: Harnby N, Edwards MF, Nienow AW, editors. Mixing in the Process Industries. Oxford: Butterworth-Heinemann. p 159-183.

Revstedt J, Fuchs L, Trägårdh C. 1998. Large eddy simulations of the turbulent flow in a stirred reactor. Chem Eng Sci 53:4041-4053.

Ross A, Schügerl K, Scheiding W. 1983. Cellulase production by *Trichoderma reesei*. Appl Microbiol Biotechnol 18:29-37.

Scargiali F, Russo R, Grisafi F, Brucato A. 2007. Mass transfer and hydrodynamic characteristics of a high aspect ratio self-ingesting reactor for gas-liquid operations. Chem Eng Sci 62:1376-1387.

Schügerl K. 1985. Nonmechanically agitated bioreactor systems, In: Moo-Young M, editor. Comprehensive Biotechnology. Volume 2. p 99-118.

Schügerl K. 1980. Neue Bioreaktoren für aerobe Prozesse. Chem Ing Tech 52:951-965.

Schügerl K. 1983. Apparatetechnische Aspekte der Kultivierung von Einzellern in Turmreaktoren. Chem Ing Tech 55:123-134.

Schügerl K. 1990. Comparison of the performances of stirred tank and airlift tower loop reactors. J Biotechnol 13:251-256.

Schügerl K. 1991. Bioreaction engineering: characteristic features of bioreactors. Chichester: John Wiley & Son Ltd.

Schügerl K. 1993. Comparison of different bioreactor performances. Bioprocess Biosyst Eng 9:215-223.

Schügerl K, Sittig W. 1982. Bioreactors, In: Präve P, Faust U, Sittig W, Sukatsch DA, editors. Fundamentals of Biotechnology. Wiesbaden: Akademische Verlagsgesellschaft. p 179-224.

Schumpe A, Deckwer W-D. 1987. Viscous media in tower bioreactors: Hydrodynamic characteristics and mass transfer properties. Bioprocess Biosyst Eng 2:79-94.

Schuster A, Schmoll M. 2010. Biology and biotechnology of *Trichoderma*. Appl Microbiol

Biotechnol 87:787-799.

Simmons, E. G. 1977. Classification of some cellulase-producing *Trichoderma* species. Proceedings of the Second International Mycological Congress, University of South Florida, Tampa, Florida. p 618.

Sin G, Gernaey KV, Lantz AE. 2009. Good modeling practice for PAT applications: Propagation of input uncertainty and sensitivity analysis. Biotechnol Prog 25:1043-1053.

Sittig W. 1982. The present state of fermentation reactors. J Chem Technol Biotechnol 32:47-58.

Smith SRL. 1980. Single Cell Protein. Philosophical Transactions of the Royal Society of London B 290:341-354.

Soderberg AC. 1997. Fermentation design, In: Vogel HC, Todaro CL, editors. Fermentation and Biochemical Engineering Handbook. Westwood, NJ: William Andrew Publishing. p 67-121.

Streiff F. A, Mathys P, Fischer TU. 1997. New fundamentals for liquid – liquid dispersion using static mixers. Paris: Proc. 9th European Conference on Mixing. p 307-314.

Sukumaran RK, Singhania RR, Pandey A. 2005. Microbial cellulases - Production, applications and challenges. J Sci Ind Res 64:832-844.

Tengerdy RP. 1996. Cellulase production by solid substrate fermentation. J Sci Ind Res 55:313-316.

Tolan JS, Foody B. 1999. Cellulase from submerged fermentation. Adv Biochem Eng Biotechnol 65:41-67.

U.S.Congress. 2007. Energy Independence and Security Act of 2007. US Congress.

Viniegra-González G, Favela-Torres E, Aguilar CN, Rómero-Gomez SdJ, Díaz-Godínez G, Augur C. 2003. Advantages of fungal enzyme production in solid state over liquid fermentation systems. Biochem Eng J 13:157-167.

Votruba J, Sobotka M. 1992. Physiological similarity and bioreactor scale-up. Folia Microbiol 37:331-345.

Walker J, Wilkinson GW. 1979. The treatment of industrial effluents using the deep shaft process. Ann N Y Acad Sci 326:181-191.

Wang DIC, Cooney CL, Demain AL, Dunnill P, Humpfrey AE, Lilly MD. 1979. Fermentation and enzyme technology. New York: Wiley & Sons.

Ward OP. 2011. Production of recombinant proteins by filamentous fungi. Biotechnol Adv. Article in press.

Westlake R. 1986. Large-scale continuous production of single cell protein. Chem Ing Tech 58:934-937.

Yang H, Allen DG. 1999. Model-based scale-up strategy for mycelial fermentation processes. Can J Chem Eng 77:844-854.

Zaidi A, Ghosh P, Schumpe A, Deckwer WD. 1991. Xanthan production in a plunging jet reactor. Appl Microbiol Biotechnol 35:330-333.

Zhang YHP, Lynd LR. 2004. Toward an aggregated understanding of enzymatic hydrolysis of cellulose: Noncomplexed cellulase systems. Biotechnol Bioeng 88:797-824.

Zhou G, Kresta SM. 1996. Impact of tank geometry on the maximum turbulence energy dissipation rate for impellers. AIChE J 42:2476-2490.

Zlokarnik M. 1975. Der Schaufelradreaktor - ein spezieller Reaktortyp für Reaktionen im System gasfürmig/flüssig. Verfahrenstechnik 9:442-445.

Zlokarnik M. 1978. Sorption characteristics for gas-liquid contacting in mixing vessels. Adv Biochem Eng Biotechnol 8:133-151.